CHAPTER IV

RESULTS AND DISCUSSION

1. Preparation and Characterization of Liposomes

Hydrogenated soybean phosphatidylcholine (HPC) was selected for studying the preparation methods of liposomes and the spray-dried liposomal powders because of its commercial availability and reasonable cost. Moreover, HPC has high gel-to-liquid crystalline phase transition temperature (T_m), displays good stability and gives high entrapment of peptides (Weiner, 1989). Desai et al. (2003) explained a crucial role of the T_m of the phospholipids in determining the aerodynamic size of phospholipids-based powders and found that the higher the T_m of the phospholipid, the lower the mass median aerodynamic diameter (MMAD) of particles would be. Phospholipids with T_m below 10 °C (such as unsaturated phosphatidylcholine) form highly cohesive powders after spray drying which result in sticky powders (Weers et al., 2002). This is because of their hygroscopic property and the presence of double bonds in the fatty acyl chains. HPC is composed of saturated fatty acid chains, giving it a crystalline appearance. However, when high content of HPC was present in formulations in this present study, its T_m was not sufficient to avoid softening of the powders during the spray drying process and consequently did not prevent aggregation of particles. This finding is consistent with previous studies by Sebti and Amighi (2006) and Gaete et al. (2008). Therefore, an additive was added into the formulations to reduce aggregation of particles and to increase the collector yield of the liposomal powders by spray drying process.

In the preliminary study, coarse lipid dispersion with only HPC was prepared by dispersing HPC under mechanical stirring in Ultrapure® water at 65 °C for 2 hours (Figure 18a). Then, a high speed homogenizer was used to disperse lipid in Ultrapure® water at 65 °C for 5 min (Figure 18b). Volume mean diameter of the lipid dispersion was 6.69 μm and span was 1.78. The lipid dispersion was mixed with

mannitol (M) solution in a HPC/M weight ratio of 5:5 and spray-dried into the powders. The spray drying process parameters used in the study were the condition commonly reported in the spray drying of proteins (Platz et al., 2003; Grenha et al., 2008). The SEM micrographs in Figure 19 show that this spray-dried formulation resulted in mostly spherical particles with rough surface but appeared to be broken and aggregate. The size of most particles was larger than 10 μm which might be corresponding to the size of lipid droplets prior to spray drying. When the spray-dried powders were reconstituted with HBS at 37 °C, decent liposomes did not adequately form as evident by optical microscopy (Figure 20). Nonuniform large size of lipid droplets before spray drying resulted in inconsistent drying during the spray drying process which allowed segregation of the mixture of lipid and mannitol. Consequently, aggregation and/or fusion of these lipid droplets took place. Therefore, the method using high speed homogenizer was not used in the study.

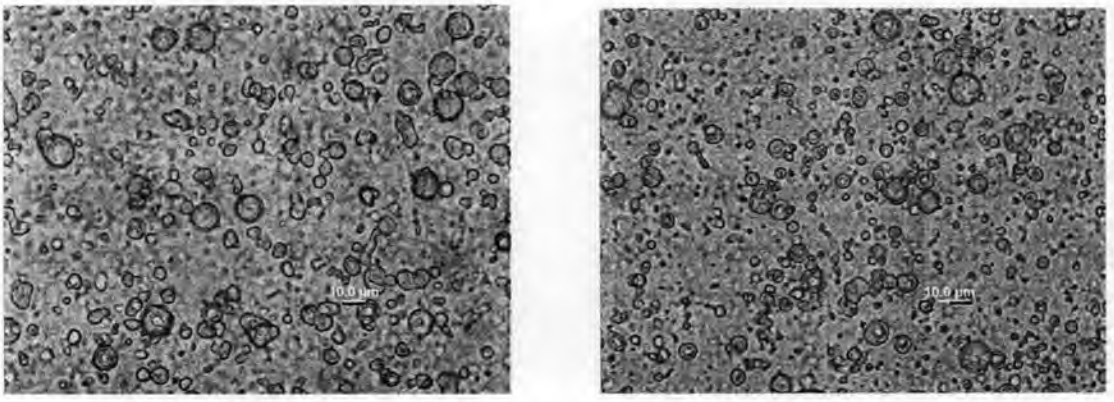

(a) (b)

Figure 18 Optical micrographs of (a) HPC lipid dispersions prepared by dispersing HPC in Ultrapure® water at 65 °C for 2 hours and then (b) after high speed homogenization. Magnification 400x. Scale bar = 10 μm.

For liposomes composed of HPC and Chol, a homogeneous distribution of the two lipids all over the bilayer was required. Therefore, liposomes constituted of HPC and Chol were prepared by film hydration method. Finally, all formulations of liposomes were extruded through two-stacked 0.2 μm PC filters to obtain homogeneous vesicles prior to spray drying process. Nano-size range of liposomes resulted in uniform

distribution in the bulk of spray-dried powders. TEM micrographs of the extruded liposomes composed of HPC and HPC/Chol (8:2) are illustrated in Figure 21. The effective diameters of the extruded liposomes prior to spray drying were about 130-190 nm and polydispersity values were around 0.15-0.19, independent of the lipid compositions. The polydispersity values indicate narrow size distribution.

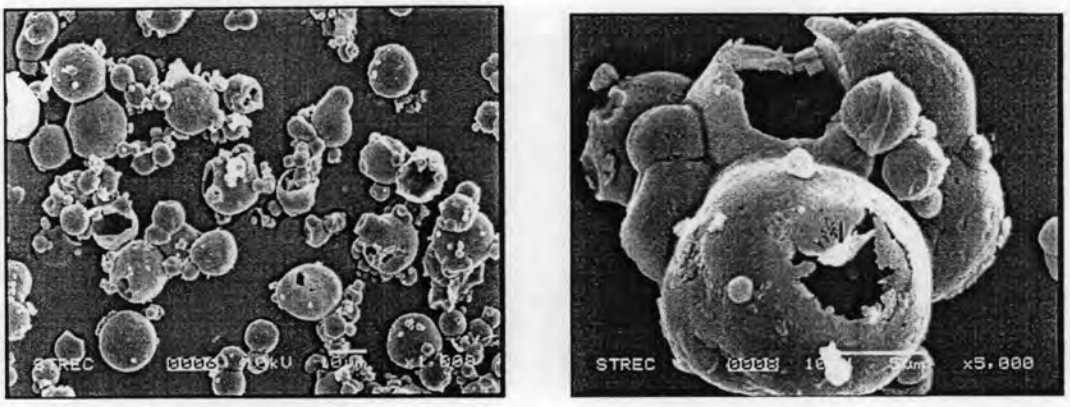

(a) (b)

Figure 19 Scanning electron micrographs of the spray-dried powders of lipid dispersion prepared by high speed homogenizer. (a) Magnification 1000x. Scale bar = 10 μm. (b) Magnification 5000x. Scale bar = 5 μm.

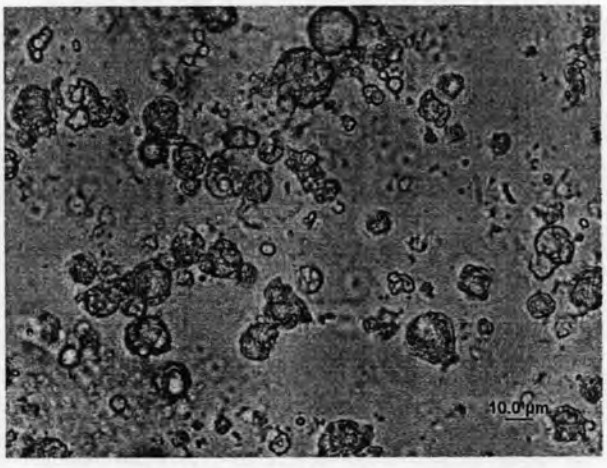

Figure 20 Optical micrograph of the spray-dried powders of lipid dispersion prepared by high speed homogenizer reconstituted in HBS at 37 °C. Magnification 400x. Scale bar = 10 μm.

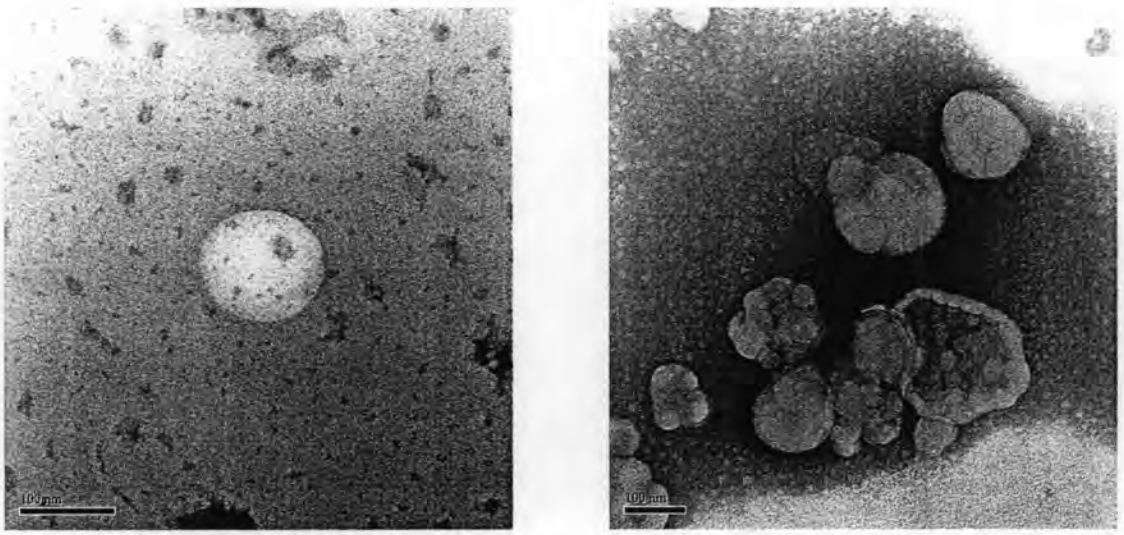

(a) (b)

Figure 21 Transmission electron micrographs of the liposomes composed of (a) HPC and (b) HPC/Chol (8:2) extruded through two-stacked 0.2 μm PC filters. Scale bar = 100 nm.

2. Preparation of Spray-dried Liposomal Powders

Carbohydrates including sucrose, trehalose, lactose and mannitol were evaluated as an additive in the preliminary study for preparing the liposomal powders by spray drying technique. There are many researches which can prepare spray-dried powders of proteins using sucrose, lactose or trehalose as an additive (Goldbach et al., 1993a, b; Lo et al., 2004). Because of very humid atmosphere of Thailand, however, sucrose, lactose and trehalose were not able to be prepared into dry powders by spray drying technique in this present study. This may be due to the production of essentially amorphous material which is typical of the spray-drying process (Chidavaenzi et al., 1997; Chidavaenzi, Buckton, and Koosha, 2001). Due to their high hygroscopic properties, some minutes after recovering the spray-dried pure sugars, they became sticky and handling was not easy. This result is consistent with earlier findings (Grenha, Seijo, and Remunan-Lopez, 2005). In addition, lactose which is reducing sugar can influence the stability of proteins and peptides (Dubost et al., 1996; Li et al.,

1996). The use of lactose with protein powders may lead to a reaction with lysine residues present in the protein, producing lactosylated protein molecules.

Mannitol is a non-reducing sugar and has non-hygroscopic property. It was able to be prepared into fine powders by spray drying technique. Moreover, mannitol is known for its non-toxic and degradable properties (Bosquillon et al., 2001). In addition, Steckel and Bolzen (2004) reported that mannitol was the best candidate for DPI formulations. Therefore, mannitol was considered appropriate to use as an additive for preparation of liposomal powders by spray drying technique in this study. Mannitol formed the backbone structure of the solid particles during the spray drying process and might help in pulmonary delivery of liposomes. The effects of various formulation variables (lipid/mannitol ratios and liposome compositions) were investigated on the physicochemical properties of the spray-dried liposomal powders and the reconstituted liposomes.

3. Chemical Stability of Phospholipids

From data obtained in Table 10 and Figure 22, the liposomal and spray drying processes had no statistically significant ($P > 0.05$) destructive effect on the chemical stability of the major structural phospholipid, both hydrolysis and oxidation, when compared to the HPC starting material (see ANOVA tables in Appendix II). This may be due to the mild condition of liposomal process by the one-step method and the short exposure to heat during spray drying process. This result is consistent with a previous study by Goldbach et al. (1993a). Thus, the spray drying condition at inlet temperature of 120 °C was feasible in producing HPC liposomal powders.

Table 10 Hydrolysis and oxidation stability of HPC in the starting material and various formulations (mean ± SD, n=4)

Formulation	Hydrolysis (%)	Oxidation index
HPC starting material	4.02 ± 0.13	0.179 ± 0.043
HPC liposomes	3.94 ± 0.07	0.140 ± 0.034
HPC/M 10:0	4.21 ± 0.17	0.184 ± 0.013
HPC/M 5:5	3.93 ± 0.12	0.147 ± 0.028

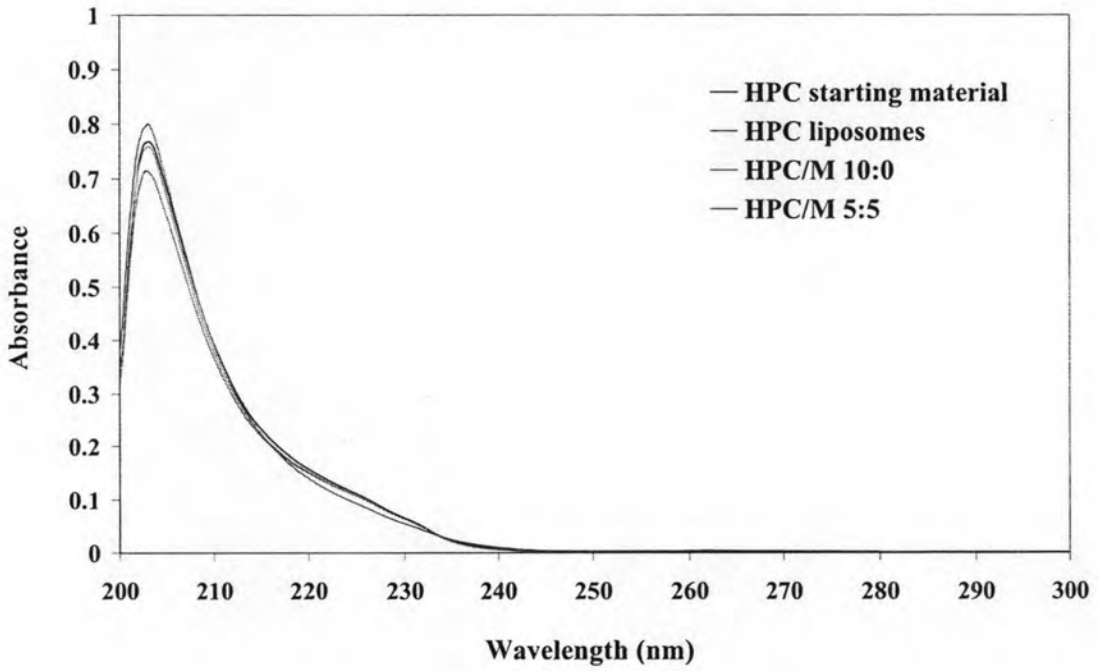

Figure 22 UV absorption spectra of HPC in the starting material and various formulations dissolved in absolute ethanol

4. Effect of HPC/Mannitol Weight Ratio on the Properties of Spray-Dried Liposomal Powders

The spray-dried powders were prepared with various HPC/M weight ratios without lysozyme. The properties of the spray-dried powders obtained are presented in Table 11. The spray-dried powders were recovered from the cyclone and the collector of the spray dryer with a total yield range between 54-74 % (Table 11). The spray-dried powders obtained from the only collector were further characterized. The loss of product was due to sticking on the drying chamber wall, the piping leading from the drying chamber to the cyclone and the loss of too fine particles which were not dissociated from the air by the cyclone separator. The spray-dried liposomal powders with only HPC stuck strongly to the cyclone separator wall of the spray dryer. Addition of mannitol decreased the amount of powders adhering to the cyclone wall of the spray dryer because of its non-hygroscopic property.

Table 11 Properties of the spray-dried powders with various HPC/M weight ratios

HPC/M weight ratio	Yield (%) in		Total yield (%)	Moisture content (%w/w)*	Particle size ($D_{0.5}$, μm (span))**	Physical appearance
	Collector	Cyclone				
10:0	2.92	61.74	64.66	6.68 ± 0.36	ND	aggregates
9:1	52.36	11.58	63.94	3.65 ± 0.17	ND	aggregates
7:3	34.24	20.00	54.24	3.73 ± 0.29	ND	aggregates
5:5	44.18	16.28	60.46	3.84 ± 0.23	7.76 (1.09)	fine powders
3:7	62.78	6.31	69.08	1.71 ± 0.12	8.45 (1.77)	fine powders
1:9	46.18	10.47	56.60	0.80 ± 0.03	6.59 (2.60)	fine powders
0:10	74.00	-	74.00	0.39 ± 0.04	0.66 (17.26)	fine powders

* mean ± SD, n = 3

** mean of $D_{0.5}$ (mean of span), n = 3; Measured by Mastersizer S

- denotes nil (not adhere the cyclone).

ND denotes not determined.

Owing to non-hygroscopic property of mannitol, the moisture content of the spray-dried liposomal powders decreased with increasing mannitol content except the formulations with HPC/M ratios of 9:1 to 5:5 which gave similar moisture content about 3.6-3.8 % (Figure 23). Mannitol was able to draw water from the liposomes in the terminal stages of drying and reduce the tendency of the particles to aggregate.

The particle size of the spray-dried powders was measured except the formulations with HPC content of 70-100 %w/w giving highly aggregate and fused powders (see SEM in Figure 24a-c). As shown in Table 11, there was no much difference among the particle sizes of the spray-dried formulations with the HPC/M ratios of 5:5 to 1:9 (see SEM in Figure 24d-f). The span value measures the width of the particle size distribution, and small span value indicates narrow particle size distribution (Chew and Chan, 2002). The spray-dried formulation with only mannitol gave the smallest particle size but high span value which may be due to agglomeration of particles by surface electrostatic forces. The particle agglomeration is a common problem in redispersion of micronized powders (< 5 μm) (Malcolmson and Embleton, 1998) (Figure 24g).

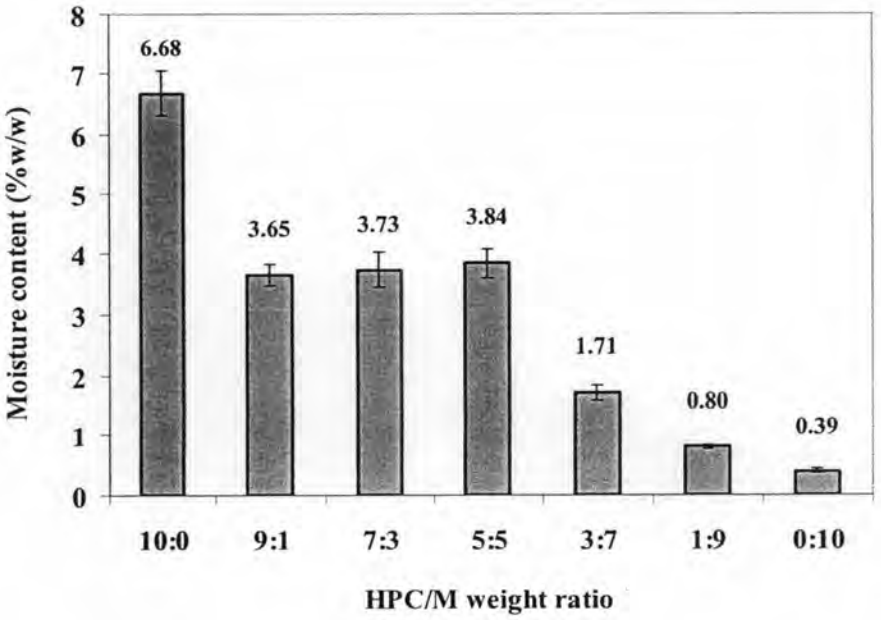

Figure 23 Histogram of moisture content of the spray-dried powders with various HPC/M weight ratios

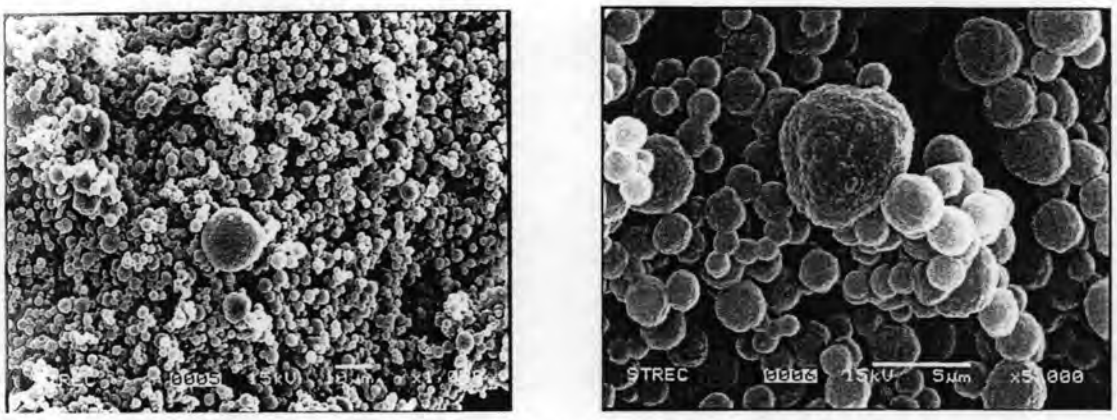

(a) HPC/M 10:0

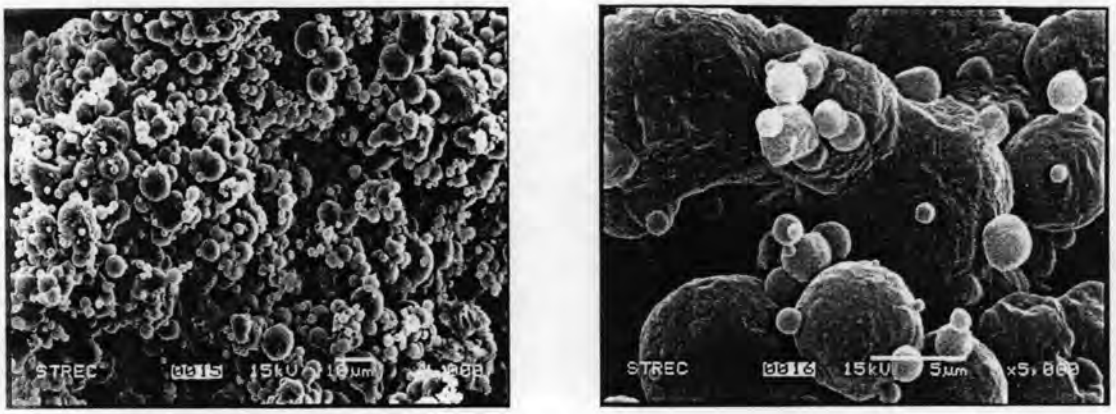

(b) HPC/M 9:1

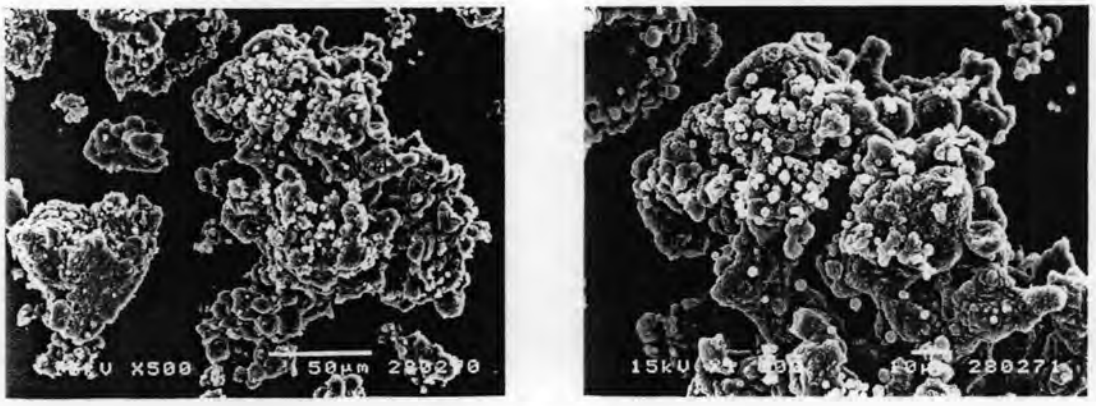

(c) HPC/M 7:3

Figure 24 Scanning electron micrographs of the spray-dried powders with different HPC/M weight ratios. On the left side: magnification 1000x and scale bar = 10 µm. On the right side: magnification 5000x and scale bar = 5 µm. Except the ratio of 7:3, on the left side: magnification 500x and scale bar = 50 µm and on the right side: magnification 1000x and scale bar = 10 µm.

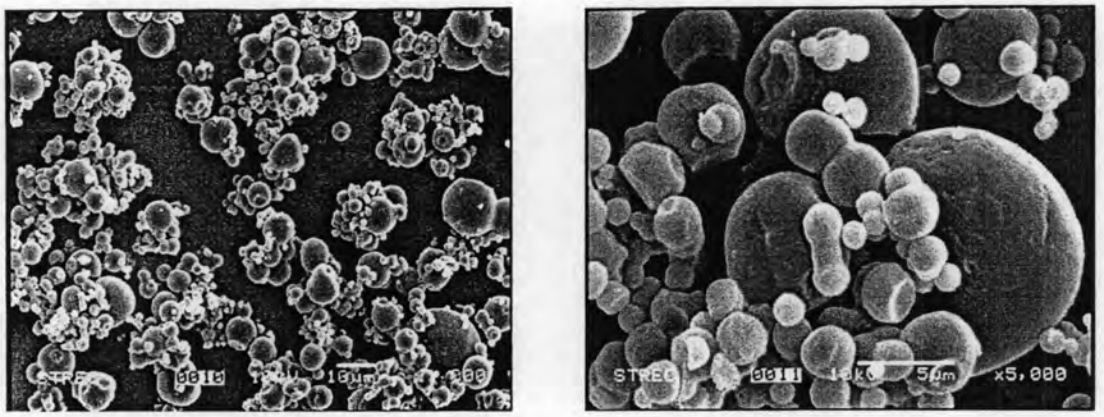

(d) HPC/M 5:5

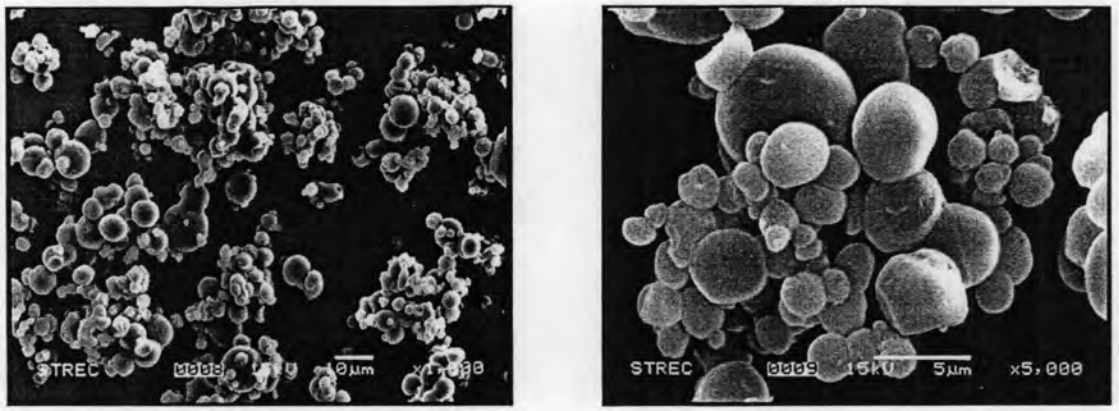

(e) HPC/M 3:7

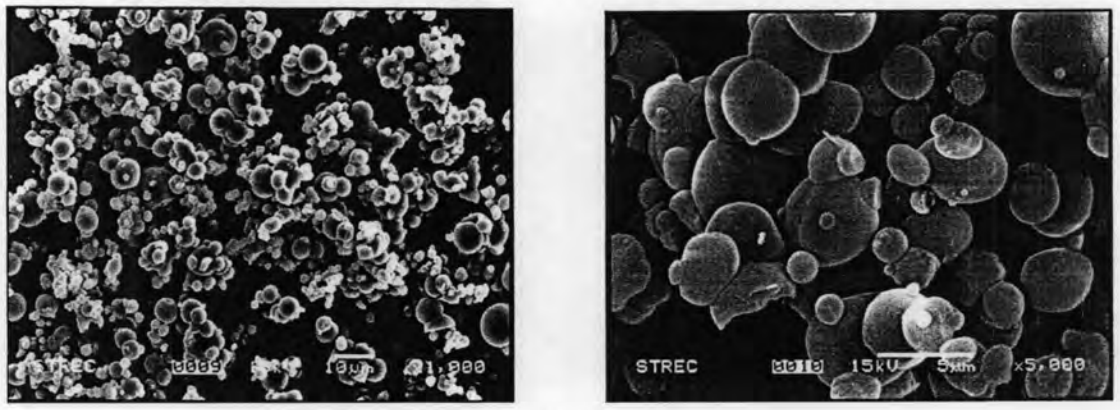

(f) HPC/M 1:9

Figure 24 (Continued)

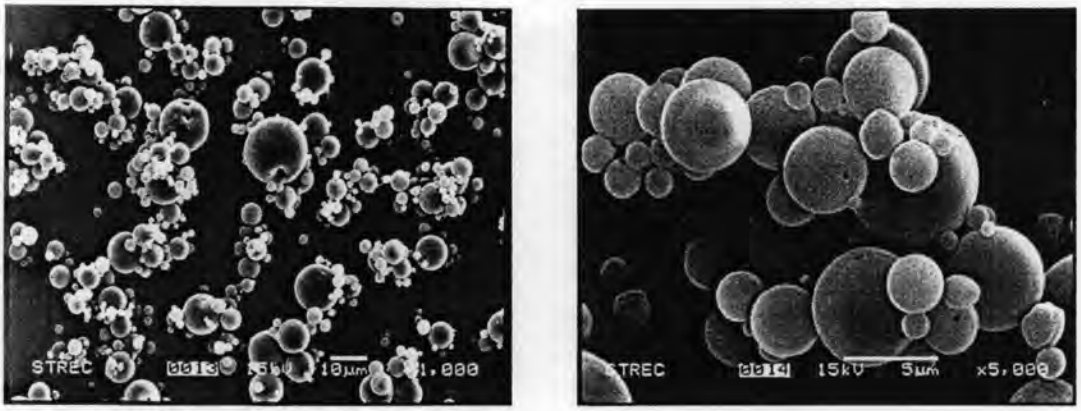

(g) HPC/M 0:10

Figure 24 (Continued)

SEM images in Figure 24 show that the spray-dried powders had wide size distribution and their morphology was dependent on the HPC/M ratios. The spray-dried liposomal powders without mannitol were large aggregates of a few microns spherical particles with irregular surface that appeared to be melted/annealed (Figure 24a). The small particle size of this formulation may be because of surfactant property of phospholipid which was reported to facilitate droplet formation in the atomization step of spray drying and decrease particle surface energy (Lo et al., 2004; Padhi, Chougule, and Misra, 2006). The formulation without mannitol was difficult to prepare fine powders by spray drying. This may be due to T_m value of lipid in the spray-dried form (84.56 °C, Figure 26 and Table 12) which was close to with the outlet temperature of this spray drying process (about 80 °C). Another reason may be because the spray-dried only HPC was partially amorphous, as shown by XRPD patterns in Figure 27, which resulted in highly sticky powders difficult to deaggregate and aerosolize (Weers et al., 2002).

The addition of mannitol resulted in an increase in particle size and a decrease in cohesion of particles. The spray-dried formulation with the HPC/M ratio of 9:1 gave strongly fused and aggregate spherical particles similar to that without mannitol but larger particle size (Figure 24b). At the ratio of 7:3, irregular mass was formed instead of spherical particles (Figure 24c). This result was consistent in both of the

two batches prepared. The formulations with HPC content less than or equal to 50 %w/w gave slightly aggregate spherical powders (Figure 24d-g). The surface of the spray-dried particles got smoother as the amount of mannitol increased. The spray-dried mannitol had a spherical shape with smooth surface.

Some mannitol particles had blowholes indicating an under- or over-pressure in the particles during drying (Elversson and Millqvist-Fureby, 2005). SEM image of some broken particles in Figure 25 indicates that some of the spray-dried powders with HPC/M 5:5 had hollow interior with dense shell. This result is consistent with a previous study by Grenha et al. (2005). Mannitol in the liposomal mixture did not have the time to diffuse towards the center of the droplet as it dried. Therefore, mannitol was trapped at the drying front leading to the earlier formation of a hollow shell. The earlier solidification of the shell during the drying process may explain an observed increase in particle size.

Figure 25 Scanning electron micrographs of the broken spray-dried powders with HPC/M ratio of 5:5. Magnification 8500x. Scale bar = 2 µm.

Characterization of thermal properties and X-ray powder diffraction of the spray-dried formulations is very important in determining the crystalline nature of the product and in discussion of the major physical transformations.

A comparison of DSC thermograms (Figure 26) and XRPD patterns (Figure 27) of the HPC starting material (Phospholipon® 90H) and the spray-dried HPC liposomal powders without mannitol revealed that HPC was transformed to partially amorphous form under the spray drying process used. The melting peak of the HPC starting material was detected at 122.50 °C while T_m of lipid in the spray-dried powders was at 84.56 °C corresponding to the melting of the aliphatic chains (Table 12). The T_m value of the liposomal powders was higher than that of the hydrated liposomes (about 52.83 °C, Table 14). The higher transition temperature agrees with the well established result that phospholipid melting temperature increases as hydration decreases (Grabielle-Madelmont and Perron, 1983). Removal of water results in reduction of the area occupied by each head group, with the important consequence that the packing density of the hydrocarbon chains increases, leading to increased opportunities for Van der Waal's interactions. As a result, the temperature at which the transition from gel to liquid crystalline phase occurs is increased (Crowe et al., 1988).

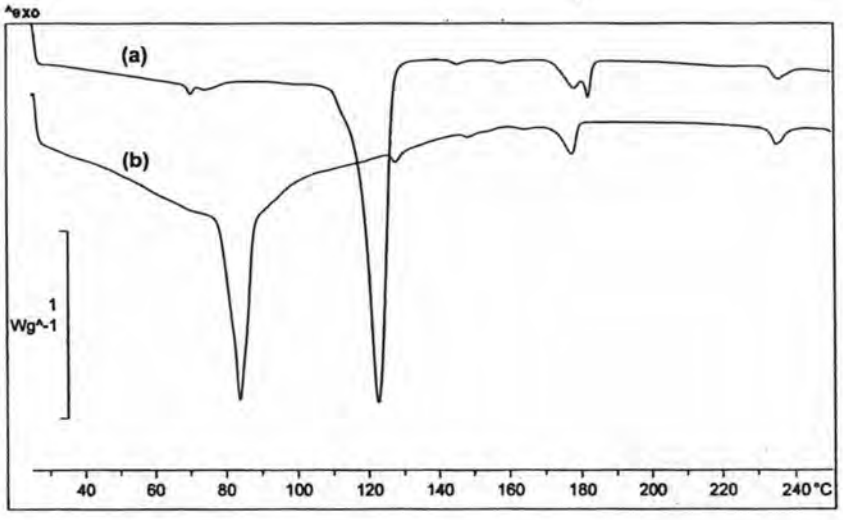

Figure 26 DSC spectra of (a) the HPC starting material and (b) the spray-dried HPC liposomal powders

The XRPD pattern of the spray-dried HPC only liposomal powders showed the main single peak at 2θ around 21° that was close to one of the major peaks of the initial crystalline Phospholipon® 90H (Figure 27).

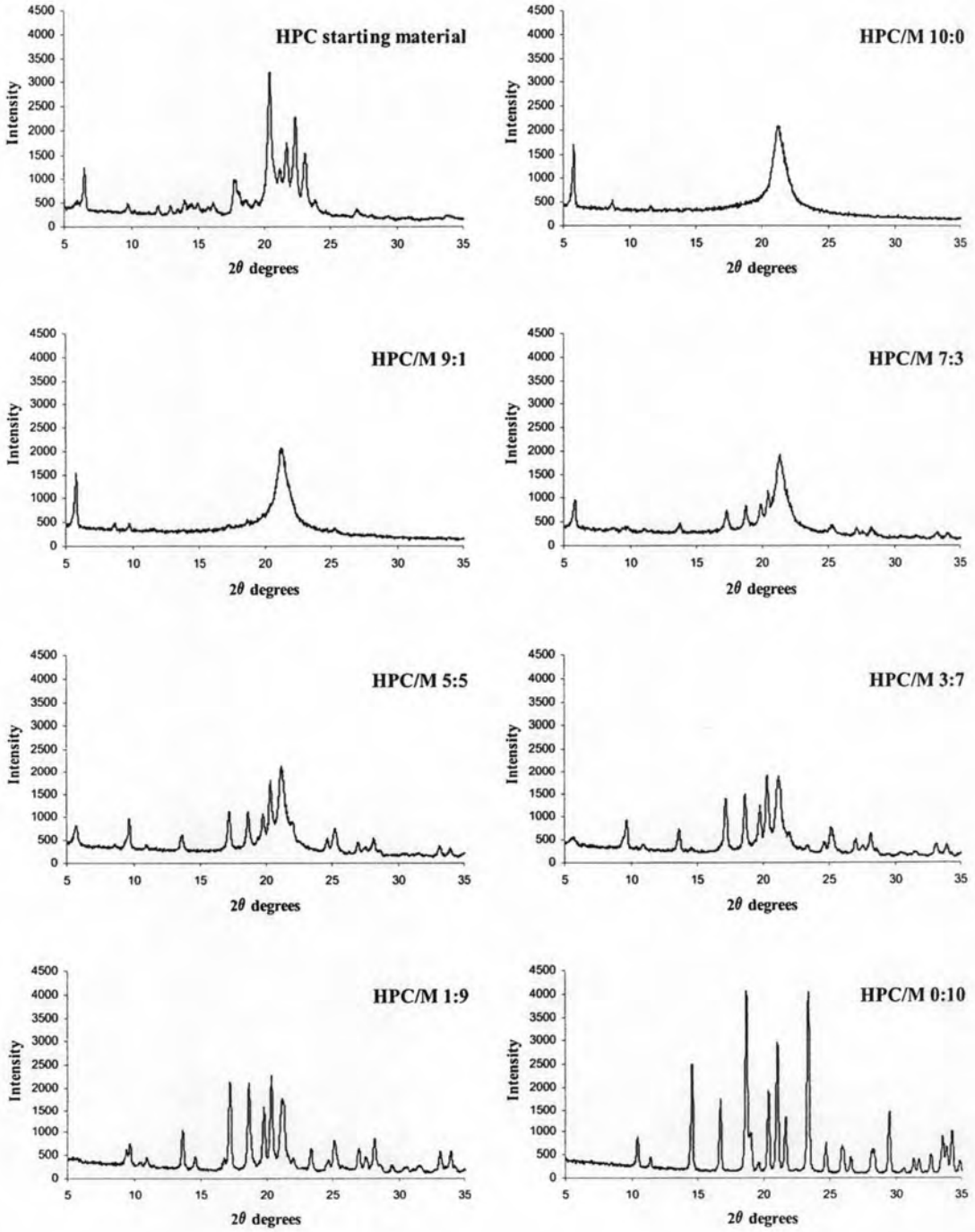

Figure 27 X-ray diffraction patterns of the HPC starting material and the spray-dried powders with various HPC/M weight ratios

DSC spectra and thermal properties of the spray-dried powders with various HPC/M weight ratios are shown in Figure 28 and Table 12. The T_m values of the lipid in the spray-dried liposomal powders decreased with increasing mannitol content up to the HPC/M ratio of 5:5. The lipid-mannitol interaction weakened the phospholipid interaction in the spray-dried powders, leading to lower phase transition temperature. This result is consistent with a previous study that sugars depress T_m in dry phospholipids to a temperature close to that of the hydrated phospholipid because of lipid-sugar interactions (Crowe et al., 1988; Hauser, 1993). Addition of mannitol in various ratios had no affect the melting peak of mannitol (around 166 °C, Table 12) in the spray-dried liposomal powders except the HPC/M ratio of 7:3 (152.52 °C). The different melting peak of mannitol in the formulation with HPC/M (7:3) might relate to its unusual morphology as shown in Figure 24c.

The XRPD patterns in Figure 27 show the effect of HPC/M ratio on the crystallinity of the spray-dried powders. The crystallinity of samples is characterized by the shape (intensity or height and width) of the peaks in X-ray diffractograms (Alves and Santana, 2004). The narrower the peaks, the more crystalline the structures. Wide or small peaks indicate the presence of amorphous domains in the structures. The XRPD pattern of the formulation with HPC/M 9:1 showed a single main peak (around 21°) similar to the formulation without mannitol which indicated the occurrence of identical amorphous form under the spray drying condition used. This result was not due to dilution effect because the XRPD pattern of the physical mixture of the spray-dried HPC and the spray-dried mannitol in the ratio of 9:1 revealed additional peak of the spray-dried mannitol (Figure 29). When the content of mannitol increased more than or equal to 30 %w/w, the intensity of the additional peaks, being characteristic of the spray-dried mannitol, was higher (Figure 27), meaning that the major component in the formulation was higher crystalline.

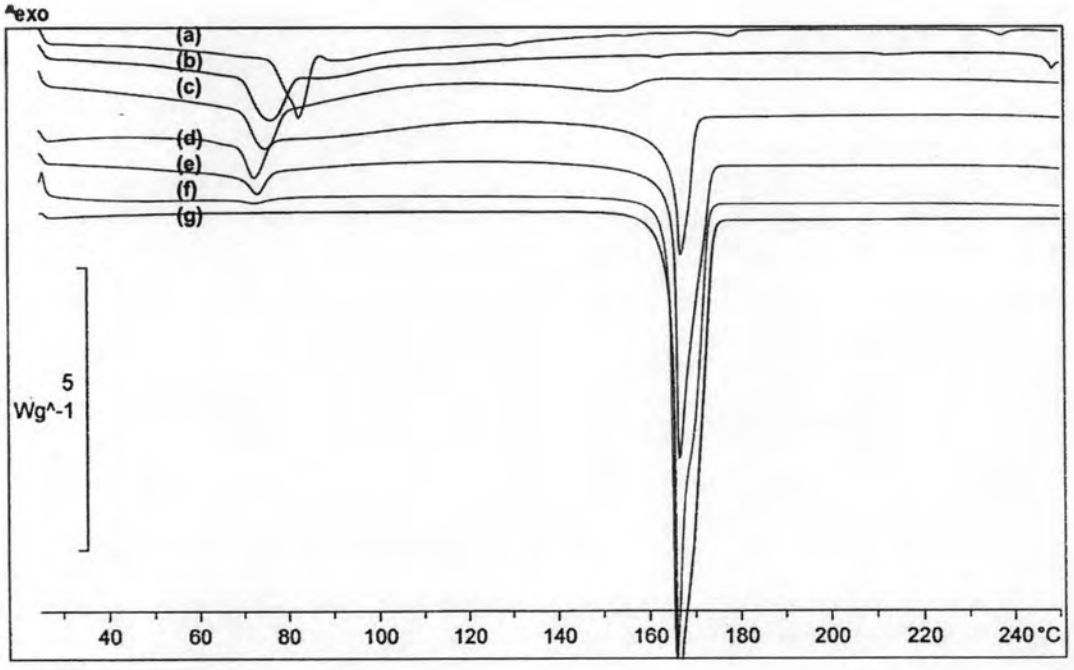

Figure 28 DSC spectra of the spray-dried powders with different HPC/M weight ratios. (a) 10:0; (b) 9:1; (c) 7:3; (d) 5:5; (e) 3:7; (f) 1:9; (g) 0:10.

Table 12 Thermal properties of the starting materials and the spray-dried powders with various HPC/M weight ratios (mean ± SD, n =3)

Formulation	T_m of lipid (°C)	MP of mannitol (°C)
HPC starting material	122.50 ± 0.72	-
Mannitol starting material	-	166.24 ± 0.44
HPC/M 10:0	84.56 ± 0.74	-
HPC/M 9:1	76.73 ± 0.81	162.27 ± 0.14
HPC/M 7:3	74.84 ± 0.18	152.52 ± 0.15
HPC/M 5:5	72.59 ± 0.68	167.03 ± 0.73
HPC/M 3:7	72.98 ± 0.28	166.36 ± 0.56
HPC/M 1:9	72.37 ± 0.35	166.13 ± 0.60
HPC/M 0:10	-	165.97 ± 0.45

- denotes nil.

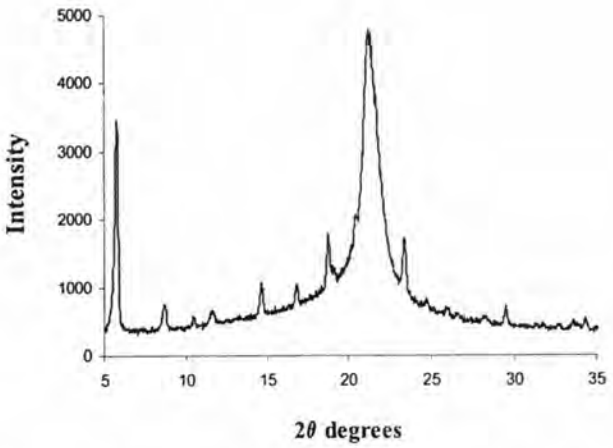

Figure 29 X-ray diffraction pattern of physical mixture of the spray-dried HPC and the spray-dried mannitol in weight ratio of 9:1

DSC thermograms of the spray-dried mannitol and the crystalline starting material both showed a sharp peak at 166 °C (Figure 28 and Table 12) corresponding to the melting of crystalline mannitol modifications I or II (Burger et al., 2000). This result agrees with a previous research by Naini, Byron, and Phillips (1998) in that spray-dried mannitol is crystalline modification I despite the high drying rate favors formation of an amorphous state as observed for lactose, sucrose and trehalose. Because of short average droplet drying times, spray drying is often believed to offer insufficient opportunity for nucleation and crystal growth. Nevertheless, there is clearly sufficient time to enable crystallization of mannitol, an additive known to crystallize readily in other circumstances (Korey and Schwartz, 1989). Mannitol crystallization depends on the formulation composition (Andya et al., 1999). The intensity of peak in the XRPD pattern of the spray-dried mannitol was lower than that of the starting material which indicated that the spray-dried mannitol prepared by this process was not 100 % crystalline (Figure 30).

The reconstitution of the spray-dried liposomal powders was performed using 10 mM HEPES and 140 mM NaCl, pH 7.4 (HBS) as medium. It is assumed that the airway surface liquid has a pH of approximately 7, close to that of the interstitial fluid and plasma (Kyle, Ward, and Widdicombe, 1990). In addition, HBS did not also have

any impact on the phospholipid assay by Bartlett method for entrapment study of lysozyme in liposomes.

Figure 31 and Table 13 show the optical photomicrographs and volume mean diameter of the reconstituted liposomes prepared from the spray-dried liposomal powders with various HPC/M weight ratios, respectively. These images indicated that the spray drying process led to aggregation and/or fusion of liposomes after reconstitution of the HPC liposomal powders with and without mannitol. This result was observed by the increased sizes of the reconstituted liposomes when compared to those of the initial liposomes before spray drying. An increase in the size of the reconstituted liposomes could be mainly attributed to thermal stress-induced lysis of lipid bilayer that may have occurred during the spray drying process. Another cause was aggregation and/or fusion of liposomes. Aggregation and/or fusion of liposomes are a mechanism to dissipate the excess surface energy originating from the distorted molecular packing to attain a state of greater stability (Lentz et al., 1985). From Table 13, there was no significant difference among the volume mean diameter of the reconstituted liposomes from the spray-dried liposomal powders with various HPC/M ratios except the formulations with only HPC and the ratio of 7:3. The formulation with HPC/M 7:3 was not able to form liposomes after reconstitution corresponding to

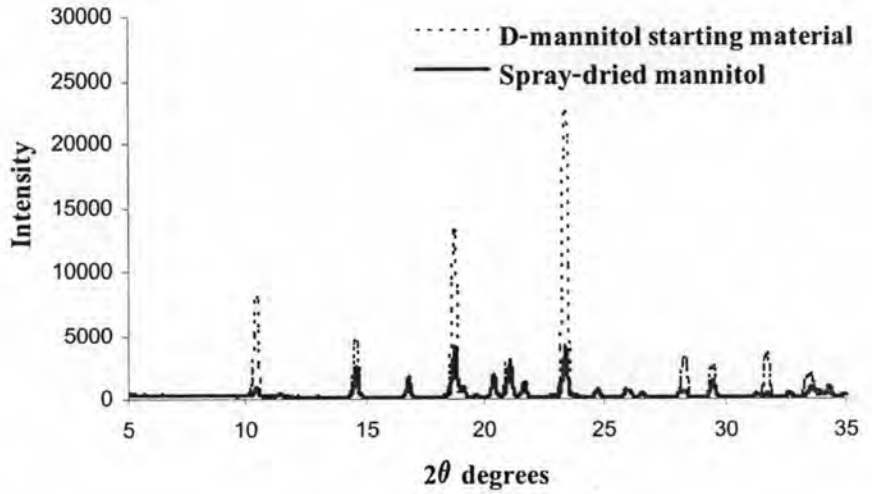

Figure 30 X-ray diffraction patterns of D-mannitol starting material and the spray-dried mannitol

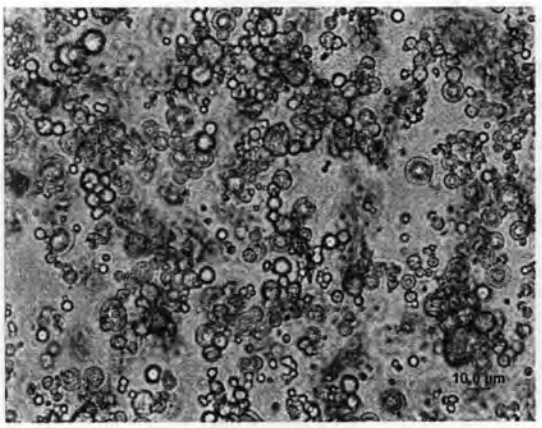

(a) 10:0

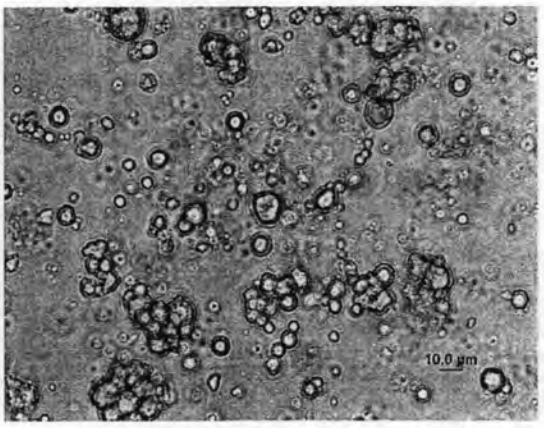

(b) 9:1

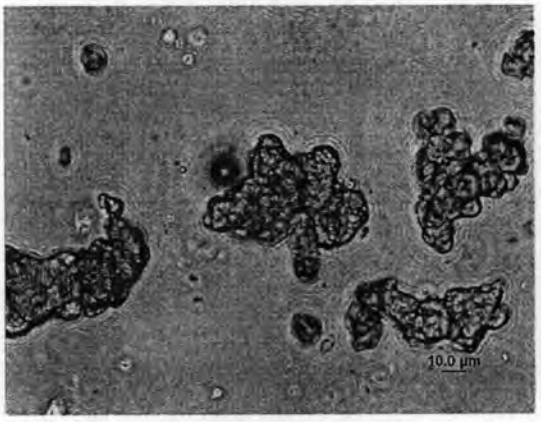

(c) 7:3

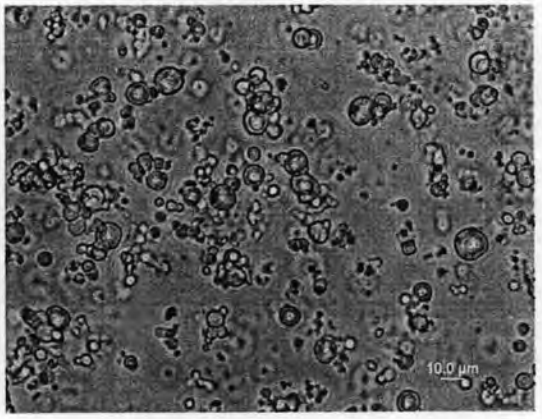

(d) 5:5

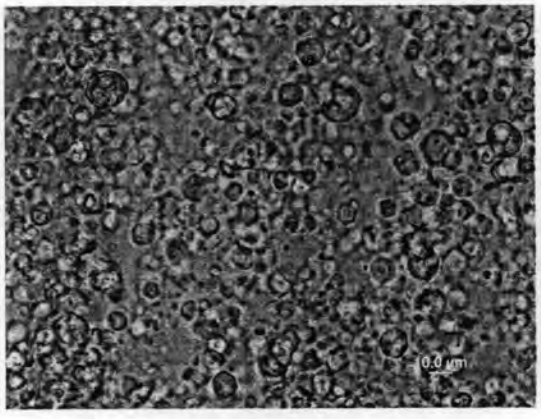

(e) 3:7

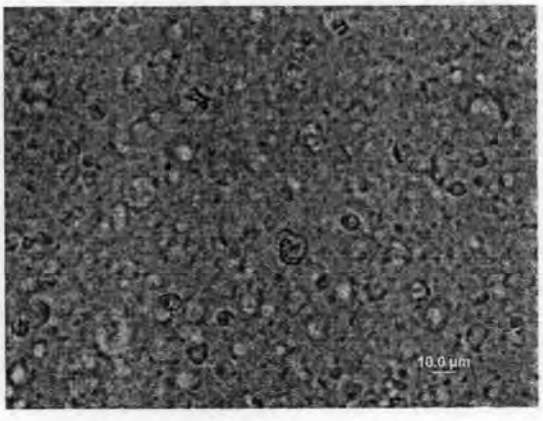

(f) 1:9

Figure 31 Optical micrographs of the reconstituted liposomes from the spray-dried liposomal powders with different HPC/M weight ratios: (a) 10:0; (b) 9:1; (c) 7:3; (d) 5:5; (e) 3:7; and (f) 1:9 in HBS at 37 °C. Magnification 400x. Scale bar = 10 µm.

Table 13 Volume mean diameter of the reconstituted liposomes from the spray-dried liposomal powders with various HPC/M ratios in HBS at 37 °C (mean ± SD, n = 3)

HPC/M weight ratio	$D_{[4,3]}$ (μm)*	Span
10:0	6.19 ± 0.05	1.45 ± 0.01
9:1	9.38 ± 0.03	1.87 ± 0.01
7:3	23.08 ± 0.16	1.76 ± 0.01
5:5	9.95 ± 0.02	1.52 ± 0.00
3:7	9.93 ± 0.02	0.99 ± 0.00
1:9	8.17 ± 0.18	1.05 ± 0.12

* Measured by Mastersizer 2000

the morphology of the spray-dried powders. Overall results indicated that the formulation with mannitol gave larger sizes of the reconstituted liposomes than the HPC only formulation (Table 13). This may be because mannitol can readily dissolve in water. Dissolution of mannitol might reduce free water for rehydration of liposomes leading to an increase in fusion of HPC liposomes after reconstitution. The size characterization of the reconstituted liposomes using laser diffraction technique (Table 13) indicated that addition of mannitol in various ratios did not have an effect on the size of the reconstituted liposomes. Therefore, mannitol was not effective in preserving the HPC liposome integrity during spray drying process. Mannitol is a monosaccharide alcohol that easily crystallizes and has the tendency of phase separation of the lyophilized cake which is deleterious to the stability of dry liposomes (Lu and Hickey, 2005). A similar mechanism might also operate in spray drying of liposomes as well.

The DSC thermograms (Figure 32) of the initial HPC liposomes and the reconstituted liposomes showed the typical pretransition of phospholipid in liposomes. The pretransition corresponds to the conversion of the lamellar gel phase L_β into the ripple gel phase P_β'. The main transition relates to the passage from the P_β' phase to the lamellar liquid-crystalline phase L_α (Torchillin and Weissig, 2003).

There was not difference between the thermal property (Table 14) of the reconstituted liposomes from the spray-dried liposomal powders without (Figure 32b) and with mannitol (Figure 32c). Mannitol did not affect the organization of the rehydrated HPC liposomes. However, the pretransition peak temperature of both spray-dried formulations increased slightly from 46.14 °C to 47.73 °C and the transition enthalpy increased from 1.86 to 4.66 J/g when compared to those of the initial liposomes. The increasing of the peak temperature and the transition enthalpy indicated an increase in the phospholipid molecular packing in the bilayer of the reconstituted liposomes when compared to the initial liposomes extruded through 0.2 μm PC filters. The effect was more pronounced with pretransition phase which indicated more tightly packed hydrocarbon chains (Torchilin and Weissig, 2003). In general, large liposomes have lesser surface curvature of lipid bilayer than small liposomes (Huang and Mason, 1978). Liposomal curvature had influence on the molecular packing of the phospholipid molecules in a bilayer. However, the adverse effect of curvature on molecular packing is usually more significant in small unilamellar vesicles which might not be the case here.

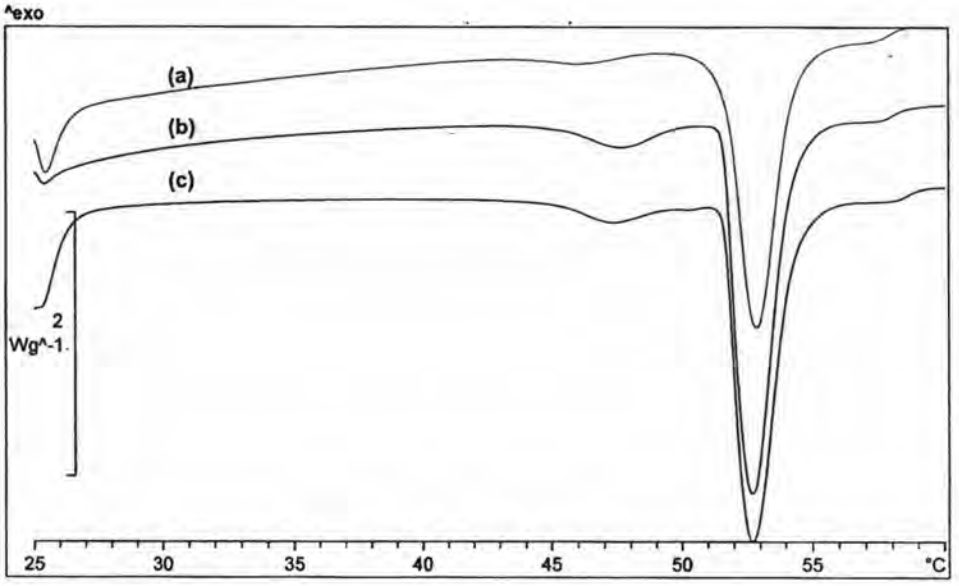

Figure 32 DSC spectra of (a) the initial HPC liposomes, and the reconstituted liposomes from the spray-dried liposomal powders composed of (b) only HPC and (c) HPC/M (5:5)

Table 14 Thermal properties of the initial HPC liposomes and the reconstituted liposomes from the spray-dried liposomal powders without and with mannitol (mean ± SD, n=3)

Formulations	Pre-transition		Main transition	
	Peak temp. (°C)	Enthalpy (ΔH, J/g)	Peak temp. (°C)	Enthalpy (ΔH, J/g)
HPC liposomes	46.14 ± 0.05	1.86 ± 0.02	52.83 ± 0.05	46.07 ± 0.51
HPC/M 10:0	47.73 ± 0.05	4.66 ± 0.42	52.99 ± 0.18	51.12 ± 2.86
HPC/M 5:5	47.27 ± 0.10	4.67 ± 0.93	52.78 ± 0.08	51.90 ± 1.20

5. Effect of Glycine on the Properties of Spray-Dried Liposomal Powders

Glycine is one of polar and uncharged amino acids. Glycine is used as an bulking agent and an anti-adherent to prevent tendency of the particles to bond strongly, and results in light particles with good flow behavior, deaggregation properties and dose reproducibility of dry powder inhalers (Chougule et al., 2006). Table 15 shows the effect of glycine amount based on the total weight of lipid and mannitol on the properties of the spray-dried HPC liposomal powders. The addition of glycine decreased the amount of powders adhering to the cyclone of spray dryer because of its anti-adherent property but did not affect total process yield except the formulation with 10 %w/w glycine. High glycine content (10 %w/w) gave low process yield of the spray-dried liposomal powders which may be due to very fusion of the powders (Figure 33d) and a large amount of powders sticking on the drying chamber wall.

Table 15 Properties of the spray-dried liposomal powders with HPC/M (5:5) and various glycine concentrations (%w/w of total lipid and mannitol)

Glycine concentrations (%w/w)	Yield (%) in		Total yield (%)	Moisture content (%) (mean ± SD)	Physical appearances
	Collector	Cyclone			
0	46.08	26.15	72.23	3.84 ± 0.23	fine powders
0.5	65.97	10.15	76.12	3.44 ± 0.29	fine powders
1	75.60	-	75.60	3.26 ± 0.35	fine powders
5	72.86	2.17	75.03	3.24 ± 0.14	aggregates
10	43.88	4.82	48.70	2.80 ± 0.03	aggregates

- denotes nil (not adhere the cyclone).

The addition of glycine in high amount resulted in a smaller particle size of the spray-dried liposomal powders but more fused (Figure 33c-d). The increase in fusion of particles may be due to incomplete drying of spray droplets and consequent droplet coalescence during drying process. If this was the case, increasing inlet temperature should decrease fusion of the spray-dried liposomal particles with high glycine amount which requires further investigation. Alternatively, presence of more than one solute in the mixture might cause an alteration in crystallization behavior of these solutes during spray drying process. Further study is still required to support this hypothesis.

After reconstitution of the spray-dried powders with HBS, the liposomes were formed in the size range between 9-11 μm (Table 16) independent of the glycine amount except the formulation with 10 %w/w glycine giving more fused liposomal powders difficult to rehydrate (Figure 34).

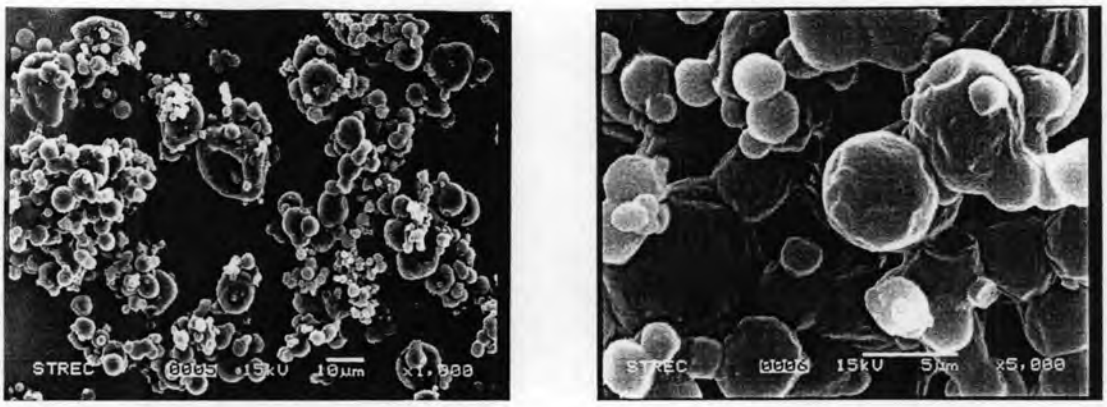

(a) glycine 0.5%

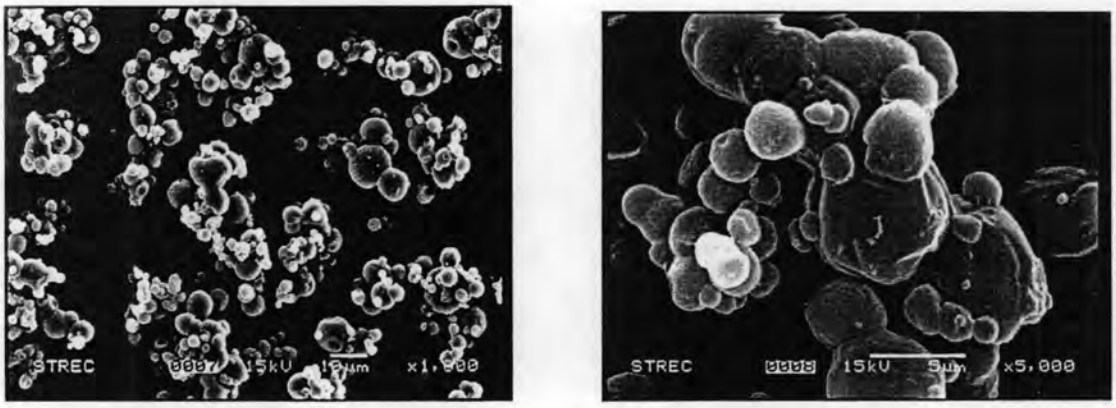

(b) glycine 1%

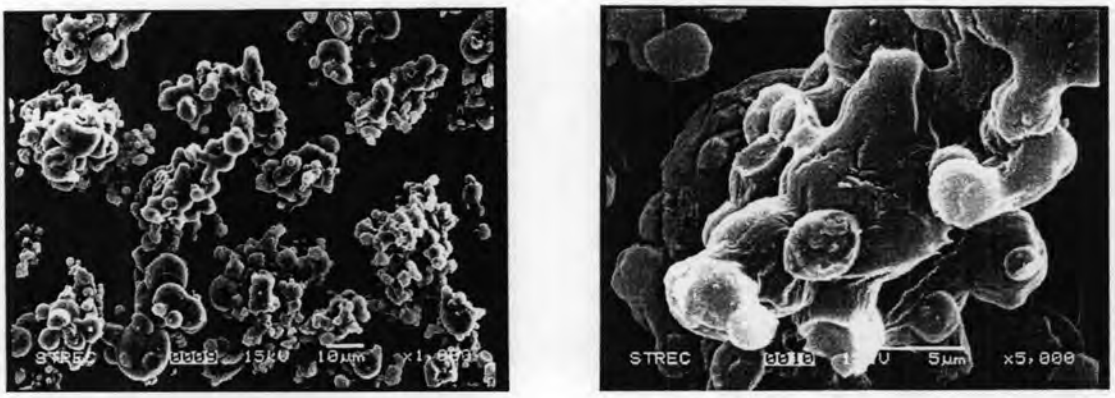

(c) glycine 5%

Figure 33 Scanning electron micrographs of the spray-dried liposomal powders with HPC/M (5:5) and various glycine concentrations (%w/w of total lipid and mannitol). On the left side: magnification 1000x and scale bar = 10 µm (except (d) glycine 10%: magnification 500x and scale bar = 50 µm). On the right side: magnification 5000x and scale bar = 5 µm.

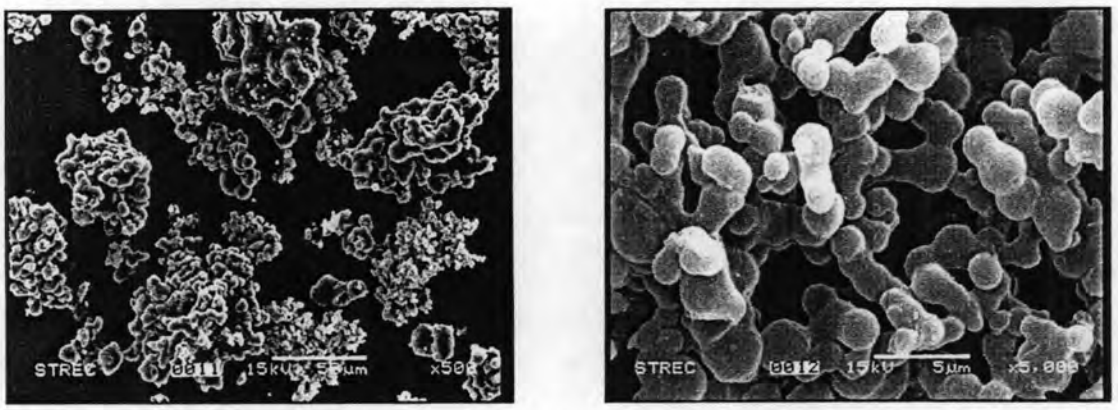

(d) glycine 10%

Figure 33 (Continued)

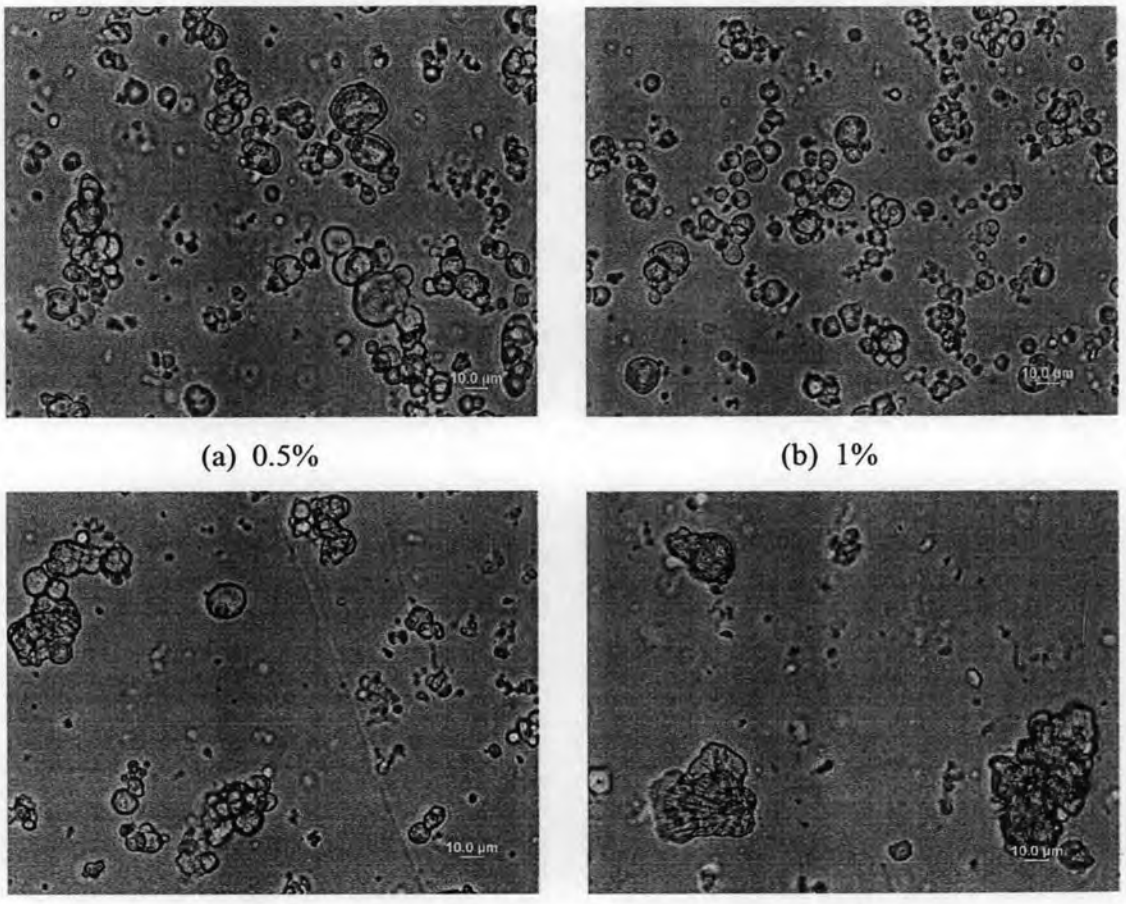

(a) 0.5% (b) 1%

(c) 5% (d) 10%

Figure 34 Optical micrographs of the reconstituted liposomes from the spray-dried liposomal powders with HPC/M (5:5) and various glycine concentrations in HBS at 37 °C. Magnification 400x. Scale bar = 10 µm.

Table 16 Volume mean diameter of the reconstituted liposomes from the spray-dried liposomal powders with HPC/M (5:5) and various glycine concentrations in HBS at 37 °C (mean ± SD, n = 3)

Glycine concentrations (%w/w)	$D_{[4,3]}$ (μm)*	Span
0	9.95 ± 0.02	1.52 ± 0.00
0.5	11.13 ± 0.02	1.49 ± 0.00
1	9.33 ± 0.03	1.17 ± 0.00
5	11.20 ± 0.02	1.64 ± 0.00
10	17.20 ± 0.04	1.97 ± 0.00

* Measured by Mastersizer 2000

DSC thermograms and thermal properties of the spray-dried liposomal powders with various glycine concentrations are shown in Figure 35 and Table 17. Addition of glycine had no effect on the T_m of lipid in the spray-dried liposomal powders. However, the melting peak temperature of mannitol decreased from 167.03 °C to 156.33 °C with increasing glycine content from 0 to 10 %w/w. The mechanism underlying effect of glycine on the melting peak of mannitol in the spray-dried liposomal powders requires further study. However, when mannitol was used in combination with glycine in freeze-dried formulations, each solute influenced the extent of crystallization of the other (Pyne, Chatterjee, and Suryanarayanan, 2003). Pikal et al. (1991) reported that glycine could prevent conversion of amorphous form of mannitol to crystalline one during freeze drying and upon storage. Nevertheless, changes in crystallinity of the powders with glycine amounts of 0.5-10 %w/w were not clearly seen as observed by XRPD in this present study (Figure 36). However, additional peaks at around 18° and 23.7° were evident and increased with glycine content (Figure 36). The peaks at 23.7° may indicate more crystallinity of mannitol.

Because glycine could interfere the determination of lysozyme content by QPBCA assay kit and might affect the entrapment of lysozyme in the reconstituted liposomes, it was not used for the study in the next Section.

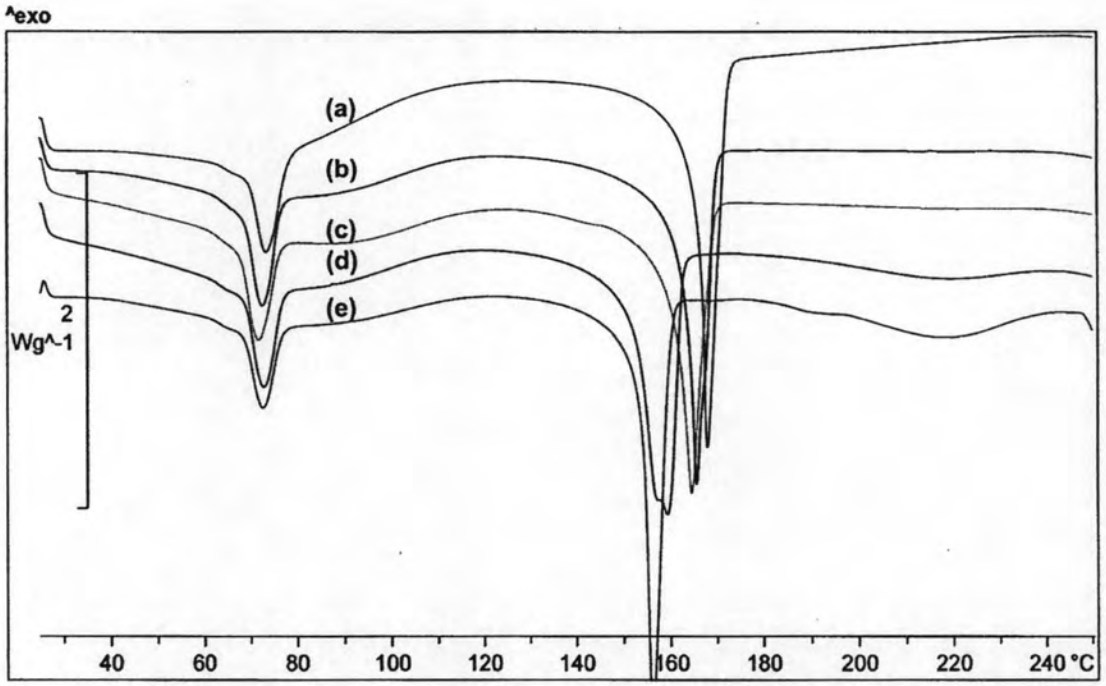

Figure 35 DSC spectra of the spray-dried liposomal powders with various glycine concentrations: (a) 0%; (b) 0.5%; (c) 1%; (d) 5%; (e) 10%

Table 17 Thermal properties of the spray-dried liposomal powders with HPC/M (5:5) and various glycine concentrations (mean ± SD, n = 3)

Glycine concentrations (%w/w)	T_m of lipid (°C)	MP of mannitol (°C)
0	72.59 ± 0.68	167.03 ± 0.73
0.5	72.46 ± 0.15	165.52 ± 0.32
1	72.25 ± 0.54	164.74 ± 0.59
5	72.65 ± 0.33	159.02 ± 0.36
10	72.67 ± 0.16	156.33 ± 0.56

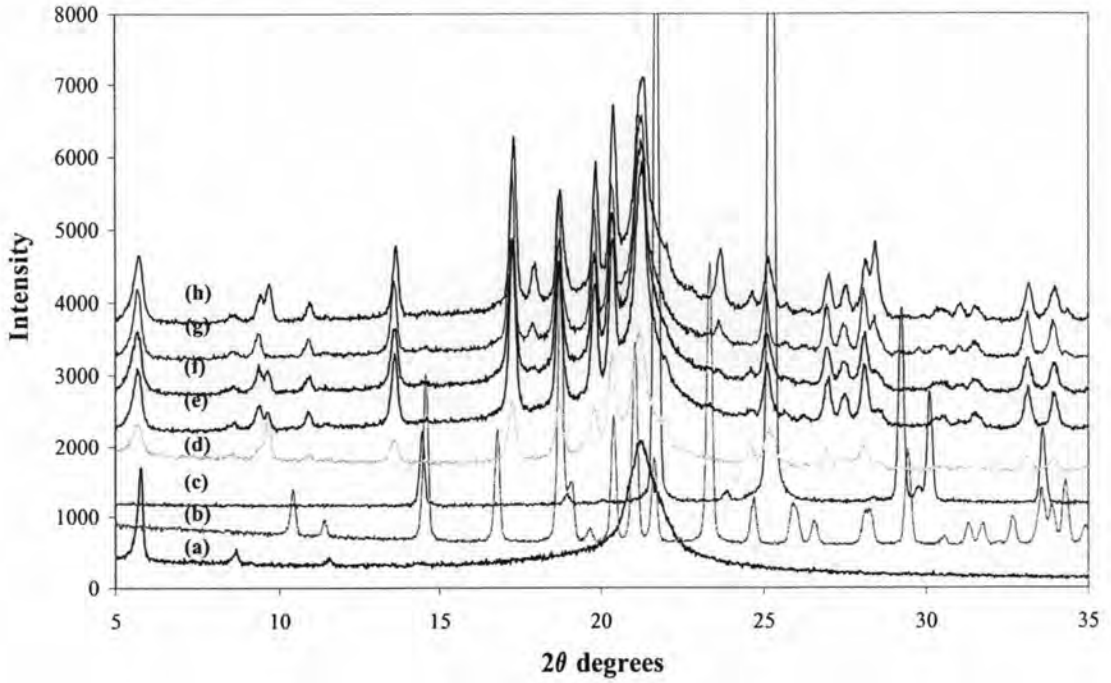

Figure 36 X-ray diffraction patterns of (a) HPC/M 10:0; (b) HPC/M 0:10; (c) the spray-dried glycine; and HPC/M 5:5 with various glycine concentrations: (d) 0 %; (e) 0.5 %; (f) 1 %; (g) 5 %; (h) 10 %

6. Analysis of Phospholipid and Lysozyme

6.1 Quantification of Phospholipids by the Bartlett Assay

Phospholipid content of the liposome dispersion could be determined by Bartlett assay. A standard curve for phospholipid assay was plotted between the net absorbance at 800 nm and the concentrations of phosphate in μmol/mL, and then was fitted using linear regression analysis. Table 18 and Figure 37 show calibration curve data of phosphate standard solutions at various concentrations. A straight line was obtained with a coefficient of determination (R^2) of 0.9997. The regression equation of this line is

$$y = 0.0003 + 2.4422x \quad (14)$$

where y is the net absorbance at 800 nm and x is the concentration of phosphate solution in μmol/mL.

Table 18 Calibration curve data of phosphate standard solutions by the Bartlett assay

Concentration of phosphate (μmol/mL)	Absorbance at 800 nm	Net absorbance at 800 nm
0	0.2740	0.0000
0.0641	0.4283	0.1543
0.0962	0.5126	0.2386
0.1283	0.5858	0.3118
0.1604	0.6670	0.3930
0.1924	0.7491	0.4751
0.2245	0.8180	0.5440

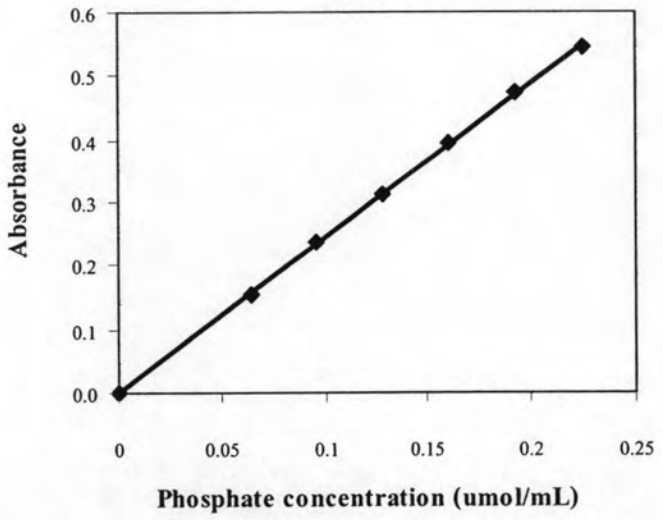

Figure 37 Calibration curve of phosphate standard solutions by the Bartlett assay (R^2 = 0.9997)

6.2 Quantitative Assay of Lysozyme by QuantiPro BCA Assay Kit

The amount of lysozyme could be determined using QPBCA assay kit. The measurement filter of a microplate reader used to analyze lysozyme in this study was 550 nm since it gave the maximum absorbance value. Figure 38 shows the spectra of lysozyme standard solutions in Ultrapure® water at various concentrations. A standard curve was plotted between the net absorbance at measurement filter of 550 nm and its concentrations, and was fitted using linear regression analysis. The results are shown in Table 19 and Figure 39. A straight line was obtained with a coefficient of determination (R^2) of 0.9992. The regression equation of this line is

$$y = -0.0001 + 0.0273x \quad (15)$$

where y is the net absorbance of lysozyme in Ultrapure® water at measurement filter of 550 nm and x is the concentration of lysozyme solution in μg/mL. This equation was then used to calculate the amount of lysozyme in the spray-dried lysozyme.

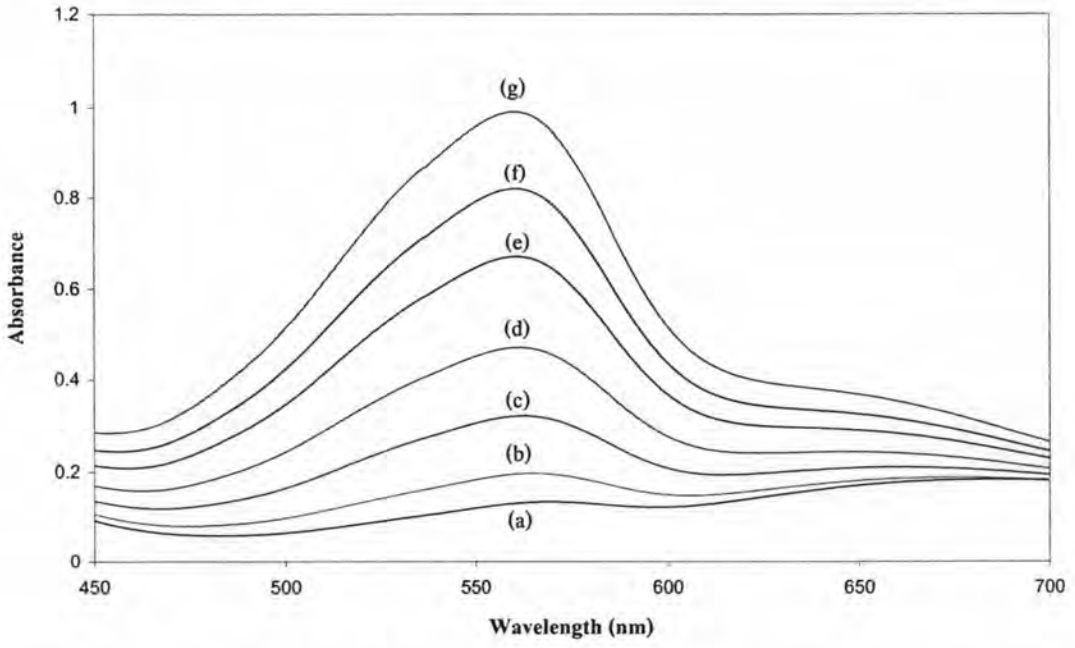

Figure 38 Spectra of standard solutions of lysozyme in Ultrapure® water at the concentrations of 0 (a), 2 (b), 5 (c), 10 (d), 15 (e), 20 (f), and 25 (g) μg/mL

Table 19 Calibration curve data of lysozyme in Ultrapure® water assayed by QPBCA method using a microplate reader

Concentration (μg/mL)	Absorbance at 550 nm	Net absorbance at 550 nm
0	0.163	0.000
2	0.210	0.046
5	0.298	0.134
10	0.446	0.282
15	0.582	0.419
20	0.708	0.544
25	0.839	0.675

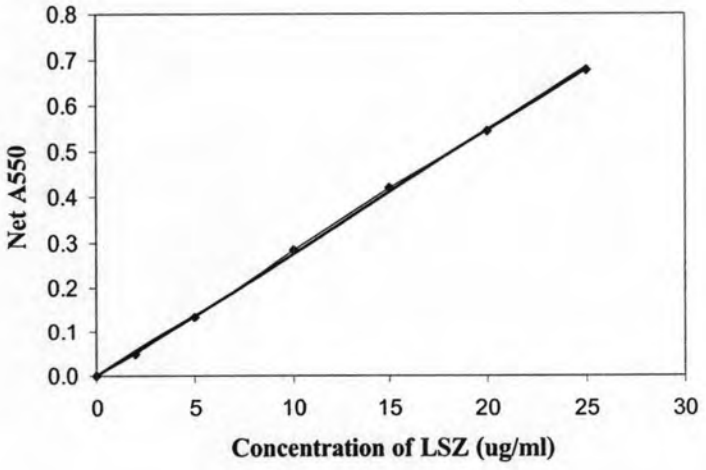

Figure 39 Calibration curve of lysozyme in Ultrapure® water assayed by QPBCA method using a microplate reader ($R^2 = 0.9992$)

For analysis of lysozyme in liposomal dispersion, liposomes were treated with Triton X-100 to disrupt liposomal bilayer. HBS, lipid and Triton X-100 affected lysozyme analysis by QPBCA assay. These effects were compensated by performing blank and lysozyme standards in the solution with equivalent amount of blank lipid and Triton X-100. Mannitol had no effect on QPBCA assay. The validation of the

QPBCA assay performed in HBS with 0.05 % HPC/Chol (8:2) and 2 % Triton X-100 is presented as follows:

6.2.1 Linearity

The spectra and the calibration curve data of lysozyme standard solutions in HBS with 0.05 % HPC/Chol (8:2) and 2 % Triton X-100 are shown in Figure 40 and Table 20, respectively. The calibration curve is presented in Figure 41 and gives a straight line with a coefficient of determination (R^2) of 0.9996. The regression equation of this line is

$$y = -0.0046 + 0.027x \quad (16)$$

where y is the net absorbance of lysozyme in HBS with 0.05 % HPC/Chol (8:2) and 2 % Triton X-100 at measurement filter of 550 nm and x is the concentration of lysozyme solution in μg/mL.

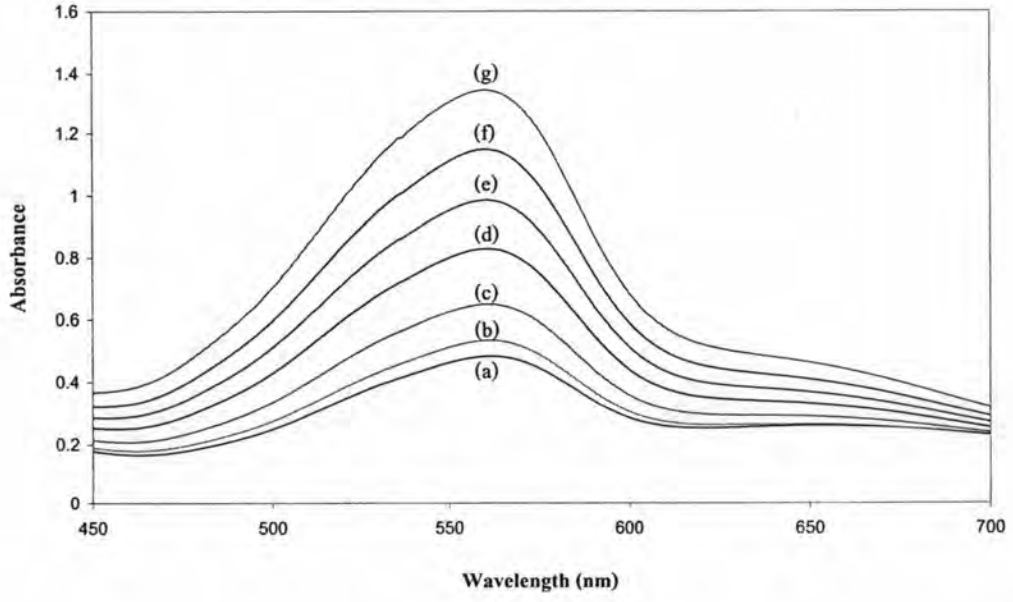

Figure 40 Spectra of standard solutions of lysozyme in HBS containing 0.05 % HPC/Chol (8:2) and 2 % Triton X-100 at the concentrations of 0 (a), 2 (b), 5 (c), 10 (d), 15 (e), 20 (f), and 25 (g) μg/mL

Table 20 Calibration curve data of lysozyme in HBS containing 0.05 % HPC/Chol (8:2) and 2 % Triton X-100 assayed by QPBCA method using a microplate reader

Concentration (μg/mL)	Absorbance at 550 nm	Net absorbance at 550 nm
0	0.427	0.000
2	0.470	0.043
5	0.552	0.125
10	0.699	0.272
15	0.830	0.403
20	0.964	0.537
25	1.093	0.666

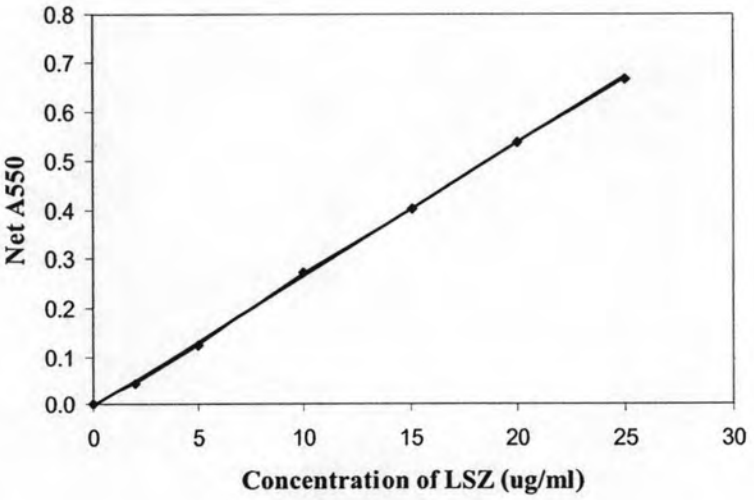

Figure 41 Calibration curve of lysozyme in HBS containing 0.05 % HPC/Chol (8:2) and 2 % Triton X-100 assayed by QPBCA method using a microplate reader (R^2 = 0.9996)

6.2.2 Accuracy

The accuracy data is presented in Table 21. The mean value of % recovery was 100.12 % and was within 15 % of the actual value of each determination. This indicated that the QPBCA method could be used to accurately determine lysozyme content within concentration range studied.

Table 21 Data of accuracy of lysozyme in HBS containing 0.05 % HPC/Chol (8:2) and 2 % Triton X-100 assayed by QPBCA method using a microplate reader

LSZ conc. (μg/mL)	**Fitted conc. (μg/mL)**	**% Recovery**
5.00	5.10	102.05
5.00	4.92	98.38
5.00	5.16	103.22
5.00	5.22	104.43
5.00	5.26	105.15
15.00	15.14	100.90
15.00	14.90	99.36
15.00	14.65	97.67
15.00	15.53	103.56
15.00	14.74	98.23
25.00	24.96	99.86
25.00	24.08	96.32
25.00	23.73	94.91
25.00	25.40	101.60
25.00	24.04	96.17
	Mean	**100.12**
	SD	**3.19**
	% CV	**3.18**

6.2.3 Precision

Tables 22 and 23 show data of within-run precision and between-run precision of lysozyme assayed by the QPBCA method, respectively. The % CV values of the fitted concentrations at each concentration level of both precisions did not exceed 15 %. This indicated that the QPBCA method could be used to determine the amount of lysozyme over a period of time studied.

Table 22 Data of within-run precision of lysozyme in HBS containing 0.05 % HPC/Chol (8:2) and 2 % Triton X-100 assayed by QPBCA method using a microplate reader

LSZ concentration (μg/mL)	Fitted conc. (μg/mL)							
	set 1	set 2	set 3	set 4	set 5	Mean	SD	% CV
5.00	5.10	4.92	5.16	5.22	5.26	5.13	0.13	2.60
15.00	15.14	14.90	14.65	15.53	14.74	14.99	0.36	2.37
25.00	24.96	24.08	23.73	25.40	24.04	24.44	0.70	2.88

Table 23 Data of between-run precision of lysozyme in HBS containing 0.05 % HPC/Chol (8:2) and 2 % Triton X-100 assayed by QPBCA method using a microplate reader

LSZ concentration (μg/mL)	Fitted conc. (μg/mL)							
	day 1	day 2	day 3	day 4	day 5	Mean	SD	% CV
5.00	5.10	4.80	5.04	4.92	5.42	5.06	0.23	4.61
15.00	15.14	15.04	14.95	15.23	14.69	15.01	0.21	1.38
25.00	24.96	25.09	24.81	25.15	24.46	24.90	0.28	1.12

In conclusion, there were linearity, accuracy, and precision in the assay of lysozyme by the QPBCA method. Therefore, the QPBCA assay could be used to determine the amount of lysozyme in liposomes.

6.3 Biological Activity Assay of Lysozyme

Stability of lysozyme after liposomal and spray drying process was evaluated by biological activity assay. Validation of biological activity assay of lysozyme in Ultrapure® water containing 0.01 % HPC/Chol (8:2) and 0.2 % Triton X-100 was presented for accuracy and within-precision (Tables 24 and 25, respectively). The specific enzyme activity of lysozyme standard was equal to 45859.11 units/mg LSZ. The mean value of % recovery was 100.23 % and was within 15 % of the actual values (Table 24). The % CV value of precision data was 2.62 % (Table 25). These results indicated that the biological activity assay could be used to determine the activity of lysozyme.

Table 24 Accuracy data of biological activity of lysozyme in aqueous solution containing 0.01 % HPC/Chol (8:2) and 0.2 % Triton X-100

Determination	Specific enzyme activity (units/mg LSZ)	% Recovery
1	47138.64	102.79
2	45936.45	100.17
3	46428.57	101.24
4	44724.19	97.53
5	46271.11	100.90
6	45298.10	98.78
	Mean	100.23
	SD	1.87
	% CV	1.86

Table 25 Precision data of biological activity of 10 μg/mL lysozyme in aqueous solution containing 0.01 % HPC/Chol (8:2) and 0.2 % Triton X-100

Determination	Specific enzyme activity (units/mg LSZ)
1	43911.70
2	45662.26
3	47391.73
4	46611.36
5	45303.71
6	46273.90
Mean	45859.11
SD	1202.21
% CV	2.62

The remaining biological activity and the circular dichroism spectra of lysozyme in aqueous solution heated at various temperatures are presented in Table 26 and Figure 42. Heating of lysozyme solution at 60 °C for 90 min did not affect the activity and conformation integrity of lysozyme. Therefore, this condition could be used for preparing liposomes by DRV method. Heating at 80 °C for 60 min (above T_m of lysozyme in solution) resulted in perturbation of secondary structure of lysozyme which subsequently led to loss of activity (about 94 %). The native structure of lysozyme was required for its enzymatic activity.

Table 26 % Remaining activity of lysozyme aqueous solution after incubation at various conditions (mean $\pm$ SD, n = 3)

Condition	% Remaining activity
60 °C 90 min	103.84 $\pm$ 3.42
80 °C 60 min	6.47 $\pm$ 0.47

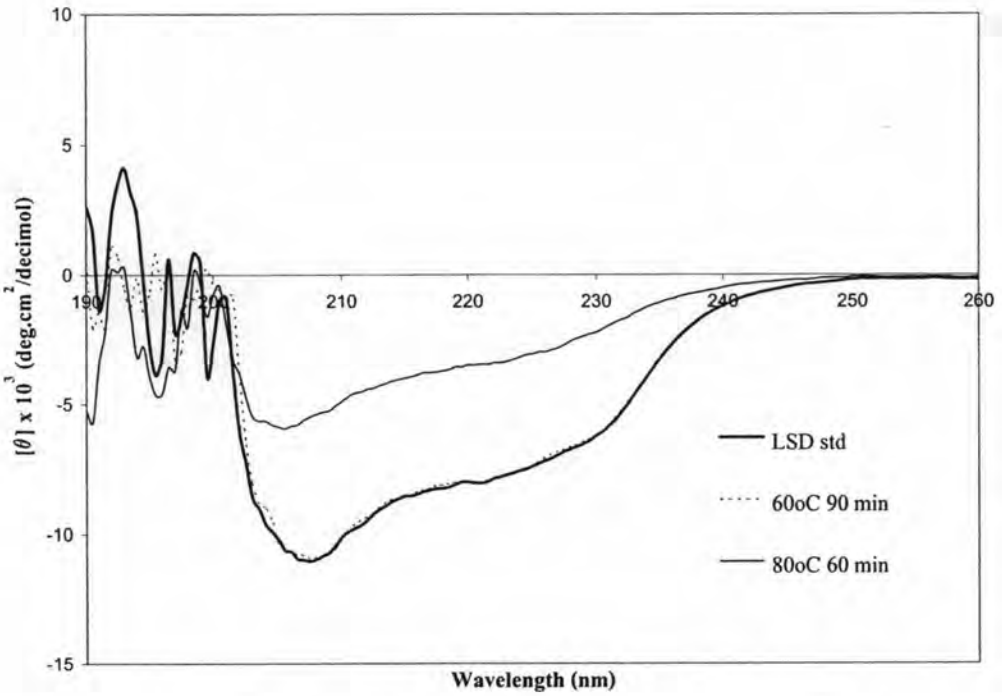

Figure 42 Far-UV CD spectra of lysozyme aqueous solution after incubation at various conditions

7. Preparation of Lysozyme-loaded Liposomal Powders by Spray Drying Technique

7.1 Effect of HPC/Chol Ratio

The formulation with the lipid/mannitol weight ratio of 5:5 was used to investigate the influence of Chol incorporation into HPC liposomal bilayer on the properties of lysozyme-loaded liposomal powders. The spray-dried lysozyme without and with mannitol were also prepared to compare the properties of the spray-dried powders. Lysozyme-loaded liposomal powders were prepared by mixing aqueous solution of lysozyme with liposome dispersion and mannitol solution prior to spray drying to avoid possible instability of lysozyme during liposomal process.

Effects of cholesterol on the characteristics of the spray-dried lysozyme-loaded liposomal powders are summarized in Table 27. The presence of lysozyme in

the spray-dried liposomal powders did not affect the physical appearance of the powders. However, when lysozyme was spray-dried into the liposomal powders, the yield ratio of the powders collected at the collector to those collected at the cyclone of spray dyer increased from 2.71 (44.18/16.28) to 7.20 (60.45/8.4) for HPC and from 1.86 (37.19/19.96) to 16.68 (56.87/3.41) for HPC/Chol ratio of 8:2. This result may be due to the anti-adherent property of lysozyme. Amino acid, peptides and polypeptides have this property by interfering with the weak bonding forces, such as Van der Waal's and Coulomb forces, between the small particles and also reducing adhesion of the particles to the walls of the device (Chougule et al., 2007). The spray drying process yield decreased with higher Chol content (Table 27). This may be because of the lower transition temperature and enthalpy of lipid in the spray-dried powders when Chol content increased (Table 28). The moisture content of the spray-dried liposomal powders with various HPC/Chol ratios was not significantly different. The spray-dried lysozyme only powders had the highest moisture content. Addition of mannitol decreased the moisture content of the spray-dried lysozyme powders.

Table 27 Characteristics of the spray-dried lysozyme powders prepared with different formulations

Formulation	Yield (%) in		Total yield (%)	Moisture content (%) (mean $\pm$ SD)	Physical appearances
	Collector	Cyclone			
Spray-dried LSZ	52.41	12.90	65.31	13.90 $\pm$ 1.41	aggregates
M/L	63.41	11.55	74.96	0.90 $\pm$ 0.01	fine powders
HPC/M/L	60.45	8.4	68.85	3.85 $\pm$ 0.06	fine powders
HPC/Chol9:1/M/L	71.66	3.44	75.10	3.78 $\pm$ 0.31	fine powders
HPC/Chol8:2/M/L	56.87	3.41	60.28	4.07 $\pm$ 0.16	fine powders
HPC/Chol7:3/M/L	43.96	8.06	52.01	2.91 $\pm$ 0.18	aggregates

SEM images in Figure 43 reveal that the morphology of the spray-dried lysozyme powders was influenced by the formulation compositions. The spray-dried lysozyme without and with mannitol were spherical in shape and had a few dimples on their surface (Figure 43a, 43b). The spray-dried lysozyme only powders were very agglomerate due to high surface electrostatic force. The morphology of the liposomal powders with various HPC/Chol molar ratios was not significantly different except the ratio of 7:3 gave the smaller size, but more aggregate, of the spray-dried powders. The reduction of particle size may be due to decreased rigidity of lipid bilayer with high cholesterol.

Representative DSC curves of the lysozyme starting material and the spray-dried lysozyme are illustrated in Figure 44. Thermal behavior of the spray-dried lysozyme was similar to that of the starting material. The curves were characterized by two endotherms, one being very broad at about 55-100 °C and a second endotherm at about 202 °C. The broad endotherm was due to water loss. The endotherm at higher temperatures was thought to represent the denaturation transition and the peak maximum was considered to reflect the denaturation melting temperature (T_m). T_m is analogous to the melting of a crystal which the native and unfolded states are in equilibrium (Hoffmann, 2000). The T_m-value of the lysozyme starting material (203.15 °C) was close to that of the spray-dried lysozyme (201.91 °C). This result indicated that the spray drying process might maintain the thermal stability of lysozyme. This finding is not consistent with the data of Elkordy, Forbes, and Barry (2002) who found that the T_m of spray-dried lysozyme was significantly higher than that of the unprocessed form. The T_m of spray-dried lysozyme was found to be markedly higher than that of the untreated enzyme in solution, the values ranging from 74-76 °C depending on the solvent used (Elkordy et al., 2002). The spray dried alone lysozyme powders was amorphous form like the starting material as proved by XRPD (Figure 45). Generally, spray drying process gives relatively low yields of crystalline products because it uses very strong drying conditions that evaporate droplets rapidly (Chidavaenzi et al., 1997; 2001).

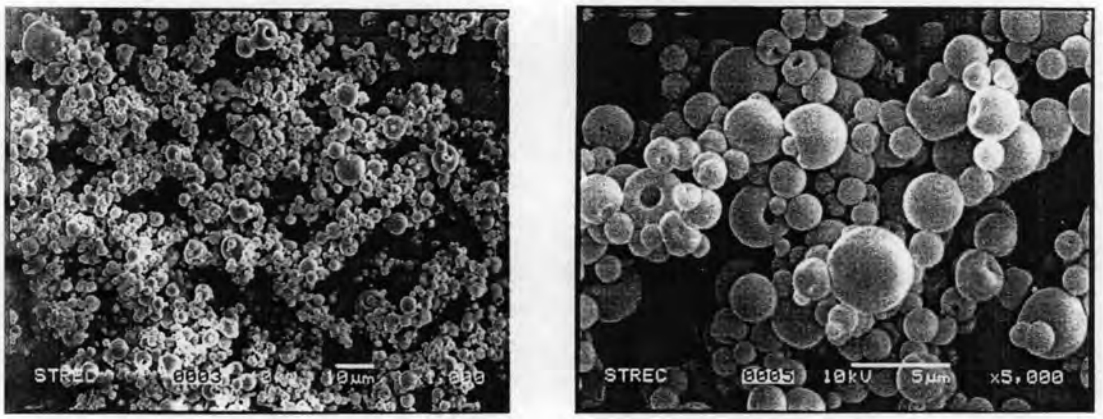

(a) Spray-dried LSZ

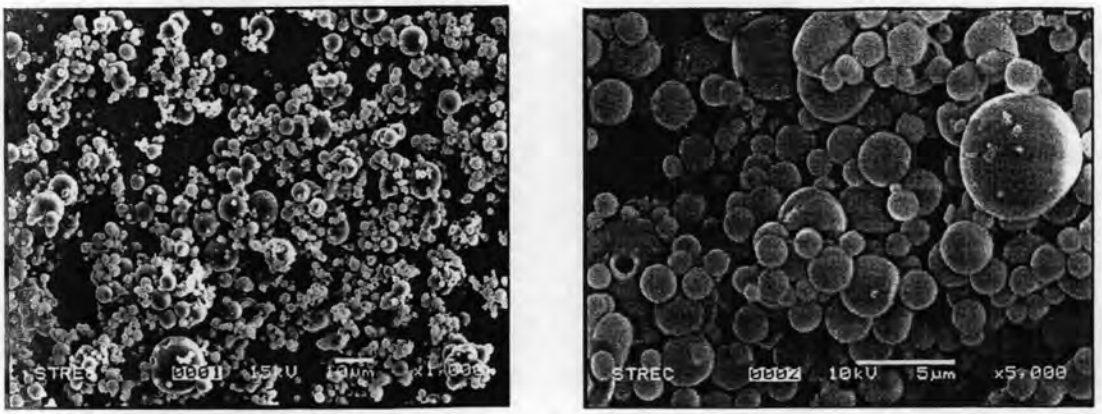

(b) M/L

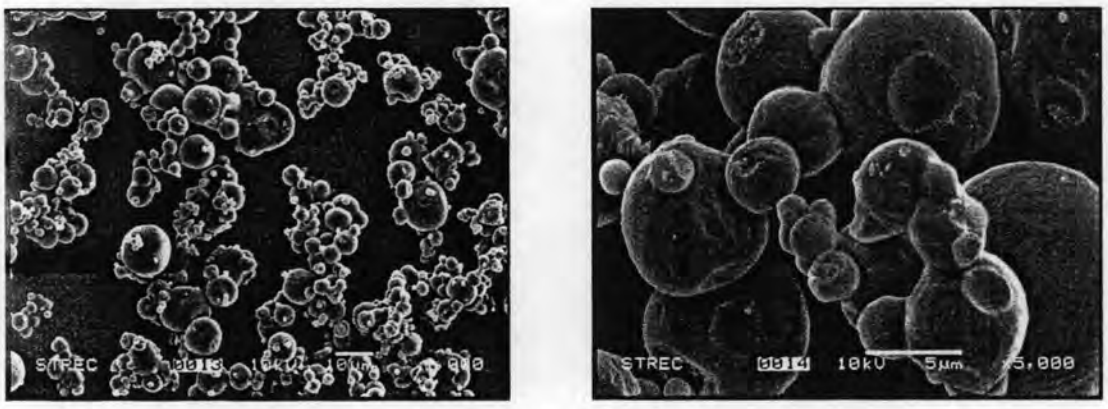

(c) HPC/M/L

Figure 43 Scanning electron micrographs of the spray-dried lysozyme powders prepared with different formulations. On the left side: magnification 1000x and scale bar = 10 μm. On the right side: magnification 5000x and scale bar = 5 μm.

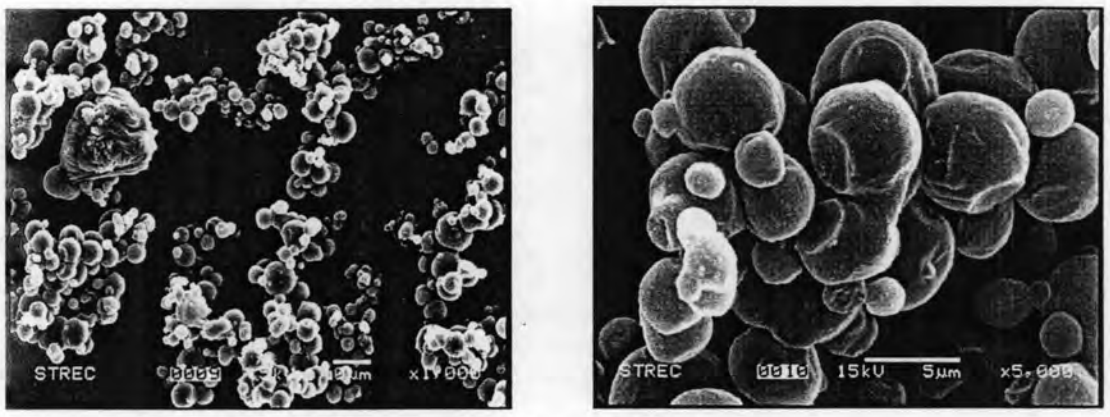

(d) HPC/Chol9:1/M/L

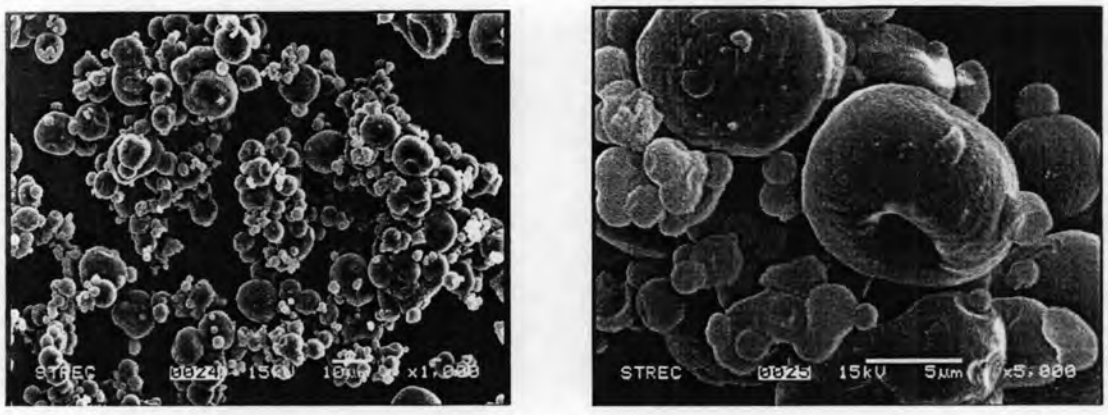

(e) HPC/Chol8:2/M/L

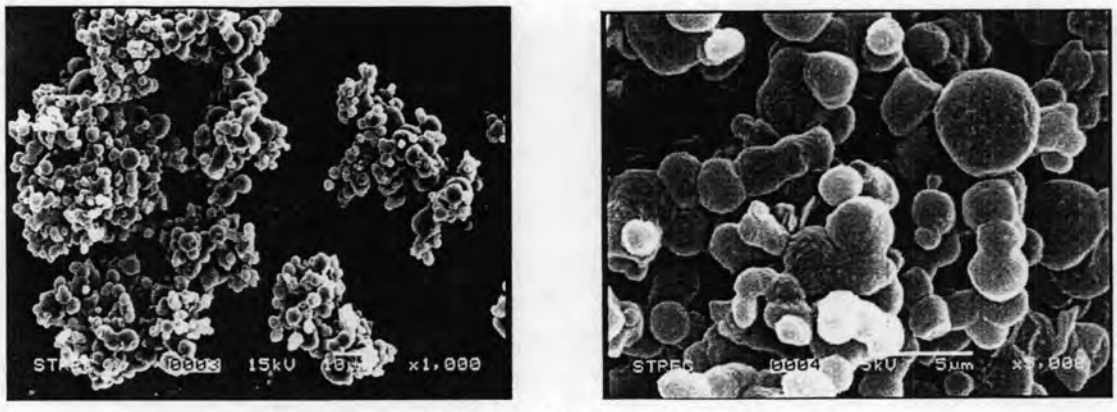

(f) HPC/Chol7:3/M/L

Figure 43 (Continued)

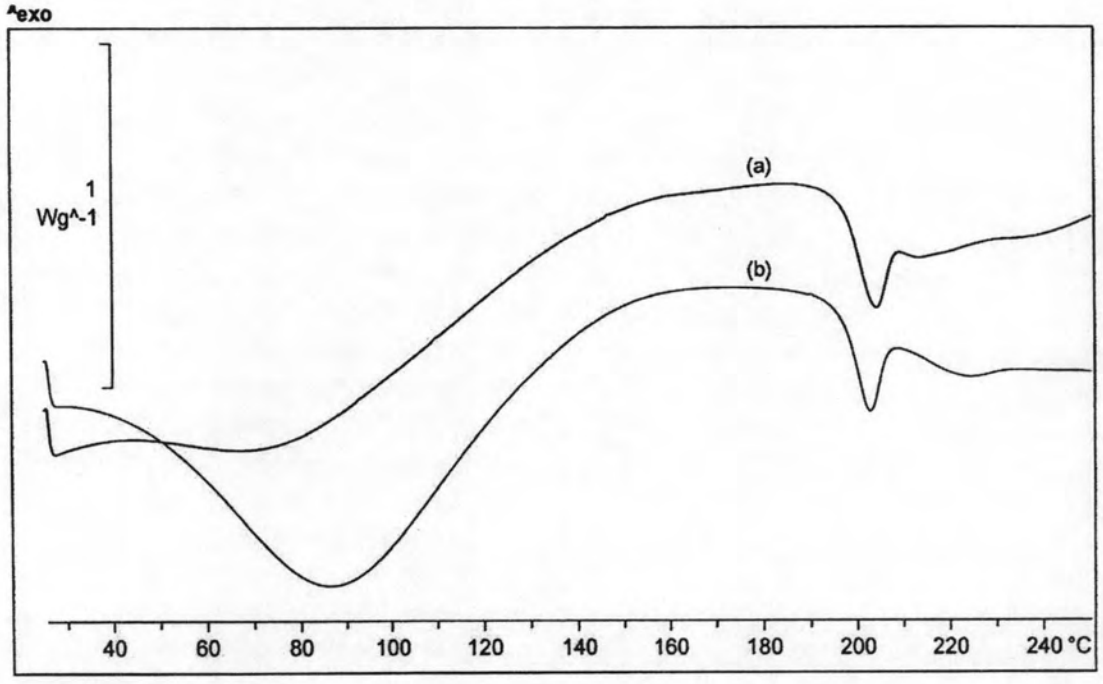

Figure 44 DSC spectra of (a) the lysozyme starting material and (b) the spray-dried lysozyme powders

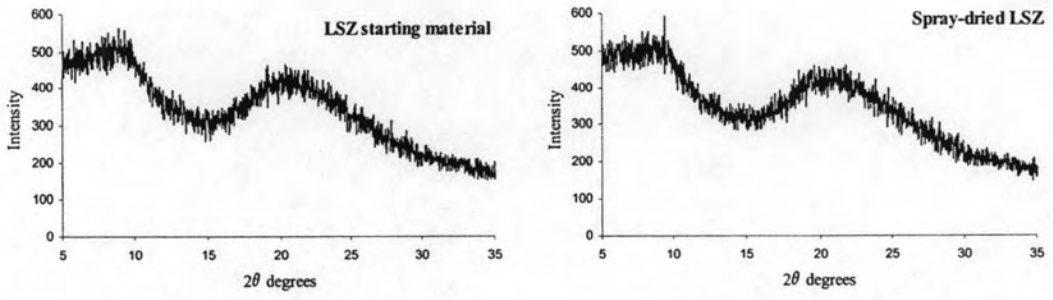

Figure 45 X-ray diffraction patterns of the lysozyme starting material and the spray-dried lysozyme

DSC spectra of the spray-dried lysozyme-loaded liposomal powders (Figure 46) did not show the endotherm peak of lysozyme. The absence of peaks characterizing lysozyme could be explained by the low drug content of the spray-dried formulations (4.76 %w/w) and the limited sensitivity of classical methods used to determine the powder crystallinity. Therefore, this part of the study was specifically purposed at investigating the crystalline nature of the lipid and mannitol additive.

A comparison of DSC spectra of the spray-dried formulations with different HPC/Chol molar ratios revealed that interactions took place between the lipid compositions under the experimental conditions (Figure 46). At the lipid to mannitol ratio of 1:1, the endothermic peak of lipid mixture shifted to a lower temperature from 72.91 °C to 66.48 °C when the Chol content increased (Table 28). The enthalpy of transition decreased from 38.29 to 18.80 J/g of lipid with increasing the Chol content. This may be because Chol weakened the phospholipid interactions considerably in the spray-dried liposomal powders which resulted in the reduction of the T_m and the enthalpy. The melting point of mannitol was not affected by the incorporation of Chol into lipid bilayer. The XRPD patterns (Figure 47) show that the HPC/Chol molar ratios studied did not affect the crystalline form of the spray-dried liposomal powders.

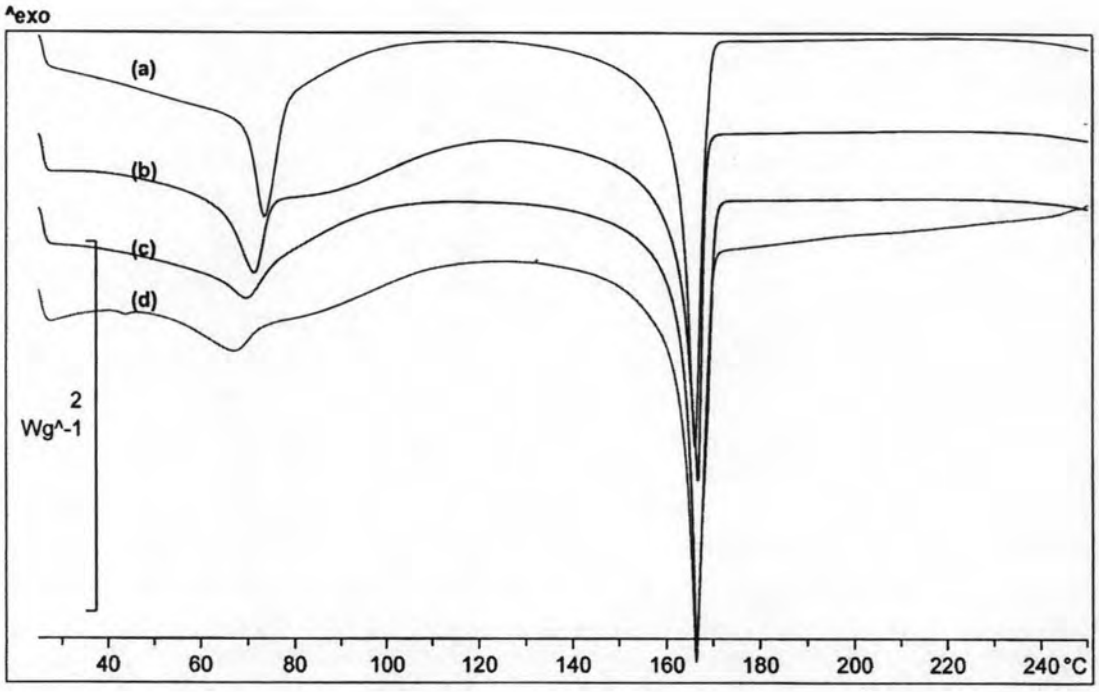

Figure 46 DSC spectra of the spray-dried lysozyme-loaded liposomal powders with different HPC/Chol molar ratios: (a) 10:0; (b) 9:1; (c) 8:2; (d) 7:3

Table 28 Thermal properties of the lysozyme starting material (LSZ) and the spray-dried lysozyme powders with different formulations (mean ± SD, n=3)

Formulation	T_m of lipid (°C)*	Enthalpy (ΔH, J/g)**	Melting peak (°C)
LSZ	-	-	203.15 ± 0.64
Spray-dried LSZ	-	-	201.91 ± 0.72
M/L	-	-	166.22 ± 0.30
HPC/M/L	72.91 ± 0.55	38.29 ± 0.32	165.87 ± 0.53
HPC/Chol9:1/M/L	71.60 ± 0.43	30.56 ± 0.31	166.37 ± 0.34
HPC/Chol8:2/M/L	68.90 ± 0.61	21.57 ± 0.36	166.22 ± 0.24
HPC/Chol7:3/M/L	66.48 ± 0.25	18.80 ± 0.61	166.05 ± 0.28

* Scan rate of 10 °C/min

** Scan rate of 1 °C/min

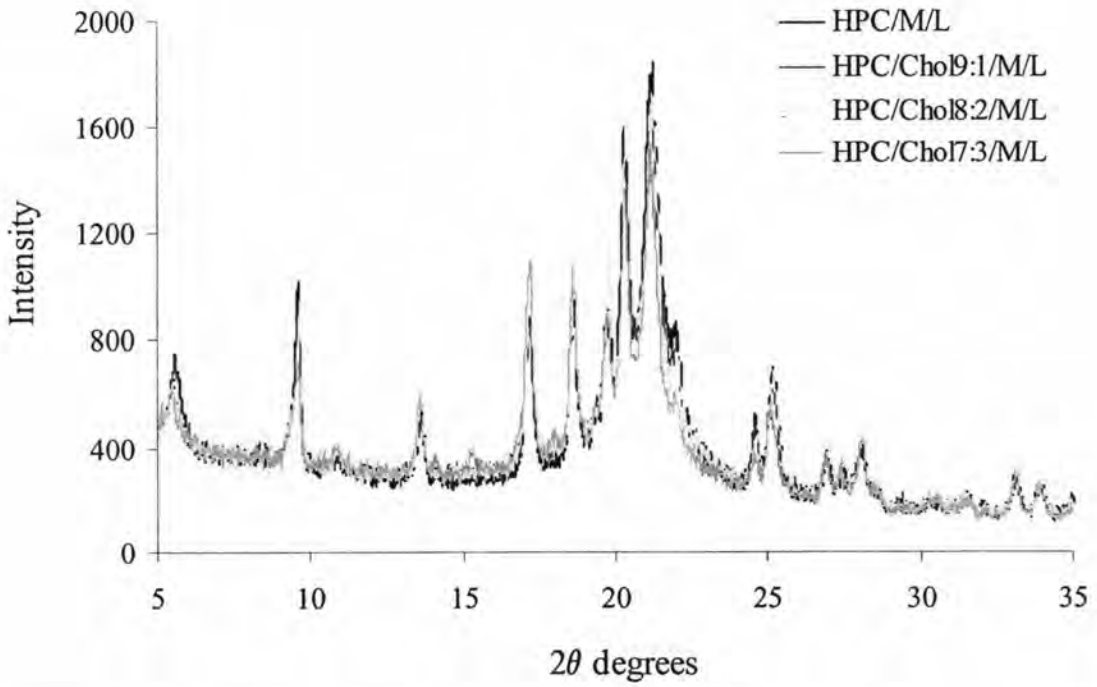

Figure 47 X-ray diffraction patterns of the spray-dried lysozyme-loaded liposomal powders with different HPC/Chol molar ratios

After the reconstitution of the spray-dried liposomal powders with various HPC/Chol ratios in HBS, the liposomes formed spontaneously with different sizes (Figure 48). The volume mean diameter ($D_{[4,3]}$) of the reconstituted liposomes decreased with increasing the Chol content (Figures 48, 49 and Table 29). This may be due to a decrease in rigidity of the HPC membrane by inclusion with Chol. The effect of Chol on HPC liposomes is pointed out in the two regions as a function of the temperature (Marsh and Smith, 1973; Coderch et al., 2000). At temperature below T_m of hydrated HPC (about 52-53 °C, Table 30), an increase in the Chol content leads to an increase in fluidity of the membrane. However, the contrary effect is observed at temperature above T_m which the membrane is condensed with Chol. This can be due to the formation of an intermediate gel state caused by a hydrophobic interaction of cholesterol with the fatty acyl chains of saturated PC (Demel and Kruyff, 1976). The enthalpy of lipid phase transition is the energy associated with the phase transition from gel to liquid crystalline state (Torchilin and Weissig, 2003). In this study, temperature for reconstitution of the powders was 37 °C (below the T_m of HPC),

therefore, the fluidity of HPC liposomal membrane was increased with increasing Chol content as observed by the decreased transition enthalpy in Table 30.

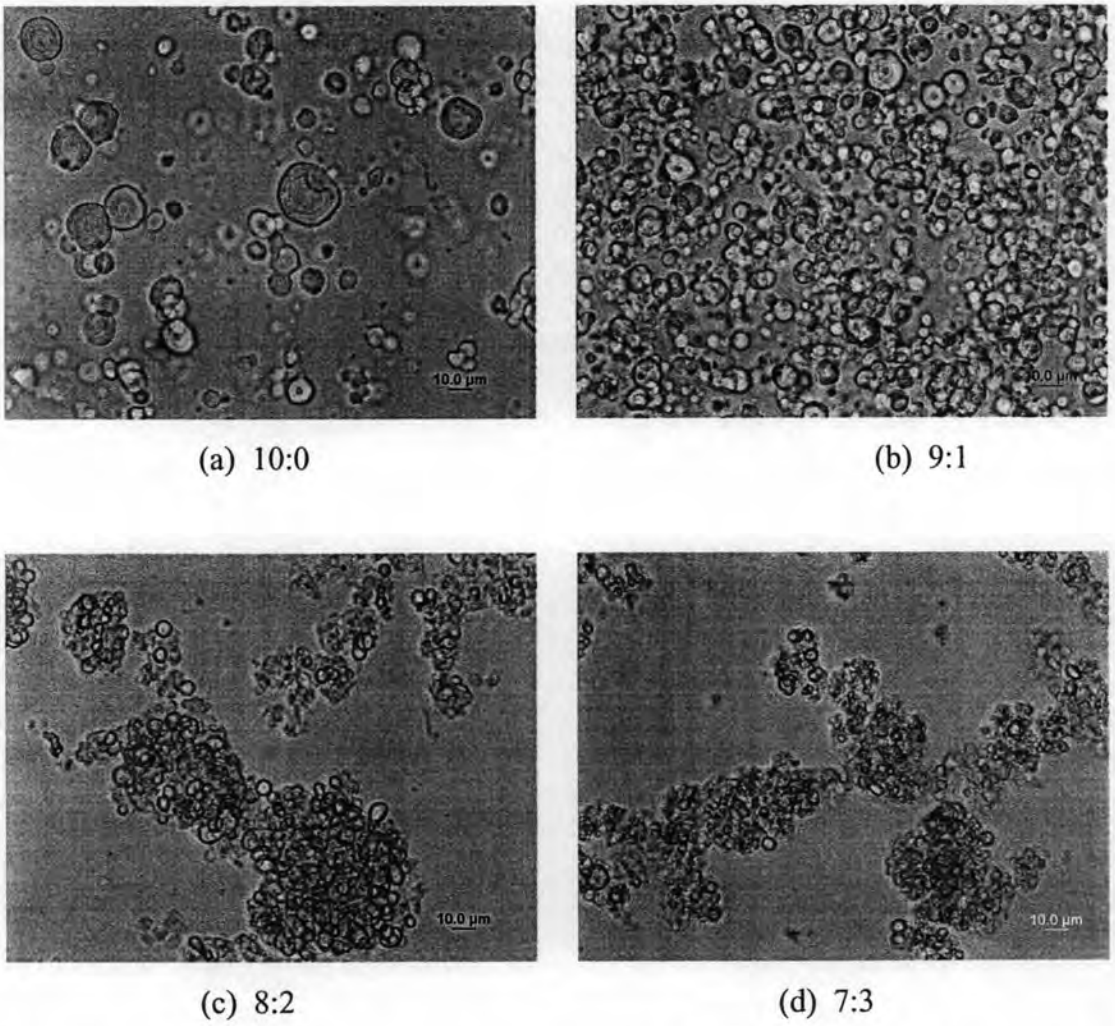

(a) 10:0 (b) 9:1

(c) 8:2 (d) 7:3

Figure 48 Optical micrographs of the reconstituted liposomes from the spray-dried lysozyme-loaded liposomal powders with different HPC/Chol molar ratios in HBS at 37 °C. Magnification 400x. Scale bar = 10 µm.

For studying the entrapment of lysozyme in liposomes, dialysis and ultracentrifugation techniques were used for separation of free lysozyme. Dialysis technique was found to be an appropriate method because of gentle and efficient method but time consuming. The entrapment efficiency of HPC/M/L formulation by dialysis was 6.74 $\pm$ 0.25 µg LSZ/mg lipid. The ultracentrifugation technique gave entrapment of 9.73 $\pm$ 0.62 µg LSZ/mg lipid which may be due to the amount of

lysozyme associated with liposomal surface. However, ultracentrifugation may result in damage of liposomal bilayer due to high centrifuge force and pellet washing process which gave the entrapment underestimate (4.50 ± 0.37 μg LSZ/mg lipid). The dialysis study using a mixture of the reconstituted empty HPC/Chol (8:2) liposomes and lysozyme solution indicated that the lysozyme amount assayed in the liposomal dispersion after dialysis process was lysozyme entrapped into liposomes, not attributed to adsorption phenomena.

The effect of HPC/Chol molar ratio on the encapsulation efficiency of lysozyme in the reconstituted liposomes is shown in Table 29 and Figure 49. The entrapment efficiency increased when the content of cholesterol increased. However, incorporation of cholesterol in the low amount of 10 mole % had no appreciable effect on the entrapment efficiency when compared to the HPC only liposomal powders. The low entrapment efficiency of the formulations with HPC/Chol ratios of 10:0 and 9:1 may be because of rigidity of the lipid membrane and high enthalpy values of lipid in the reconstituted liposomes (Figure 50 and Table 30). For the reconstitution temperature of 37 °C, most of the lipid molecules might remain in the gel phase rather than liquid crystalline, thereby yielding low entrapment.

Table 29 Entrapment efficiency (EE) and volume mean diameter of the reconstituted liposomes from the spray-dried lysozyme-loaded liposomal powders with different HPC/Chol molar ratios in HBS at 37 °C (mean ± SD, n = 3)

Formulation	EE (μg LSZ/mg lipid)	$D_{[4,3]}$ (μm)*	Span
HPC/M/L	6.74 ± 0.25	14.34 ± 0.05	1.28 ± 0.002
HPC/Chol9:1/M/L	4.60 ± 0.33	9.43 ± 0.002	1.05 ± 0.001
HPC/Chol8:2/M/L	14.81 ± 1.36	7.39 ± 0.002	1.27 ± 0.003
HPC/Chol7:3/M/L	27.88 ± 0.41	5.15 ± 0.02	1.21 ± 0.01

* Measured by Mastersizer 2000

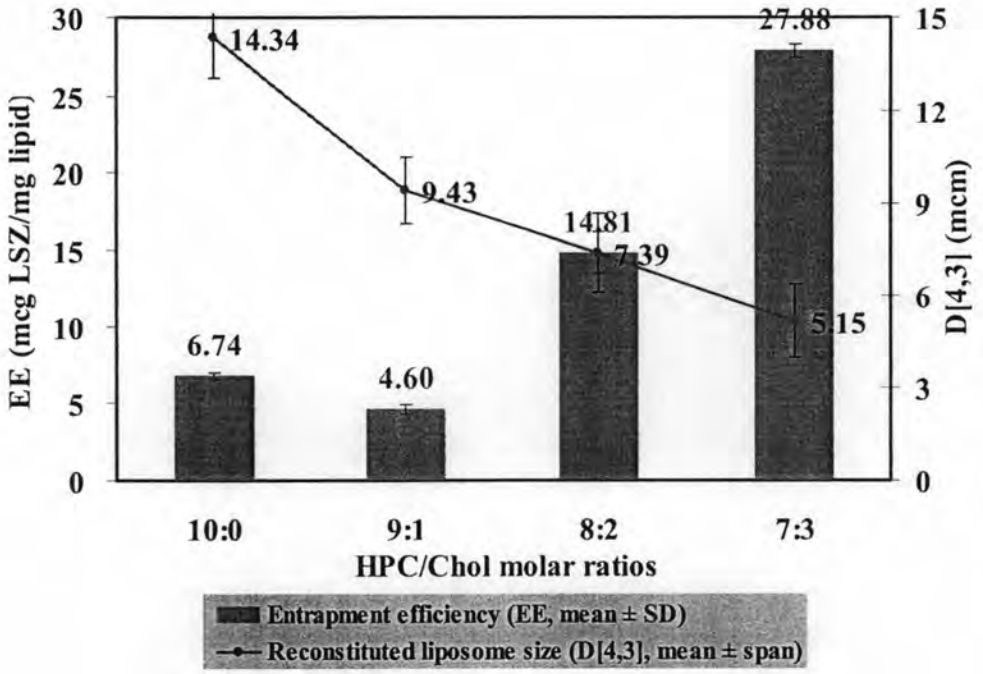

Figure 49 Entrapment efficiency and volume mean diameter of the reconstituted liposomes from the spray-dried lysozyme-loaded liposomal powders with different HPC/Chol molar ratios in HBS at 37 °C

The encapsulation efficiency of lysozyme in the reconstituted liposomes increased linearly with increasing cholesterol content from 10 to 30 mole % (Figure 49). The entrapment of lysozyme in the reconstituted liposomes might occur due to the re-encapsulation of lysozyme by the vesicles. The liposomes were spontaneously formed after reconstitution of the spray-dried powders with HBS creating reservoirs for the encapsulation of lysozyme. A higher proportion of cholesterol led to more improved fluidity of the lipid bilayer which would provide a higher re-encapsulation capacity. The increased fluidity of HPC liposomal bilayer with Chol was supported by the thermal properties of the reconstituted liposomes as shown in Figure 50 and Table 30.

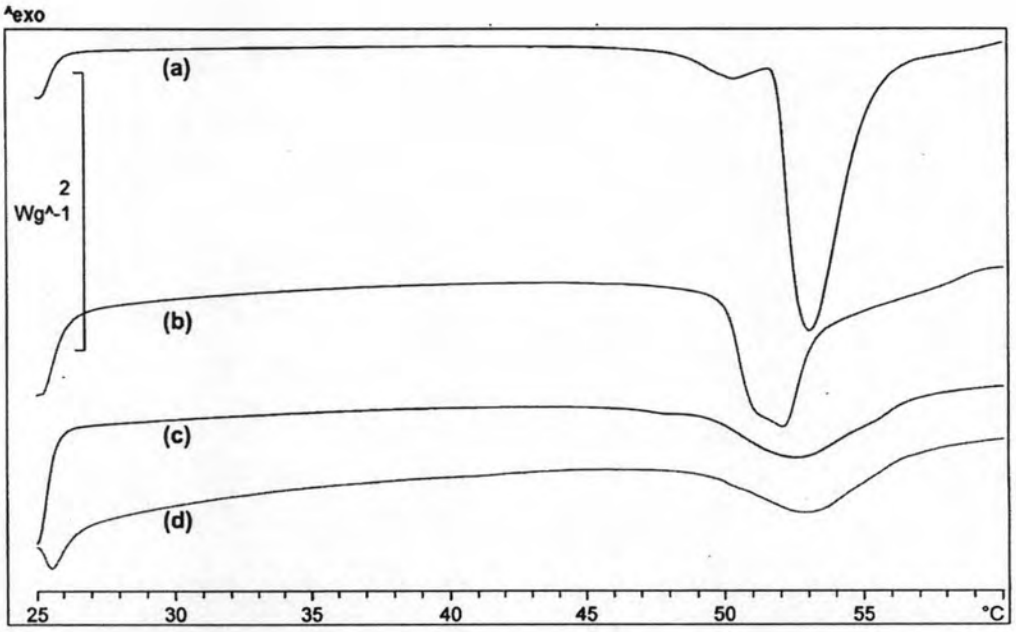

Figure 50 DSC spectra of the reconstituted liposomes from the spray-dried lysozyme-loaded liposomal powders with various HPC/Chol ratios: (a) 10:0; (b) 9:1; (c) 8:2; and (d) 7:3 in HBS at 37 ºC

Table 30 Phase transition of the reconstituted liposomes from the spray-dried lysozyme-loaded liposomal powders with various HPC/Chol molar ratios (mean ± SD, n=3)

Formulation	T_m (ºC)	Enthalpy (ΔH, J/g)
HPC/M/L	52.98 ± 0.34	50.69 ± 1.61
HPC/Chol9:1/M/L	52.29 ± 0.25	51.45 ± 0.75
HPC/Chol8:2/M/L	52.14 ± 0.73	30.83 ± 1.58
HPC/Chol7:3/M/L	53.28 ± 0.37	21.73 ± 0.77

The DSC spectra of the initial liposomes composed with various HPC/Chol molar ratios are illustrated in Figure 51. The DSC thermogram of HPC liposomes without Chol showed the small pretransition peak at 46.14 ± 0.05 °C and the enthalpy of 1.86 ± 0.02 J/g due to a rearrangement of the individual lipid molecules within the liposomal bilayer. The gel-to-liquid crystalline phase transition peaks (T_m) of the HPC liposomes with various Chol contents were not different and remained around 52-53 °C (Table 31). The transition peak of HPC liposomes was not sharp which may be due to the presence of various fatty acyl chains. Addition of Chol made the pre-transition peak disappear totally. The disappearance of the pretransition is presumably due to the conversion of the $P_{\beta'}$ phase of phospholipid bilayers into an L_{β}-like phase, in which the hydrocarbon chains become more perpendicular to the bilayer plane and the bilayer initially thickens (Finean, 1990; McMullen et al., 1993). The main transition of the formulations with Chol occurred over a broader temperature range than did the pure HPC liposomes. Incorporation of Chol progressively reduced the enthalpy of T_m of the lipid bilayer because cholesterol interacts with phospholipid in higher proportion (McMullen et al., 1993; McMullen and McElhaney, 1995). At low concentration of Chol (10 mole %), a phase separation occurred as observed by resolution of the main transition peak (Figure 51b) (New, 1989).

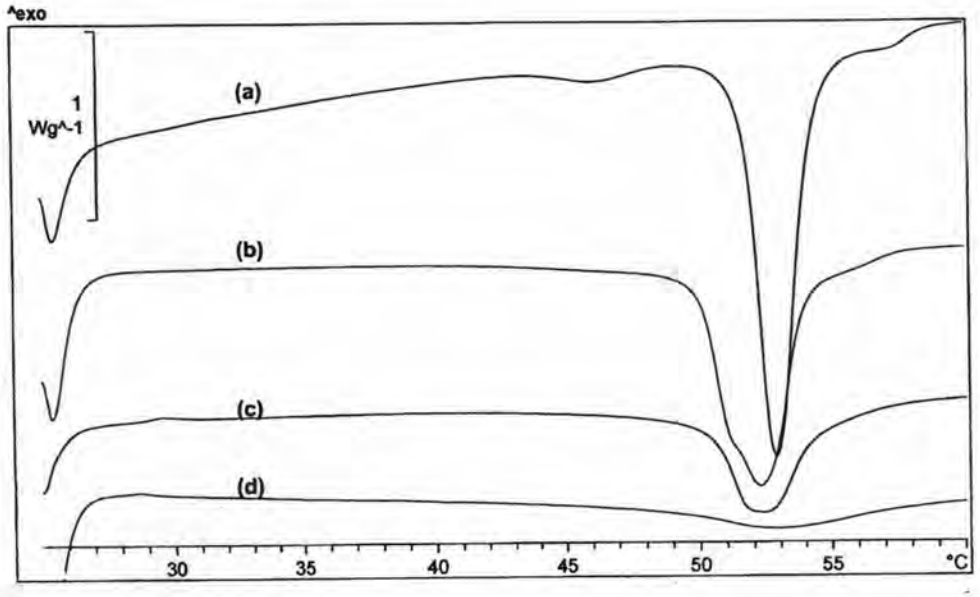

Figure 51 DSC spectra of the initial liposomes composed of various HPC/Chol ratios: (a) 10:0; (b) 9:1; (c) 8:2; and (d) 7:3

Table 31 Main phase transition of the initial liposomes with various HPC/Chol molar ratios (mean ± SD, n=3)

HPC/Chol molar ratios	T_m (°C)	Enthalpy (ΔH, J/g)
10:0	52.83 ± 0.05	46.07 ± 0.51
9:1	52.55 ± 0.27	43.74 ± 0.30
8:2	52.51 ± 0.08	23.54 ± 1.43
7:3	52.99 ± 0.39	6.94 ± 0.83

The DSC thermograms of the reconstituted liposomes (Figure 50) were similar to those of the initial liposomes with the corresponding Chol content (Figure 51). The main phase transitions (T_m) of the reconstituted liposomes were at about 52-53 °C similar to those of the initial liposomes. However, the peak of pretransition temperature shifted from 47.27 ± 0.1 °C to 50.18 ± 0.3 °C which may be due to interaction between effective hydrophobic length of lysozyme and the phospholipid hydrocarbon chains (McMullen, Lewis, and McElhaney, 1993). The transition enthalpy of the reconstituted liposomes decreased with increasing Chol content from HPC/Chol molar ratio of 9:1 to 7:3. The phase transition occurred at the ratio of 9:1 similar to the corresponding initial liposomes (Figure 50b). However, the enthalpy of the reconstituted liposomes was larger than that of the initial liposomes with the corresponding Chol content. This may be due to difference of the packing geometry (phospholipids interaction) of the hydrophobic carbon chains in the bilayer of the reconstituted liposomes in comparison to the initial extruded liposomes (Huang and Mason, 1978).

From the overall results, the formulations with only HPC and HPC/Chol (8:2) were selected for the next study because both formulations gave fine powders and the formulation with HPC/Chol (8:2) yielded high lysozyme entrapment. The mass median diameters of both liposomal powder formulations were rather large about 6-8 μm because of the aggregation of particles (Table 32).

Table 32 Particle sizes of the spray-dried lysozyme-loaded liposomal powders with only HPC and HPC/Chol molar ratio of 8:2 (mean ± SD, n=3)

Formulation	$D_{0.5}$ (μm)*	Span
HPC/M/L	7.90 ± 0.01	1.13 ± 0.00
HPC/Chol8:2/M/L	6.36 ± 0.06	1.67 ± 0.01

* Measured by Mastersizer S

The effect of temperature for reconstitution of the spray-dried liposomal powders in HBS on the properties of the reconstituted liposomes was also studied at 60 °C. As shown in Figure 52 and Table 33, the volume mean diameters of the reconstituted liposomes with HPC and HPC/Chol (8:2) decreased in comparison to reconstitution at 37 °C from 14.34 to 3.36 μm and 7.39 to 4.03 μm, respectively. On the other hand, the entrapment efficiency of lysozyme in the reconstituted liposomes increased from 6.74 to 37.43 μg LSZ/mg lipid and 14.81 to 19.00 μg LSZ/mg lipid for the formulations with HPC and HPC/Chol (8:2), respectively. The results were outstanding for the formulation with only HPC. This may be because, at the temperature 60 °C (above T_m of the hydrated HPC), fully hydrated HPC liposomes were spontaneously formed and the rigidity of the HPC lipid bilayer decreased. This resulted in the smaller liposome size and the higher re-encapsulation capacity of lysozyme into liposomes. This result is consistent with a previous study by Ma et al. (1991a, b) in that an increase in temperature decreased the surface density of the bilayer resulting in a decrease in liposome size and an increase in drug encapsulation.

Polarizing micrographs of the reconstituted liposomes from the spray-dried powders with HPC/Chol (8:2) at 37 °C confirmed the formation of spherical liposomes which lamellar structure was birefringent (Figure 53) (Giulieri and Krafft, 2003). The reconstituted liposomes with only HPC (at 37 °C) showed no birefringence and appeared dark under polarized microscope. This might imply that the reconstituted liposomes from HPC without Chol were not properly formed under this condition.

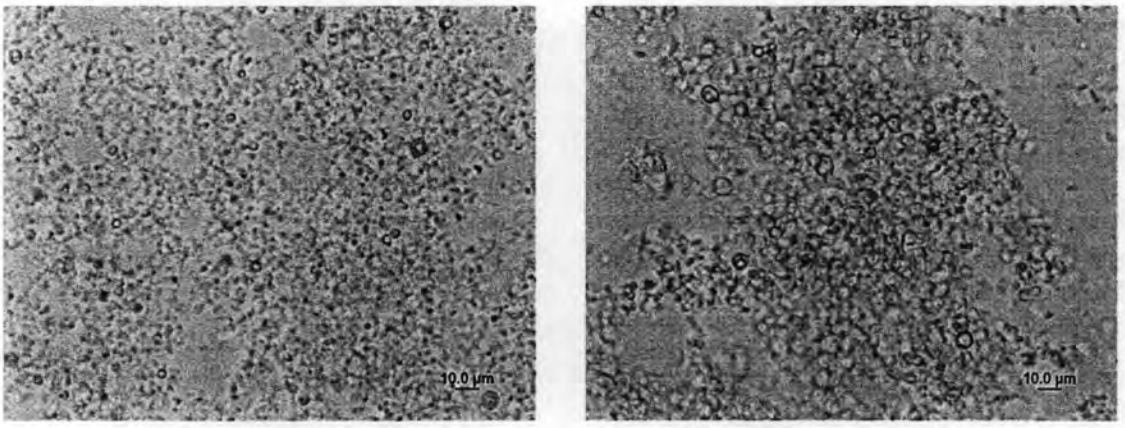

(a) HPC (b) HPC/Chol (8:2)

Figure 52 Optical micrographs of the reconstituted liposomes from the spray-dried lysozyme-loaded liposomal powders with (a) HPC and (b) HPC/Chol (8:2) in HBS at 60 °C. Magnification 400x. Scale bar = 10 µm.

Table 33 Entrapment efficiency and volume mean diameter of the reconstituted liposomes from the spray-dried lysozyme-loaded liposomal powders with HPC and HPC/Chol (8:2) in HBS at 60 °C (mean ± SD, n = 3)

Formulation	EE (µg LSZ/mg lipid)	$D_{[4,3]}$ (µm)*	Span
HPC/M/L	37.43 ± 0.81	3.36 ± 0.03	1.21 ± 0.06
HPC/Chol8:2/M/L	19.00 ± 0.77	4.03 ± 0.08	0.97 ± 0.00

* Measured by Mastersizer 2000

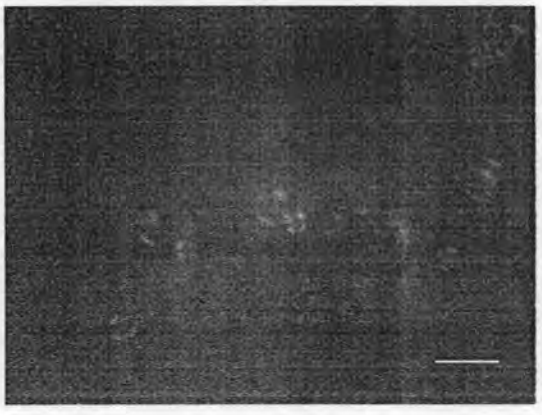

Figure 53. Polarizing micrograph of the reconstituted liposomes from the HPC/Chol 8:2/M/L formulation in HBS at 37 °C. Magnification 1000x. Scale bar = 10 µm.

7.2 Effect of Presence of Lysozyme with and without Mannitol in Liposome Structure Prior to Spray Drying

The liposomes of lysozyme were prepared by dehydration-rehydration method. Transmission electron micrographs of the extruded HPC and HPC/Chol(8:2) DRV prior to spray drying are illustrated in Figure 54. Effective diameters of the extruded DRV were about 140-170 nm and the entrapment efficiencies of lysozyme in all DRV formulations were about 25-30 μg LSZ/mg lipid (Table 34). This method gave high entrapment of lysozyme in liposomes because the freeze-dried liposomes were rehydrated with small volume of medium resulting in high lysozyme concentration (Kirby and Gregoriadis, 2003).

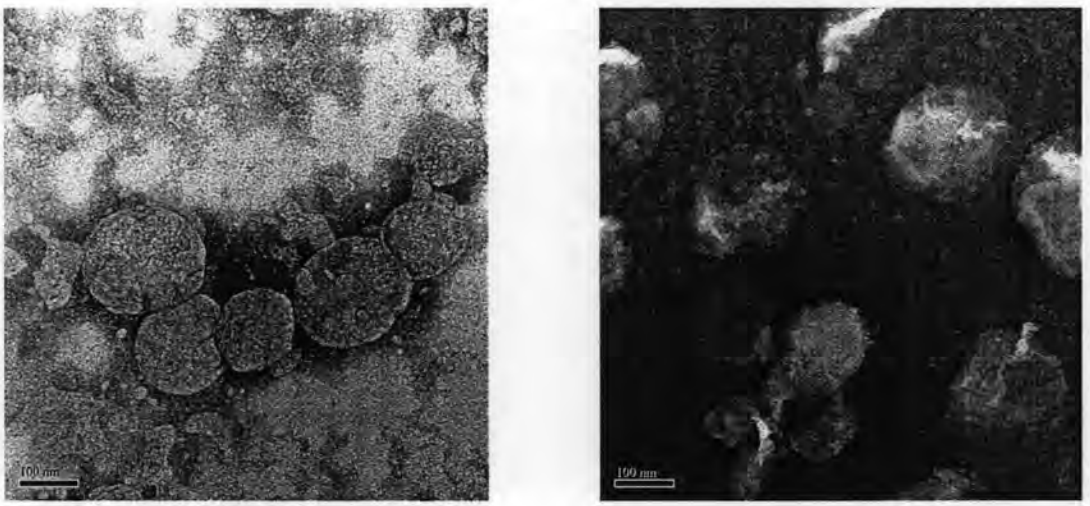

Figure 54 Transmission electron micrographs of the extruded (a) HPC and (b) HPC/Chol(8:2) DRV prior to spray drying. Scale bar = 100 nm.

The extruded DRV were spray-dried into the powders using mannitol as an additive introduced either only on the outside or on both sides of the bilayer. The yield of the formulation with mannitol on both sides of the bilayer was lower than that of the corresponding formulation with mannitol only on the outside (Table 35). The moisture content and the morphology of the four spray-dried formulations with liposomes prepared by DRV method were not significantly different (Figure 55).

Table 34 Liposome size and entrapment efficiency of lysozyme in liposomes prepared by dehydration-rehydration method prior to spray drying (mean ± SD, n =3)

Formulation code	Effective diameter (nm)*	Polydispersity	Entrapment efficiency (μg LSZ/mg lipid)
DRV HPC	141.10 ± 1.00	0.14 ± 0.04	30.54 ± 2.29
DRV HPC in M	155.80 ± 0.80	0.13 ± 0.06	25.33 ± 1.09
DRV HPC/Chol8:2	143.40 ± 0.80	0.10 ± 0.01	24.66 ± 1.11
DRV HCP/Chol8:2 in M	173.10 ± 3.90	0.18 ± 0.03	25.95 ± 0.90

* Measured by Zetaplus and Bi-mas

Table 35 Yield and moisture content of the spray-dried DRV liposomal powders

Formulation	Yield (%) in		Total yield (%)	Moisture content (%w/w) (mean ± SD)
	Collector	Cyclone		
DRV HPC	59.57	6.53	66.10	4.22 ± 0.20
DRV HPC in M	44.31	12.78	57.09	3.73 ± 0.32
DRV HPC/Chol8:2	46.24	10.37	56.61	4.92 ± 0.17
DRV HCP/Chol8:2 in M	39.65	3.97	43.62	4.31 ± 0.31

Optical micrographs of the reconstituted liposomes from the four spray-dried formulations with liposomes prepared by DRV method are illustrated in Figure 56. Volume mean diameters of the reconstituted liposomes from the spray-dried liposomal powders with the same lipid composition were not different (Table 36). The spray-dried HPC formulation with lysozyme gave the larger size of the reconstituted liposomes than that without lysozyme. This may be due to encapsulation of lysozyme into the reconstituted liposomes. However, the sizes of the reconstituted liposomes from all formulations were larger than those of the initial liposomes before spray drying.

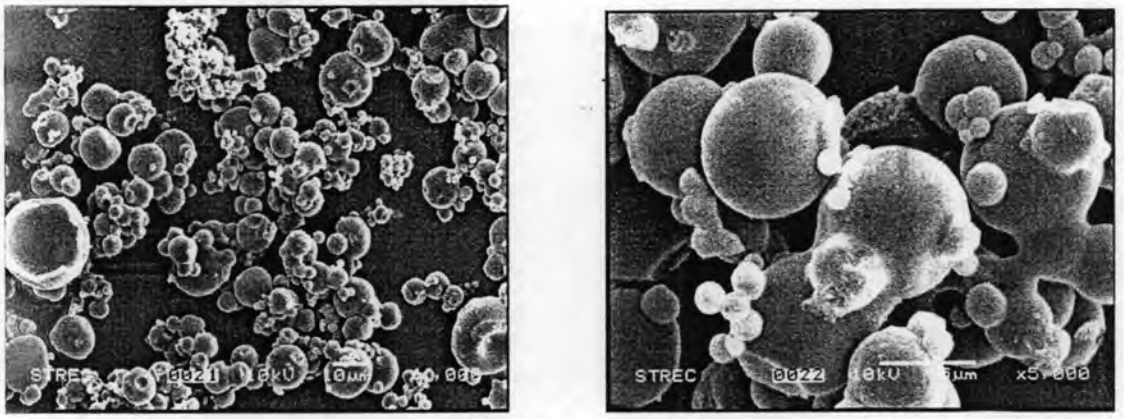

(a) DRV HPC

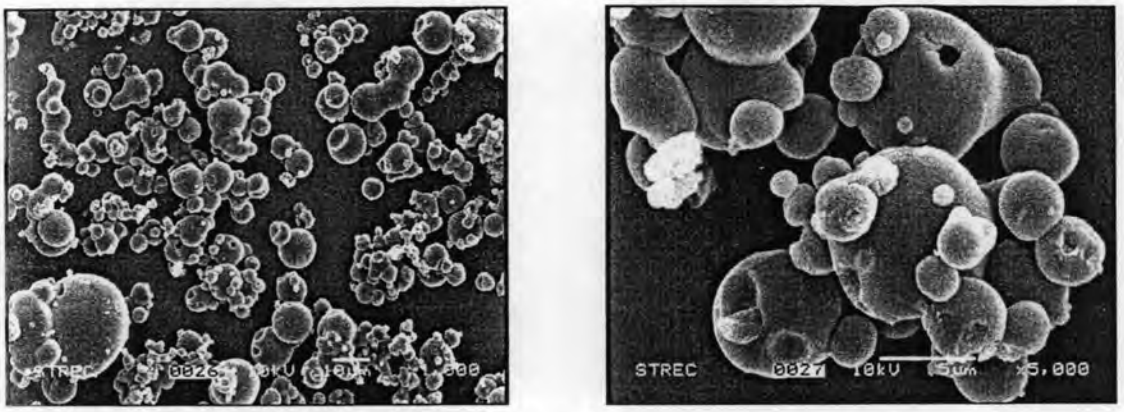

(b) DRV HPC in M

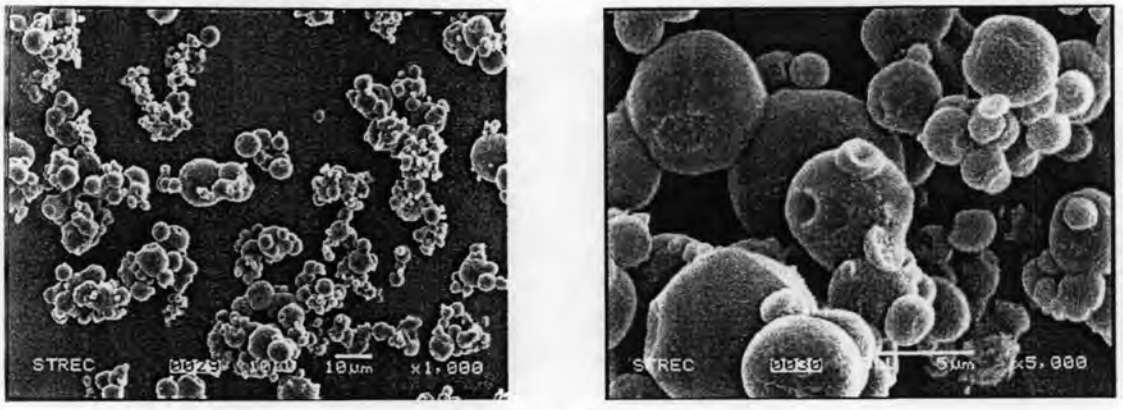

(c) DRV HPC/Chol8:2

Figure 55 Scanning electron micrographs of the spray-dried DRV liposomal powders. On the left side: magnification 1000x and scale bar = 10 μm. On the right side: magnification 5000x and scale bar = 5 μm.

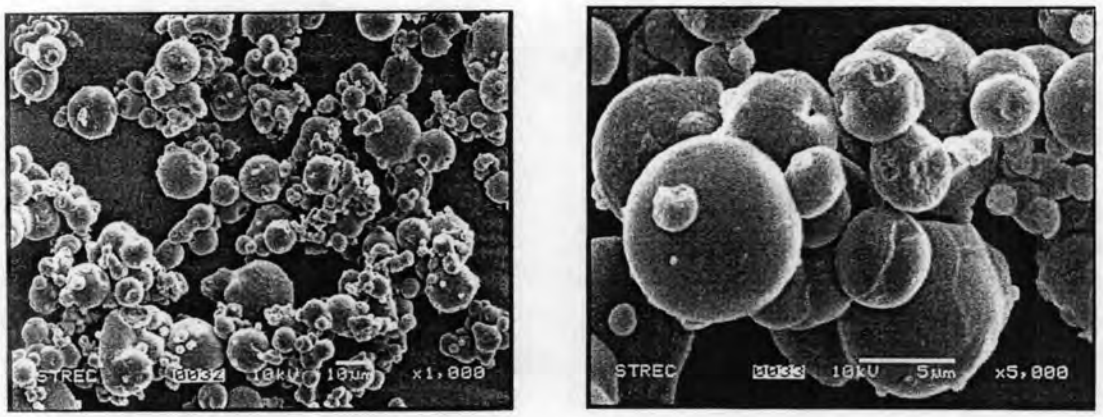

(d) DRV HPC/Chol8:2 in M

Figure 55 (Continued)

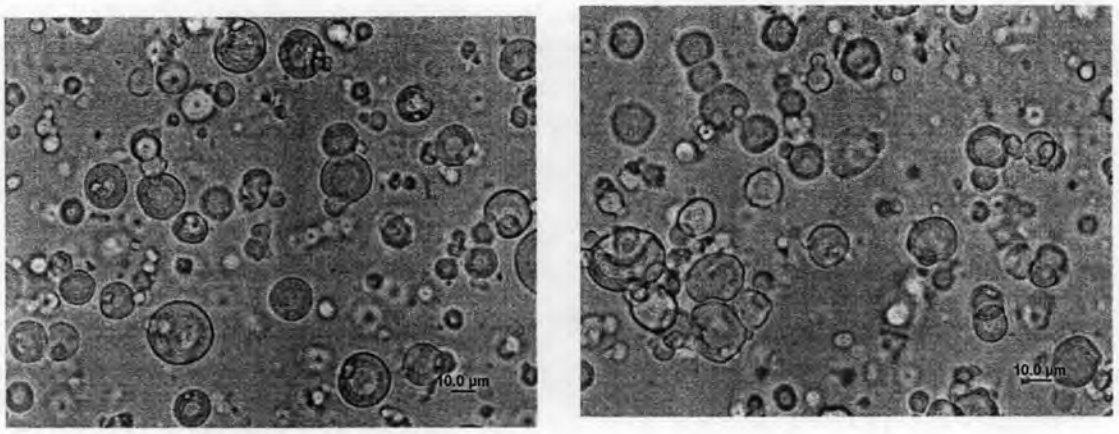

(a) DRV HPC (b) DRV HPC in M

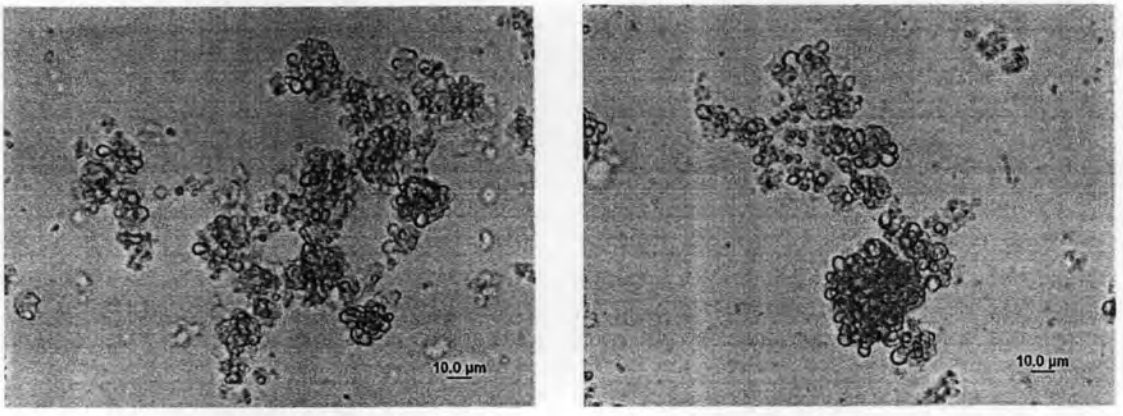

(c) DRV HPC/Chol8:2 (d) DRV HPC/Chol8:2 in M

Figure 56 Optical micrographs of the reconstituted liposomes from the spray-dried DRV liposomal powders with HBS at 37 °C. Magnification 400x. Scale bar = 10 µm.

Table 36 Entrapment efficiency and volume mean diameter of the reconstituted liposomes from the spray-dried liposomal powders with HPC and HPC/Chol (8:2) prepared with various procedures in HBS at 37 °C (mean ± SD)

Formulation	EE (μg LSZ/mg lipid)*	$D_{[4,3]}$ (μm)**	Span
HPC/M5:5	-	10.70 ± 0.27	1.62 ± 0.02
HPC/M/L	6.74 ± 0.25	14.34 ± 0.05	1.28 ± 0.00
DRV HPC	6.56 ± 0.75	14.60 ± 0.04	1.22 ± 0.00
DRV HPC in M	5.57 ± 0.36	13.93 ± 0.02	1.12 ± 0.00
HPC/Chol8:2/M	-	7.82 ± 0.01	1.40 ± 0.002
HPC/Chol8:2/M/L	14.81 ± 1.36	7.39 ± 0.002	1.27 ± 0.003
DRV HPC/Chol8:2	12.76 ± 1.60	7.65 ± 0.01	1.10 ± 0.004
DRV HPC/Chol8:2 in M	12.14 ± 0.82	8.51 ± 0.10	1.66 ± 0.08

* n = 4

** n = 3; Measured by Mastersizer 2000

After the spray drying process, the entrapment efficiency of lysozyme in the reconstituted liposomes from the spray-dried powders with only HPC prepared with all methods were about 5-7 μg LSZ/mg lipid, while those with HPC/Chol (8:2) were about 12-15 μg LSZ/mg lipid (Table 36). There was no difference among the entrapment efficiency of the corresponding formulations with mannitol introduced only on the outside and on both sides of the bilayer. Therefore, the loading of lysozyme into liposomes before spray drying process had no effect on the properties of the spray-dried liposomal powders. These results may be because, at the inlet air temperature of 120 °C, the lipid bilayers passed to the liquid crystalline state, the membrane fluidity increased a lot and the vesicles became very permeable to the entrapped material (Crowe et al., 1988; Goldbach et al., 1993b). Another reason was that mannitol could not preserve liposomal bilayer integrity during dehydration of liposomes composed of HPC with and without cholesterol by spray drying technique. Crowe et al. (1988) suggested that the leakage of contents entrapped in the inner aqueous phase of liposomes during the drying and rehydration process can be ascribed

to (1) phase separation of lipids around their T_m (in liposomes composed of only a single lipid) and to (2) membrane fusion between liposomes.

Owing to the formulation with the HPC/Chol molar ratio of 8:2 gave fine powders and high lysozyme entrapment in the reconstituted liposomes. Therefore, the formulation with HPC/Chol(8:2):M:LSZ (1:1:0.1) was considered appropriate for the further optimization of spray drying conditions.

7.3 Integrity of Lysozyme after Dehydration-rehydration Method and Spray Drying Process

7.3.1 Sodium Dodecyl Sulfate-Polyacrylamide Gel Electrophoresis

The SDS-PAGE image in Figure 57 illustrates that the spray-dried lysozyme showed a similar pattern to the lysozyme starting material. There was the only band at molecular weight 14.4 kDa which was band of lysozyme molecule (MW 14,307 Da). No low molecular weight bands could be detected on the SDS-PAGE gel. This result indicated that no cleavage of the lysozyme molecule took place during spray drying process.

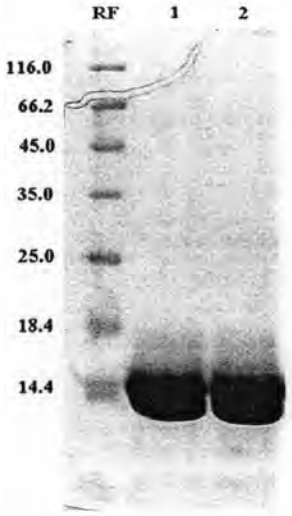

Figure 57 SDS-PAGE patterns of lysozyme. RF: molecular mass reference; Lane 1: the lysozyme starting material; Lane 2: the spray-dried lysozyme.

7.3.2 Biological Activity of Lysozyme

The biological activity of a protein depends on its native structure as determined by the three-dimensional arrangement of amino acids at the active site (Rosenberger, 1996). Tables 37 and 38 present the remaining biological activity of lysozyme in the DRV liposomes before spray drying and the reconstituted spray-dried powders, respectively, in comparison to that of aqueous solution of the lysozyme starting material. The specific enzyme activity of lysozyme in all formulations was not different from that of the lysozyme starting material. Therefore, the DRV method and the spray drying process might not affect the biological activity of lysozyme.

Elkordy et al. (2002) and Jovanovic et al. (2008) reported limitation of the use of lysozyme as a model protein. Because lysozyme is a stable protein and able to revert to its active state upon reconstitution, it is possible that the solution studies do not reflect the conformational damage that may have occurred during spray-dried processing. Therefore, circular dichroism analysis and FT-Raman spectroscopy were also used to investigate secondary structure changes of the spray-dried lysozyme.

Table 37 Remaining activity of lysozyme in the DRV liposomes before spray drying (mean $\pm$ SD, n = 3)

Formulation	Remaining activity (%)
DRV HPC	97.30 $\pm$ 5.84
DRV HPC in M	96.76 $\pm$ 3.99
DRV HPC/Chol8:2	101.84 $\pm$ 8.19
DRV HCP/Chol8:2 in M	102.21 $\pm$ 3.06

Table 38 Remaining activity of lysozyme in the spray-dried formulations prepared by different compositions and procedures (mean ± SD, n = 3)

Formulation	Remaining activity (%)
Spray-dried LSZ	101.19 ± 2.89
M/L	100.98 ± 3.35
HPC/M/L	99.41 ± 8.26
HPC/Chol8:2/M/L	101.72 ± 4.78
DRV HPC	97.52 ± 1.66
DRV HPC in M	98.33 ± 2.00
DRV HPC/Chol8:2	94.55 ± 3.75
DRV HCP/Chol8:2 in M	99.66 ± 3.45

7.3.3 Circular Dichroism Analysis

Circular dichroism is a commonly used excellent method to determine conformation of proteins in solution. Changes in CD signals in either the far-UV or the near-UV can be used to monitor the loss of structure during unfolding (Kelly and Price, 1997). The far-UV CD spectrum is directly related to the protein secondary structure due to asymmetrical packing of intrinsically achiral (planar) peptide groups (Kelly, Jess, and Price, 2005). CD was used to investigate changes of secondary structure of lysozyme after spray drying process.

Lysozyme is a small monomeric globular protein. Its structure is compact with several helices surrounding a small beta sheet region. The active site is formed at the interface between α and β–domains (Yokota et al., 2000). Therefore, the secondary structure is important for the activity of lysozyme. The far-UV CD spectra in Figure 58a indicate an increase in the α-helical content (% RHC = 108.85 %) of lysozyme in the spray-dried powders when compared with the starting material (Table 39). An increase in the molar ellipticity might be described with a shift of the

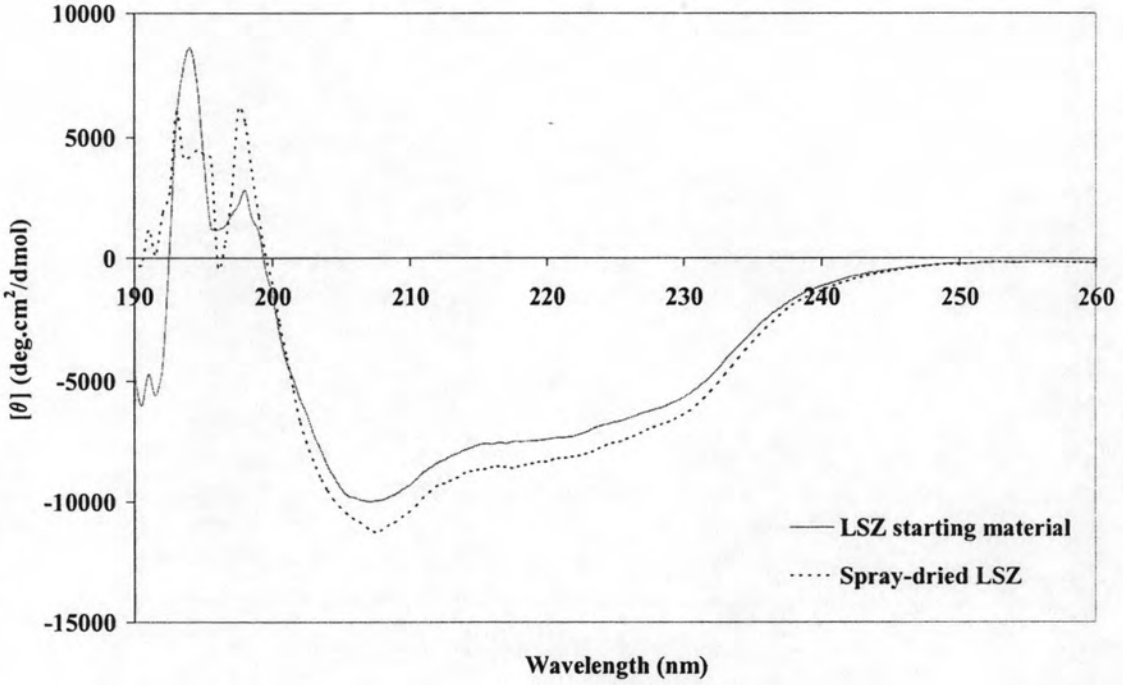

(a)

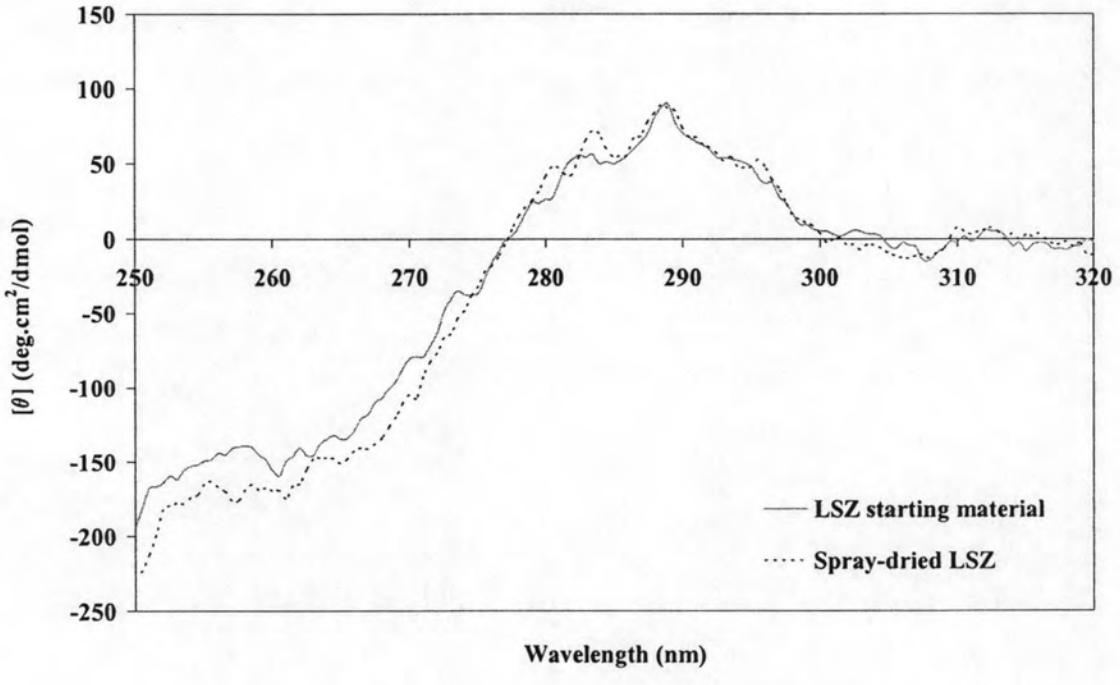

(b)

Figure 58 Circular dichroism spectra of the lysozyme starting material and the spray-dried lysozyme in the (a) far- and (b) near-UV regions

Table 39 Molar ellipticity at 222 nm and % α-helix of the lysozyme starting material and the spray-dried lysozyme (mean ± SD, n = 3)

	$[\theta]_{222}$	% α-helix
LSZ starting material	-7303.47 ± 23.18	26.42 ± 0.06
Spray-dried LSZ	-8215.37 ± 65.67	28.76 ± 0.17
% Relative α–helical content	-	108.85 %

native-state to more ordered and compact protein conformations without detectable changes in the secondary structure (Kim et al., 2003). The increased α–helix content of the spray-dried lysozyme did not have any impact on the active site of lysozyme as observed with the biological activity assay in Table 38. There was no significant change in the tertiary structure of the spray-dried lysozyme compared to the starting material as shown in the near-UV CD spectra in Figure 58b.

7.3.4 FT-Raman Spectroscopy

FT-Raman spectroscopy is a valuable tool for the investigation of peptide backbone conformation and protein secondary structure (Elkordy et al., 2002; Elkordy, Forbes, and Barry, 2004; Quinn et al., 1999). Vibrations of the peptide bond ('CONH') are termed 'amide' vibrations. The secondary structure of a protein can be determined by analysis of the amide band shape and position. Therefore, the conformation integrities of lysozyme in the starting material and the spray-dried powders were examined by comparison of FT-Raman spectra at amide I (at ~1660 cm^{-1}) for α–helix and III (1220-1300 cm^{-1}) regions which are characteristic of proteins.

Figure 59 displays the spectra of lysozyme in the starting material and the spray-dried powders over 1800-1200 cm^{-1}. Important peak positions are shown in Table 40. The lysozyme starting material was predominantly α–helical in structure as

it had a strong amide I band at ~1659 cm^{-1}. Also, the amide III band was at ~1250 cm^{-1}. The spectrum of the spray-dried lysozyme was similar to that of the starting material. However, there were slight shifts in the amide I band (+1 cm^{-1}) and in the amide III (-1 cm^{-1}) in the spectrum of the spray-dried lysozyme (Table 40) when compared to that of the lysozyme starting material. The small shifts might be due to the sensitivity limitation of the FT-Raman instrument. However, there was a new band at ~1784 cm^{-1} which indicated the presence of aggregation. The peak in the position above 1700 cm^{-1} is rarely seen for proteins and indicates physical instability and aggregation (Souillac, Middaugh, and Rrtting, 2002). Surface denaturation at the air-liquid interface of the spray droplets plays a major role in the aggregation of the protein (Maa and Prestrelski, 2000). Nevertheless, the aggregation of lysozyme was reversible upon reconstitution in diluted solution as determined by the enzymatic activity (Table 39). This finding agrees with a previous study by Jovanovic et al. (2008). However, biological enzymatic activity was the method widely used for investigation of lysozyme stability during various processes (Elkordy, Forbes, and Barry, 2004; Hulse et al., 2008).

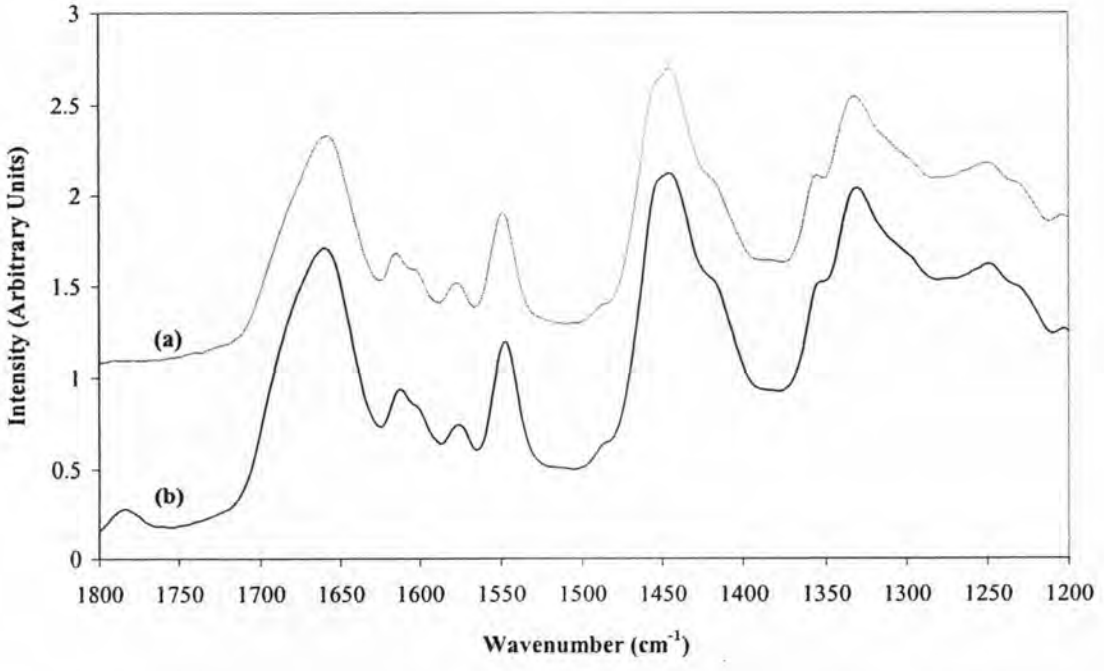

Figure 59 FT-Raman spectra of (a) the lysozyme starting material and (b) the spray-dried lysozyme in the solid state over 1800-1200 cm^{-1}

Table 40 FT-Raman peaks (cm^{-1}) of amide I and amide III bands for the lysozyme starting material and the spray-dried lysozyme in the solid state

Lysozyme	Amide I	Amide III
The starting material	1659	1250
The spray-dried powders	1660	1249

In addition, FT-Raman spectroscopy was used to characterize the conformational integrity of the lysozyme starting material and the spray-dried lysozyme in aqueous solution (7.5 %w/v) to investigate folding reversibility of the spray-dried lysozyme after reconstitution. As shown in Figure 60 and Table 41, the spectrum of lysozyme in aqueous solution is similar to published data by Elkordy, Forbes, and Barry (2008). There were shifts (+3 cm^{-1}) in amide I band and (+2 cm^{-1}) in amide III band which indicated perturbation of the secondary structure of the spray-dried lysozyme compared to the starting material in concentrated aqueous solution (Elkordy et al., 2004). However, there was no new band in the position above 1700 cm^{-1} as shown in the solid state of the spray-dried lysozyme. This indicated the absence of aggregation of the spray-dried lysozyme after reconstitution with Ultrapure® water at 7.5 %w/v.

In conclusion, the conformational integrity of lysozyme was perturbed after spray drying process as shown by FT-Raman spectroscopy in the solid-state. However, the aggregation of the spray-dried lysozyme was reversible after reconstitution with HBS in diluted solution, giving biological activity close to the starting material. According to circular dichroism spectra, there was not change in the secondary structure of the spray-dried lysozyme in diluted aqueous solution.

For other protein/peptide drugs, stabilizers should be included to improve stability of these drugs during spray drying process. Stabilizers studied widely for protein formulation were carbohydrates such as trehalose which may be combined

with mannitol as co-additives for development of spray-dried protein-loaded liposomal powders. Trehalose can stabilize proteins by a water replacement mechanism (Liao et al., 2002; Michael et al., 2005). It can interact with protein molecules via hydrogen bonding to replace the water-protein interaction.

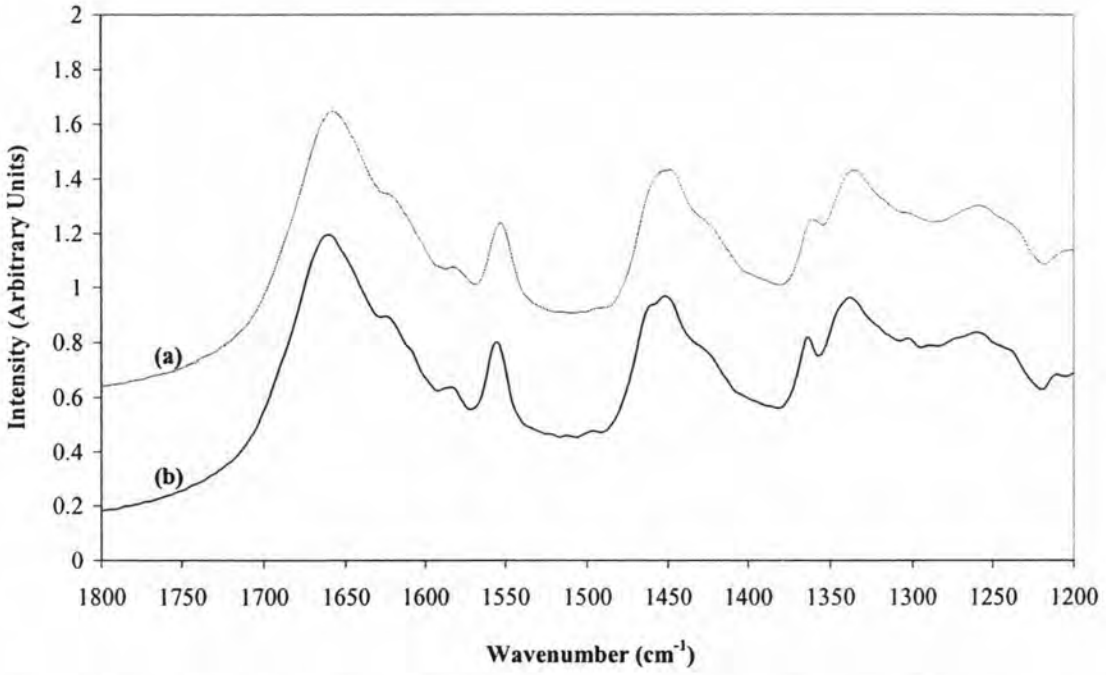

Figure 60 FT-Raman spectra of (a) the lysozyme starting material and (b) the spray-dried lysozyme in aqueous solution (7.5 %w/v) over 1800-1200 cm^{-1}

Table 41 FT-Raman peaks (cm^{-1}) of amide I and amide III bands for the lysozyme starting material and the spray-dried lysozyme in aqueous solution (7.5 %w/v)

Lysozyme	Amide I	Amide III
The starting material	1658	1259
The spray-dried powders	1661	1261

8. Experimental Design of Spray Drying Condition for Lysozyme-Loaded Liposomal Powder Formulation

The formulation composed of HPC/Chol(8:2):M:LSZ (1:1:0.1) was used for evaluation of main effects and interactions of spray drying process factors using a full 2^3 factorial design. The effects of spray drying conditions were investigated on process yield, moisture content, particle size and entrapment efficiency responses. Three center points was added to evaluate possible curvature from second-order effect. Table 42 shows the data of response variables employed to generate the factorial design to assess the effects of spray drying variables. The SEM micrographs in Figure 61 show that all spray-dried formulations studied gave slightly aggregate and rather spherical particles with wide size distribution. The particle sizes depended on the spray-drying conditions. After reconstitution of the powders with HBS at 37 °C, the liposomes were formed spontaneously and very aggregate (Figure 62).

The Design-Expert version 7.1.4 software was employed for statistical analysis of the experimental data. For a single replicate of factorial design, high-order interactions are negligible and only two factor interactions are taken into account to the model (Montgomery, 2005). Half-normal probability plot of the estimates of the effects was constructed to evaluate the important effects. This is a plot of the absolute value of the effect estimates against their cumulative normal probabilities. The effects that are negligible are normally distributed, with mean zero and variance σ^2 and will tend to fall along a straight line on this plot, whereas significant effects will have nonzero means and will not lie along the straight line (Montgomery, 2005). All main effect and interactions were used to compute the initial full model. The F-statistic was calculated for each factor and interaction terms. The *P*-values were used to check the significance of each of the coefficients. The quadratic curvature was tested for significance level at $P < 0.05$.

Table 42 The mean response variables for the 2^3 factorial design (Exp. 1-8) and the center points (Exp. 9-11)

Exp.	Factors			Response variables			
	T (°C)	Pump speed (%)	Total solid content (%)	Yield (%)	Moisture (%w/w)	Particle size* ($D_{0.5}$, μm)	EE (μg LSZ/ mg lipid)
1	110	5	2.975	61.71	3.46	6.13	13.42
2	150	5	2.975	76.68	3.39	8.35	7.64
3	110	15	2.975	56.26	3.12	6.02	15.85
4	150	15	2.975	71.77	3.05	8.05	10.88
5	110	5	8.575	62.06	3.29	7.73	14.29
6	150	5	8.575	66.04	2.43	9.20	9.00
7	110	15	8.575	56.29	3.40	8.61	15.05
8	150	15	8.575	61.5	3.63	9.81	9.92
9	130	10	5.775	65.59	3.01	8.47	13.80
10	130	10	5.775	65.12	3.00	8.39	12.70
11	130	10	5.775	64.58	2.96	8.72	13.43

* Measured by Mastersizer S

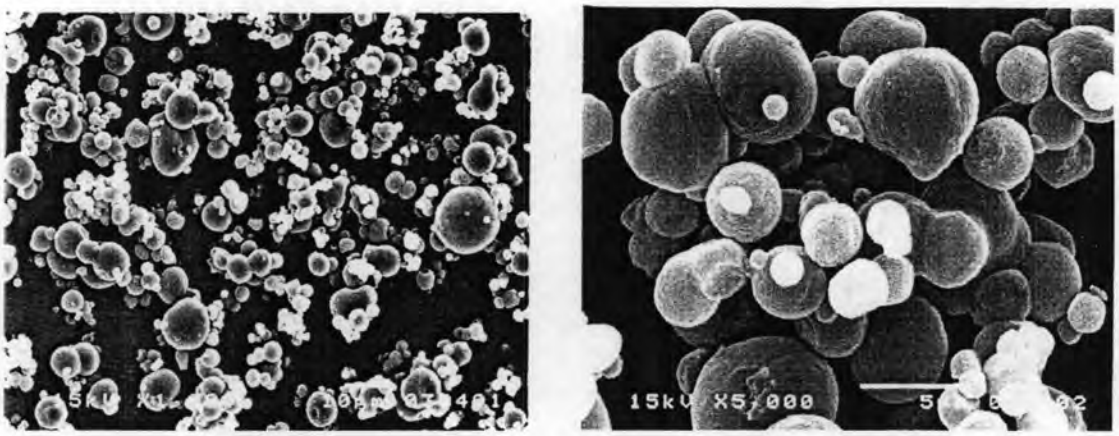

(a) Experiment no. 1: T 110 °C, P 5 %, C 2.975 %w/w

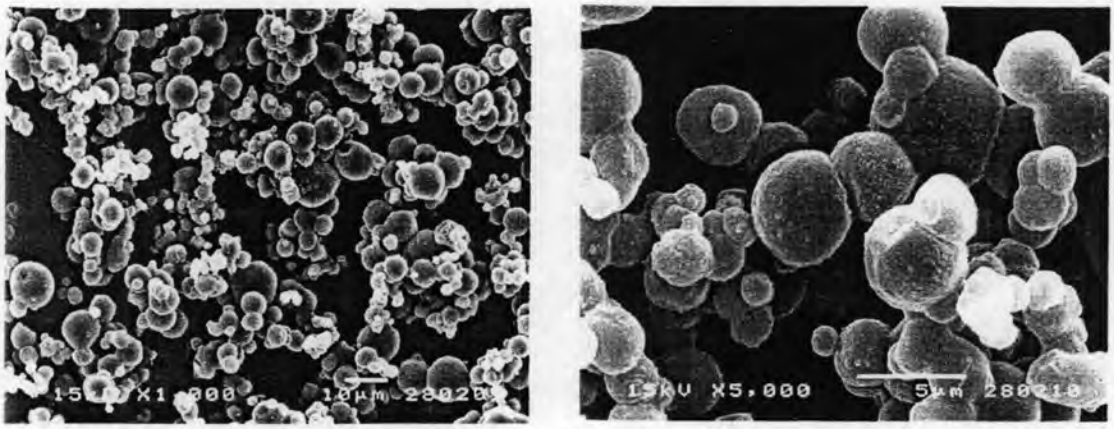

(b) Experiment no. 2: T 150 °C, P 5 %, C 2.975 %w/w

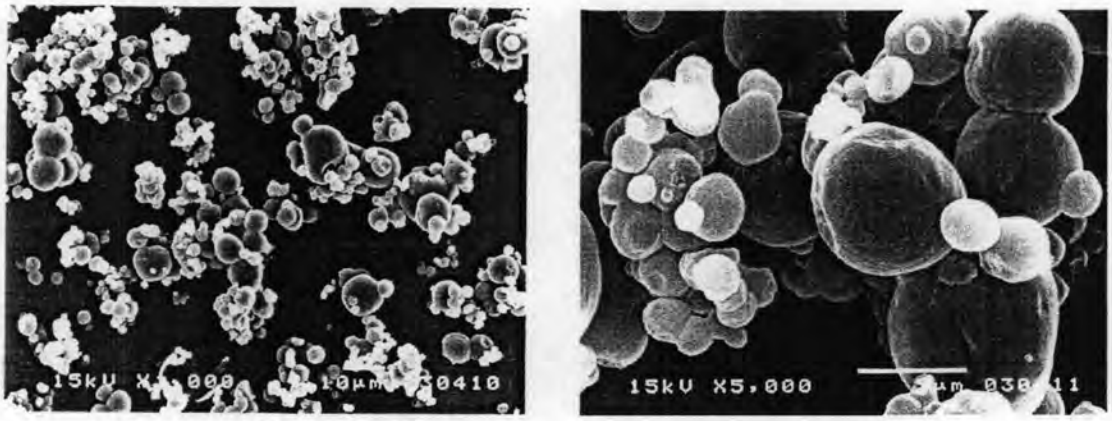

(c) Experiment no. 3: T 110 °C, P 15 %, C 2.975 %w/w

Figure 61 Scanning electron micrographs of the spray-dried powders with HPC/Chol (8/2):M:LSZ (1:1:0.1) for the 2^3 factorial design (Experiment no. 1-8) and the center point (Experiment no. 9-11). On the left side: magnification 1000x and scale bar = 10 µm. On the right side: magnification 5000x and scale bar = 5 µm.

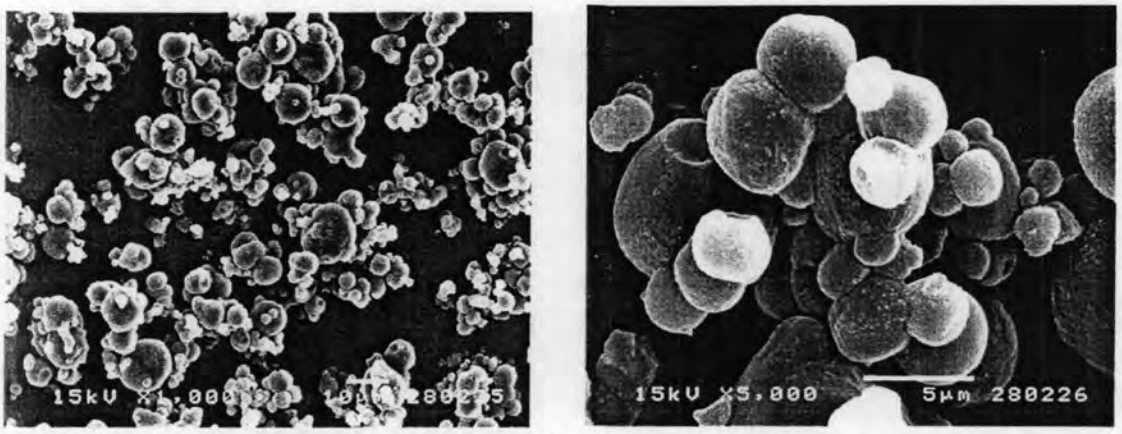

(d) Experiment no. 4: T 150 °C, P 15 %, C 2.975 %w/w

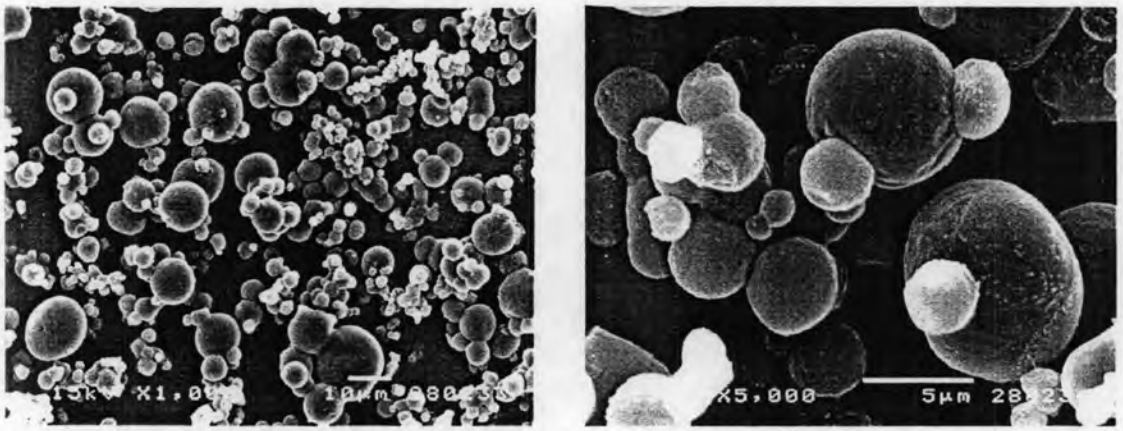

(e) Experiment no. 5: T 110 °C, P 5 %, C 8.575 %w/w

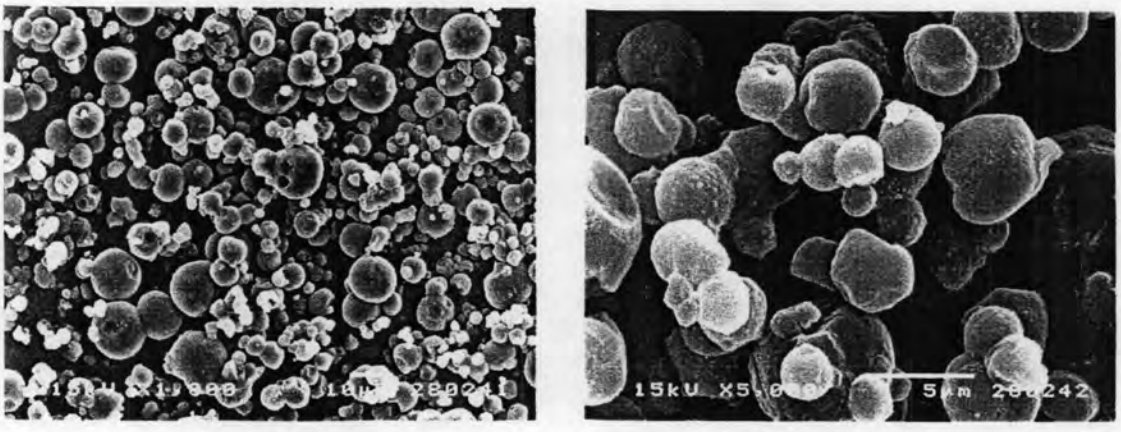

(f) Experiment no. 6: T 150 °C, P 5 %, C 8.575 %w/w

Figure 61 (Continued)

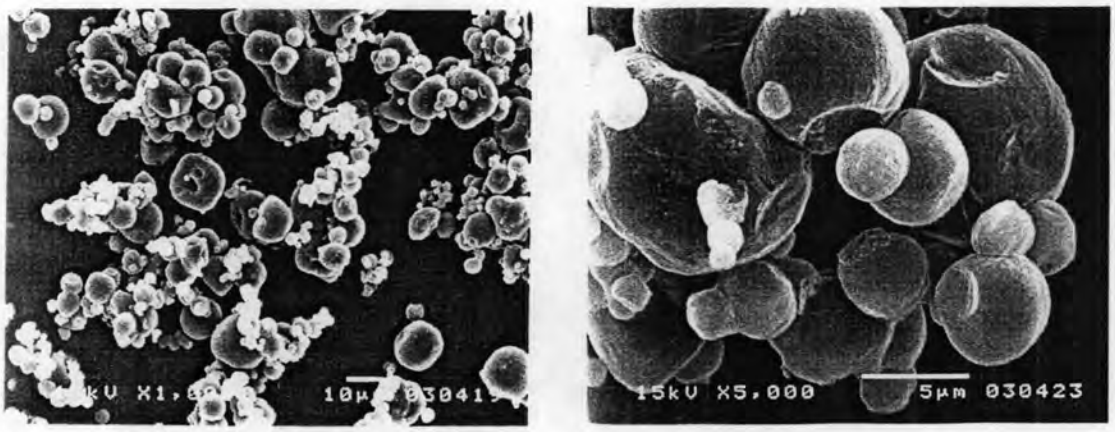

(g) Experiment no. 7: T 110 °C, P 15 %, C 8.575 %w/w

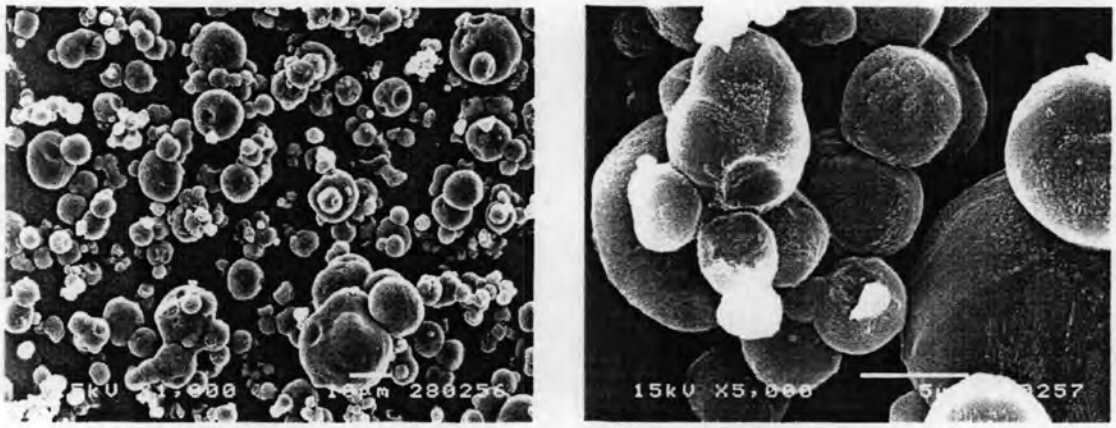

(h) Experiment no. 8: T 150 °C, P 15 %, C 8.575 %w/w

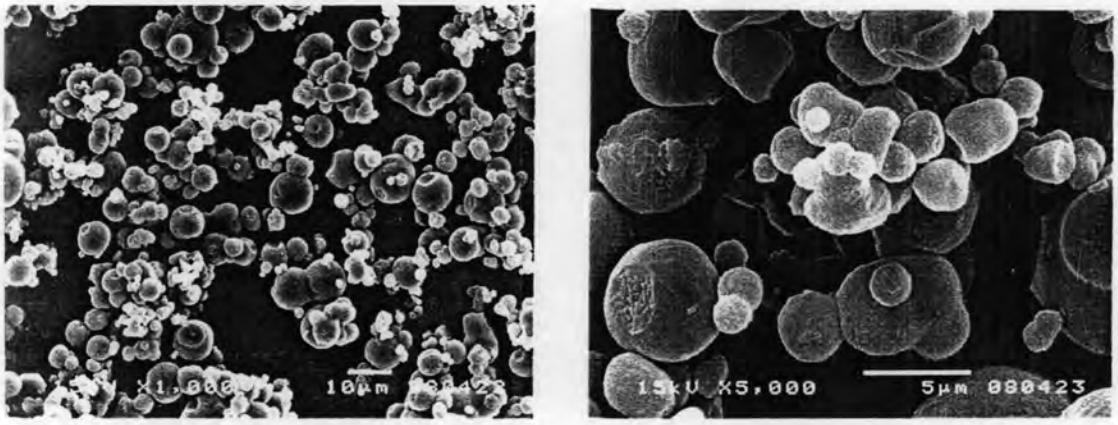

(i) Experiment no. 9: T 130 °C, P 10 %, C 5.775 %w/w

Figure 61 (Continued)

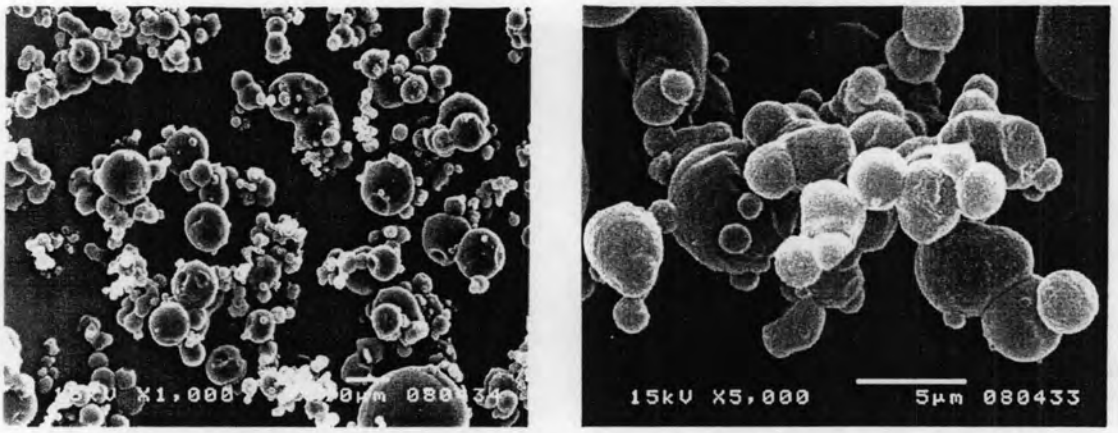

(j) Experiment no. 10: T 130 °C, P 10 %, C 5.775 %w/w

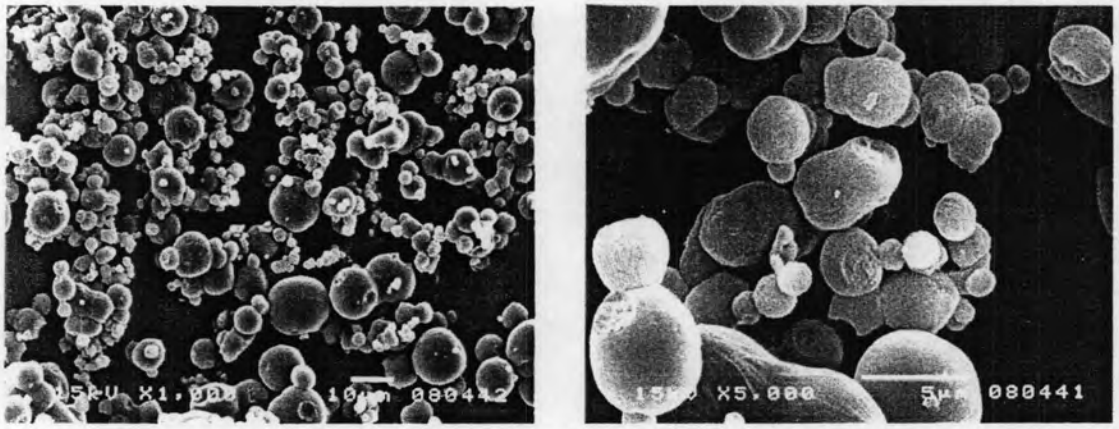

(k) Experiment no. 11: T 130 °C, P 10 %, C 5.775 %w/w

Figure 61 (Continued)

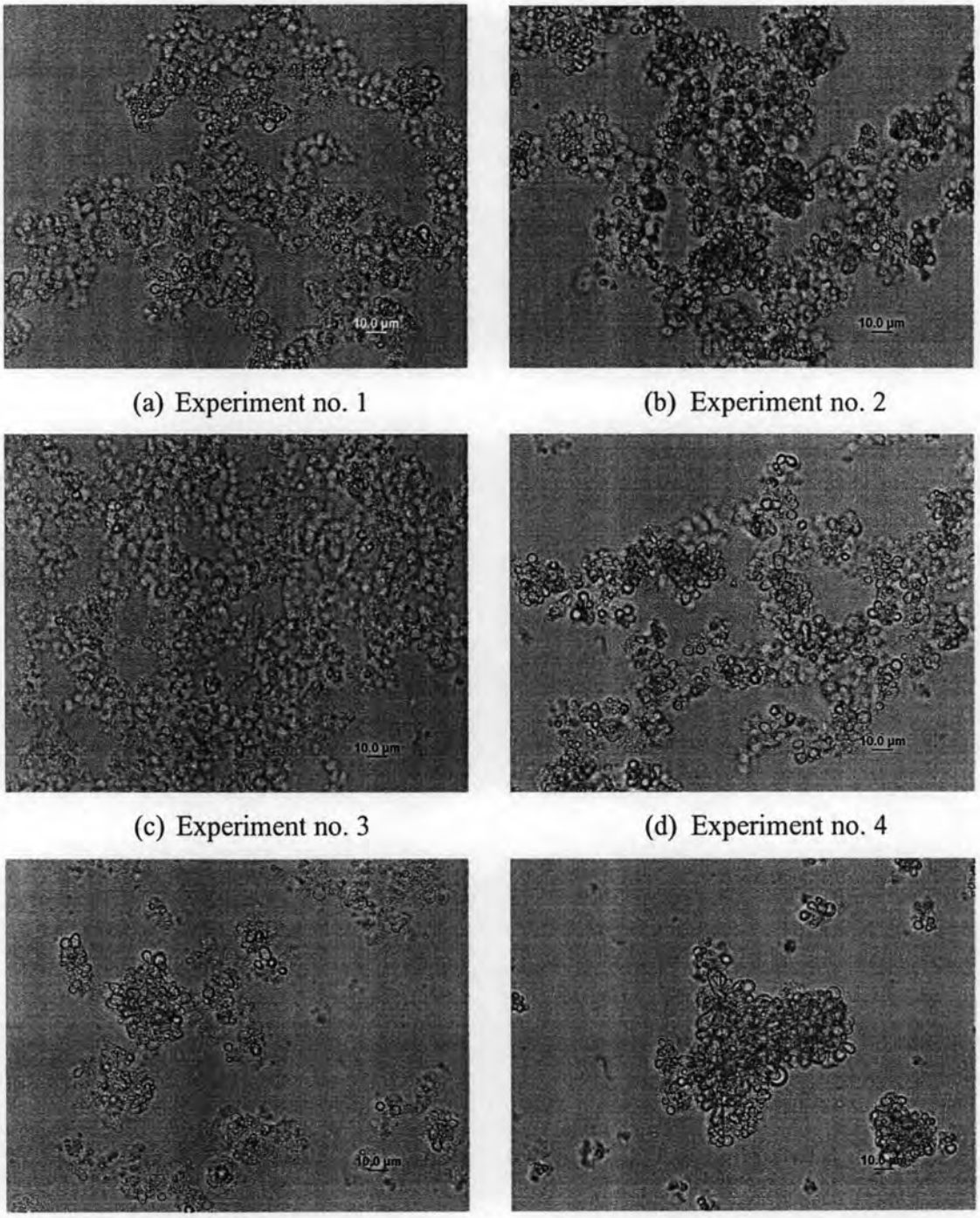

(a) Experiment no. 1 (b) Experiment no. 2

(c) Experiment no. 3 (d) Experiment no. 4

(e) Experiment no. 5 (f) Experiment no. 6

Figure 62 Optical micrographs of the reconstituted liposomes from the spray-dried lysozyme-loaded liposomal powders in HBS at 37 °C for the 2^3 factorial design (Experiment no. 1-8) and the center point (Experiment no. 9-11). Magnification 400x. Scale bar = 10 µm.

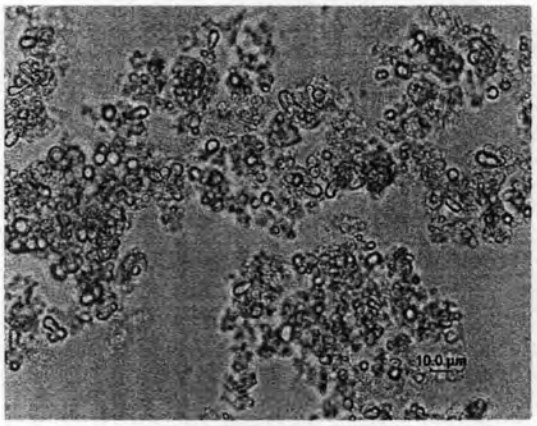

(g) Experiment no. 7

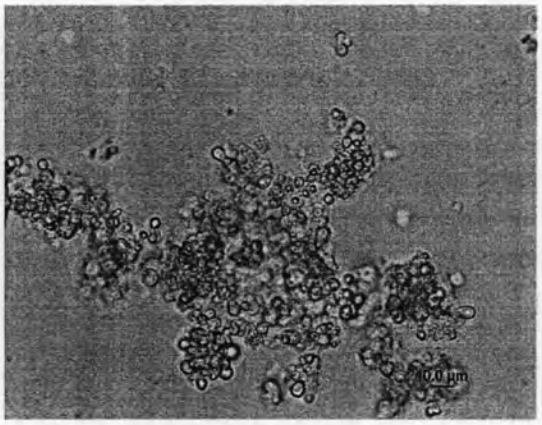

(h) Experiment no. 8

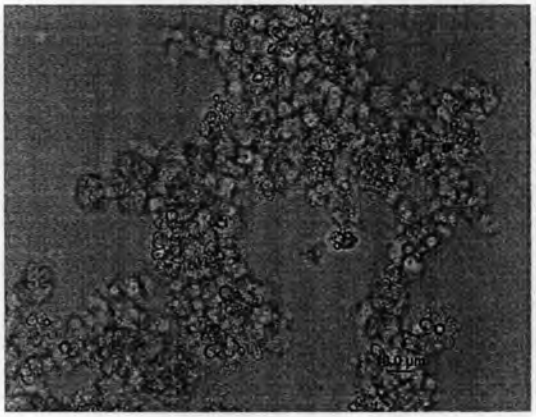

(i) Experiment no. 9

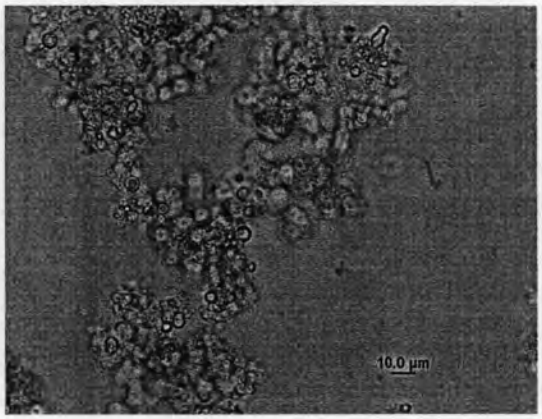

(j) Experiment no. 10

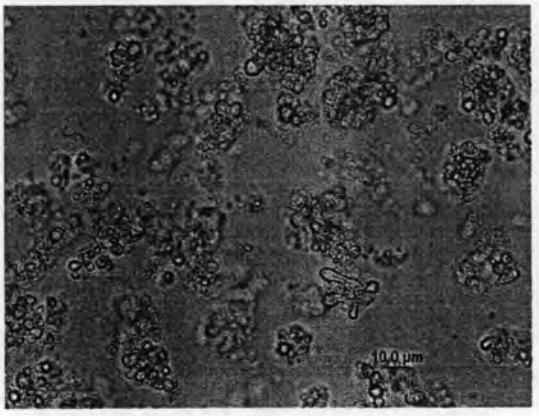

(k) Experiment no. 11

Figure 62 (Continued)

8.1 Fitting of Yield Response to the Factorial Model

Half-normal probability plot of the effects (Figure 63) showed that spray drying process yields were mainly affected by the inlet temperature followed by the pump speed and the total solid content as the estimated contribution of each term reported in Table 43. Moreover, interaction effect of the inlet temperature and the total solid content also played a role on the yield as high contribution value of the AC interaction term (Table 43). ANOVA in Table 44 reports a high significance ($P < 0.01$) of the linear model for yield response as pointed out by large F value. However, the response curvature test presented a significance ($P < 0.05$) which indicated non-linear response. Upon this observation, the study of second order model for yield response was performed by central composite design in the next section.

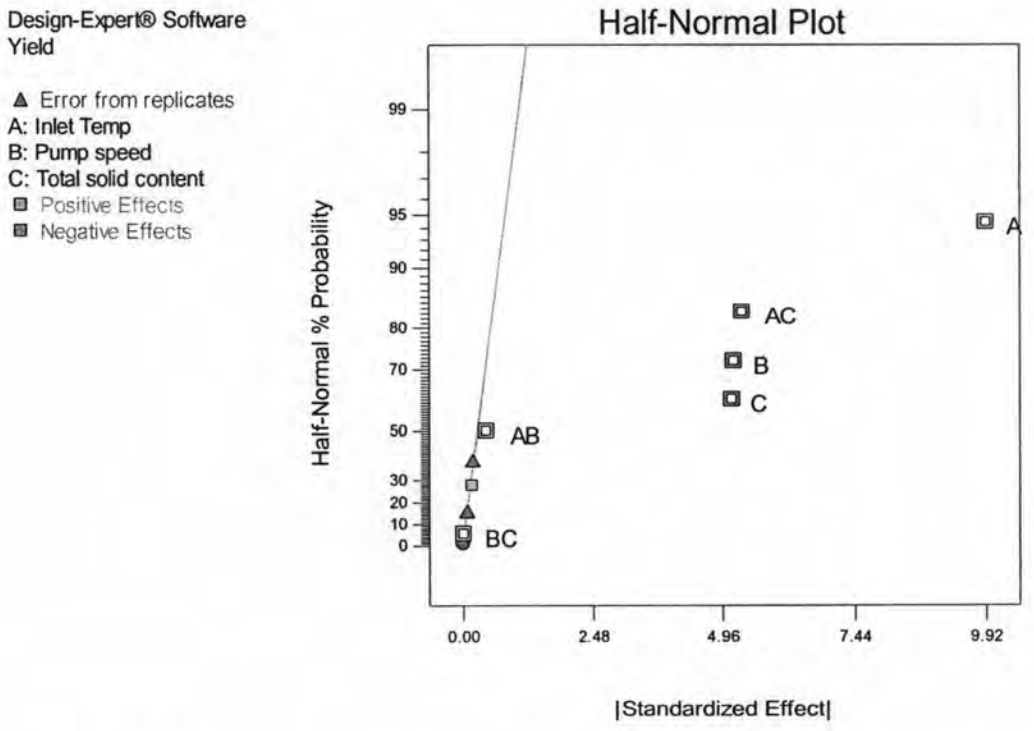

Figure 63 Half-normal probability plot of the effects for yield response in the factorial design

Table 43 Factor effect estimates for yield response in the factorial design

Model term	Effect estimate	% Contribution
A-Inlet temperature (°C)	9.918	54.211
B-Pump speed (%)	-5.168	14.718
C-Total solid content (%w/w)	-5.133	14.519
AB	0.442	0.108
AC	-5.323	15.614
BC	0.012	0.000
ABC	0.173	0.016

Table 44 ANOVA for the selected factorial model of yield response ($R^2 = 0.998$, pred $R^2 = 0.986$)

Source of Variation	df	Sum of Squares	Mean Square	*F* Value	*P*-Value
Model	6	359.855	59.976	315.452	0.0003**
A-Inlet temperature (°C)	1	196.714	196.714	1034.647	0.0001*
B-Pump speed (%)	1	53.406	53.406	280.898	0.0005**
C-Total solid content (%w/w)	1	52.685	52.685	277.106	0.0005**
AB	1	0.392	0.392	2.060	0.2467
AC	1	56.658	56.658	298.002	0.0004**
BC	1	0.000	0.000	0.002	0.9702
Curvature	1	2.442	2.442	12.843	0.0372***
Residual	3	0.570	0.190		
Lack of Fit	1	0.060	0.060	0.233	0.6770
Pure Error	2	0.511	0.255		
Cor Total	10	362.867			

* Significant at $P < 0.0001$

** Significant at $P < 0.01$

*** Significant at $P < 0.05$

8.2 Fitting of Moisture Response to the Factorial Model

The moisture content of the spray-dried liposomal powders obtained in this design ranged between 2.4 to 3.6 %w/w (Table 42). Most studies reported that an increase in inlet temperature and a decrease in feed flow resulted in a decrease in moisture content of spray-dried powders (Broadhead et al., 1994; Stahl et al., 2002). However, the data shown in Figure 64 indicate that moisture content response was not affected by all factor variables as seen from the low contribution values of all terms (Table 45) and insignificant terms in ANOVA Table (Table 46). This may be due to variation of circumstance during spray drying processing or non-hygroscopic property of mannitol resulting in similar moisture content of the powders. Therefore, the moisture content response was not further studied for the optimization of spray drying condition.

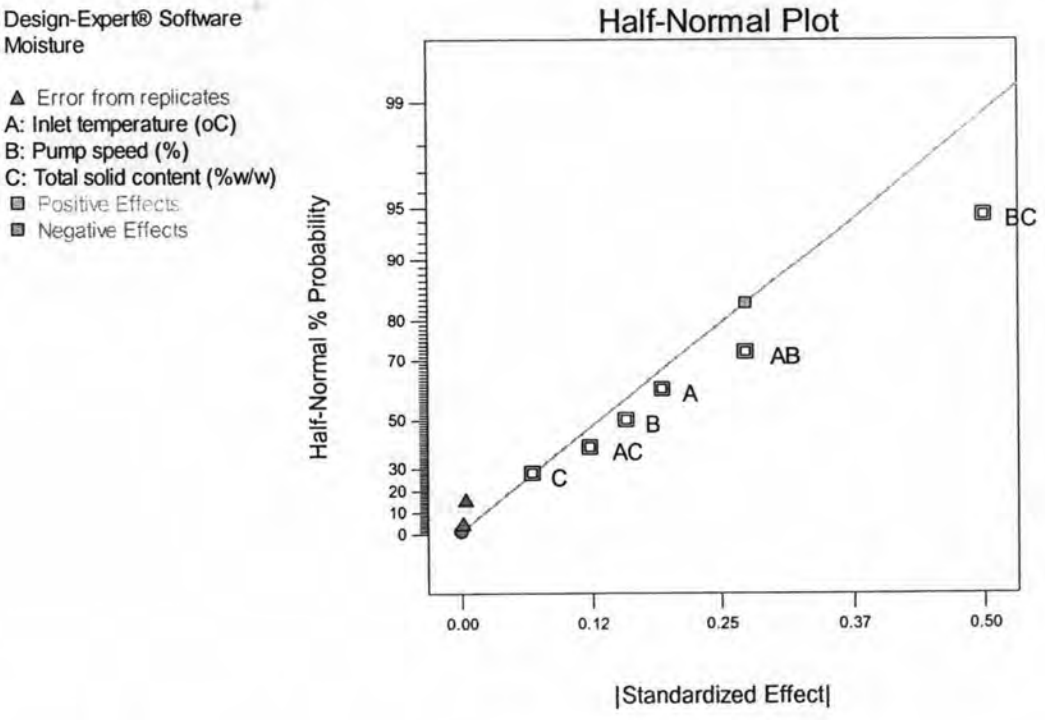

Figure 64 Half-normal probability plot of the effects for moisture response in the factorial design

Table 45 Factor effect estimates for moisture response in the factorial design

Model term	Effect estimate	% Contribution
A-Inlet temperature (°C)	-0.193	6.907
B-Pump speed (%)	0.158	4.624
C-Total solid content (%w/w)	-0.068	0.849
AB	0.273	13.841
AC	-0.123	2.797
BC	0.498	46.135
ABC	0.273	13.841

Table 46 ANOVA for the selected factorial model of moisture response ($R^2 = 0.843$, pred $R^2 = -8.942$)

Source of Variation	df	Sum of Squares	Mean Square	*F* Value	*P*-Value
Model	6	0.806	0.134	2.689	0.2233
A-Inlet temperature (°C)	1	0.074	0.074	1.483	0.3103
B-Pump speed (%)	1	0.050	0.050	0.993	0.3925
C-Total solid content (%w/w)	1	0.009	0.009	0.182	0.6981
AB	1	0.149	0.149	2.972	0.1832
AC	1	0.030	0.030	0.601	0.4948
BC	1	0.495	0.495	9.906	0.0514
Curvature	1	0.117	0.117	2.335	0.2240
Residual	3	0.150	0.050		
Lack of Fit	1	0.149	0.149	212.161	0.0047*
Pure Error	2	0.001	0.001		
Cor Total	10	1.073			

* Significant at $P < 0.01$

8.3 Fitting of Particle Size Response to the Factorial Model

Half-normal probability plot in Figure 65 shows that the particle size response was mainly affected by the inlet temperature and the total solid content variations. The estimated contribution showed an equal influence of the inlet temperature and the total solid content (Table 47). ANOVA for the first order model of particle size response showed a high significance ($P < 0.01$) (Table 48). However, the model presented the significant quadratic curvature ($P < 0.05$). The second order model for particle size response was further studied by performing central composite design.

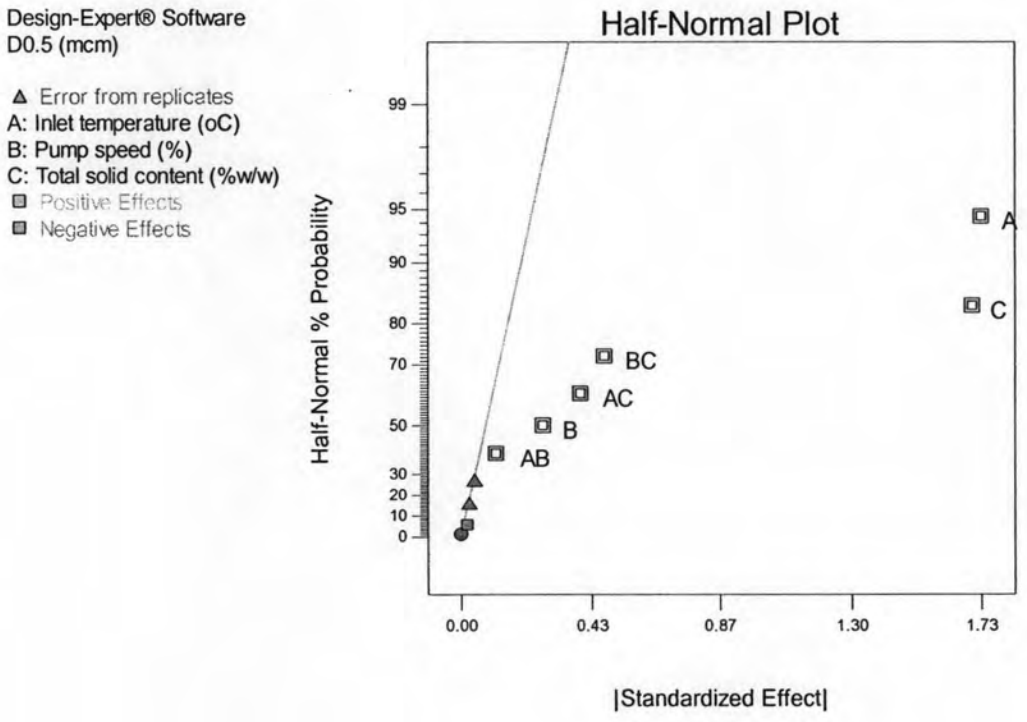

Figure 65 Half-normal probability plot of the effects for particle size response in the factorial design

Table 47 Factor effect estimates for particle size response in the factorial design

Model term	Effect estimate	% Contribution
A-Inlet temperature (°C)	1.730	44.685
B-Pump speed (%)	0.270	1.088
C-Total solid content (%w/w)	1.700	43.148
AB	-0.115	0.197
AC	-0.395	2.329
BC	0.475	3.369
ABC	-0.020	0.006

Table 48 ANOVA for the selected factorial model of particle size response (R^2 = 0.995, pred R^2 = 0.986)

Source of Variation	df	Sum of Squares	Mean Square	*F* Value	*P*-Value
Model	6	12.701	2.117	105.727	0.0014*
A-Inlet temperature (°C)	1	5.986	5.986	298.958	0.0004*
B-Pump speed (%)	1	0.146	0.146	7.282	0.0739
C-Total solid content (%w/w)	1	5.780	5.780	288.679	0.0004*
AB	1	0.026	0.026	1.321	0.3337
AC	1	0.312	0.312	15.585	0.0290**
BC	1	0.451	0.451	22.537	0.0177**
Curvature	1	0.634	0.634	31.678	0.0111**
Residual	3	0.060	0.020		
Lack of Fit	1	0.001	0.001	0.027	0.8846
Pure Error	2	0.059	0.030		
Cor Total	10	13.396			

* Significant at $P < 0.01$

** Significant at $P < 0.05$

8.4 Fitting of Entrapment Efficiency Response to the Factorial Model

The entrapment efficiency of lysozyme in the reconstituted liposomes was mainly affected by the inlet temperature followed by the pump speed as shown in Figure 66 and Table 49. ANOVA in Table 50 shows a high significance ($P < 0.01$) of the model for the entrapment efficiency response. Nevertheless, the model presented the significant quadratic curvature ($P < 0.05$). Therefore, the central composite design was further performed for the entrapment efficiency response.

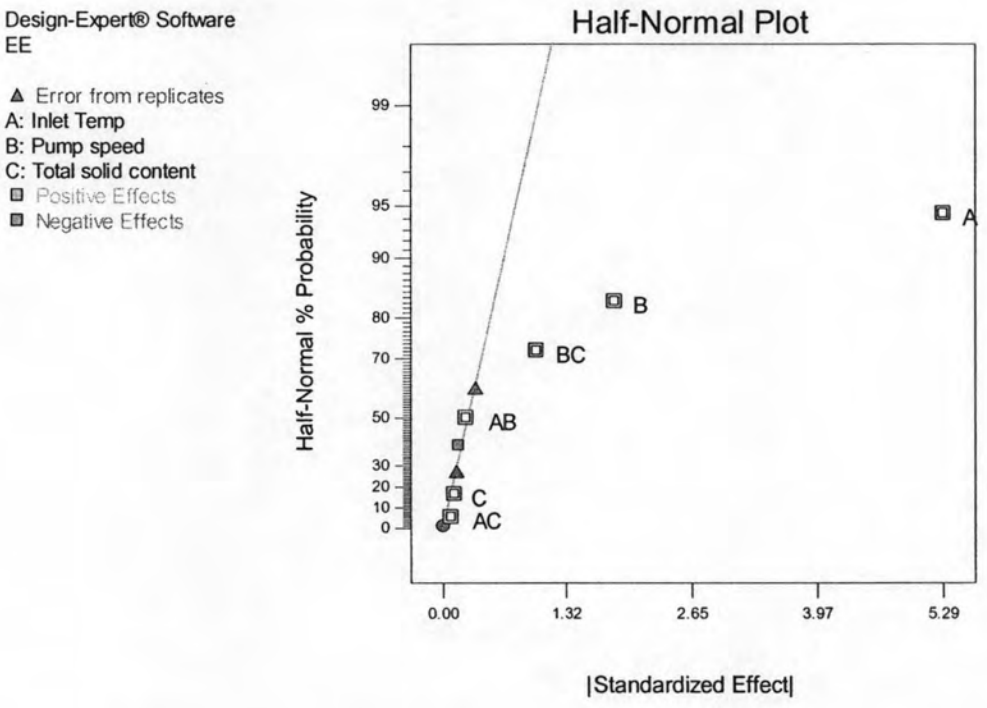

Figure 66 Half-normal probability plot of the effects for entrapment efficiency response of the factorial design

Table 49 Factor effect estimates for entrapment efficiency response in the factorial design

Model term	Effect estimate	% Contribution
A-Inlet temperature (°C)	-5.293	80.826
B-Pump speed (%)	1.838	9.743
C-Total solid content (%w/w)	0.118	0.040
AB	0.243	0.170
AC	0.083	0.020
BC	-0.998	2.871
ABC	-0.163	0.076

Table 50 ANOVA for the selected factorial model of entrapment efficiency response ($R^2 = 0.990$, pred $R^2 = 0.927$)

Source of Variation	df	Sum of Squares	Mean Square	*F* Value	*P*-Value
Model	6	64.923	10.820	47.779	0.0046*
A-Inlet temperature (°C)	1	56.021	56.021	247.366	0.0006*
B-Pump speed (%)	1	6.753	6.753	29.818	0.0121**
C-Total solid content (%w/w)	1	0.028	0.028	0.122	0.7500
AB	1	0.118	0.118	0.519	0.5232
AC	1	0.014	0.014	0.060	0.8221
BC	1	1.990	1.990	8.787	0.0593
Curvature	1	3.709	3.709	16.376	0.0272**
Residual	3	0.679	0.226		
Lack of Fit	1	0.053	0.053	0.169	0.7212
Pure Error	2	0.627	0.313		
Cor Total	10	69.311			

* Significant at $P < 0.01$

** Significant at $P < 0.05$

9. Central Composite Design: Effects of Spray Drying Conditions on Yield, Particle Size and Entrapment Efficiency Responses

The linear regression models of yield, particle size and entrapment efficiency responses showed the significant curvature, therefore, the central composite design were built. Six experiments including axial points were added to the experimental design. Table 51 shows the response data of the axial points. The morphological characteristics of the spray-dried liposomal powders and the reconstituted liposomes are illustrated in Figures 67 and 68, respectively.

Quadratic regression model fitting was done using Design-Expert 7.1.4 software. ANOVA was performed to determine the significance of the full model, each factor and interaction terms. The coefficient estimates of each term for the quadratic model were calculated for each response linking to the experimental factors and interactions. The signs in front of the coefficient estimates are interpreted as follows: a positive sign means that an increase in the variable value is followed by an increase in the response value. On the contrary, when the sign is negative, an increase in the variable value results in a decrease in the response value (Montgomery, 2005). After that, the insignificant terms were eliminated from the full model using backward elimination regression with alpha to exit = 0.05. Romoving the insignificant terms has produced a final model that is likely to function more effectively as a predictor of new data (Montgomery, 2005).

Residual analysis was used to check normality assumptions and model adequacy (Montgomery, 2005). A normal probability plot of the residuals shows that if the underlying error distribution is normal, this plot will resemble a straight line. A plot of the residuals versus the predicted values shows that if the model is adequate, the residuals should be structureless (no obvious patterns). Quadratic polynomial equations were generated to establish the relationship between the factors and the responses. Adequate models were accepted at no lack of fit ($P > 0.05$), regression model test ($P < 0.05$), high and similar goodness of fit (R^2) and prediction estimates (pred R^2), which are ideally above 0.9 and 0.7, respectively (Stahl et al., 2002). The

R^2 measures percent of total variability explained by the model in the response data. The pred R^2 indicates percent of the variability explained by the full model in new data (Montgomery, 2005).

Table 51 Mean response variables of the axial points for central composite design

Exp.	Factors			Response variables			
	T (°C)	P (%)	C (%)	Yield (%)	Moisture (%w/w)	Particle size* ($D_{0.5}$, μm)	EE (μg LSZ/ mg lipid)
12	96	10	5.775	51.18	4.18	4.69	16.02
13	164	10	5.775	65.65	2.97	8.57	7.13
14	130	2	5.775	75.47	2.77	8.70	9.09
15	130	18	5.775	70.97	3.28	8.57	11.98
16	130	10	1.05	60.75	3.14	6.17	14.53
17	130	10	10.5	61.16	3.19	10.17	14.30

* Measured by Mastersizer S

9.1 Fitting of Yield Data to the Quadratic Model

The yields varied between 51.18 and 76.68 % (Tables 42 and 51). ANOVA in Table 52 shows a high significance ($P < 0.01$) of the quadratic model for yield response. However, the lack of fit of this model was significant ($P < 0.05$). Insignificant lack of fit is good (Montgomery, 2005). After removing the insignificant terms, ANOVA (Table 53) for the reduced quadratic model of yield response showed insignificant lack of fit ($P = 0.0554$). Table 53 indicates that the process yield obtained depended on all spray drying variables. It was mainly influenced by the inlet temperature ($P < 0.0001$) followed by the pump speed ($P < 0.01$), the total solid content ($P < 0.05$) and the interaction between the inlet temperature and the total solid content ($P < 0.01$).

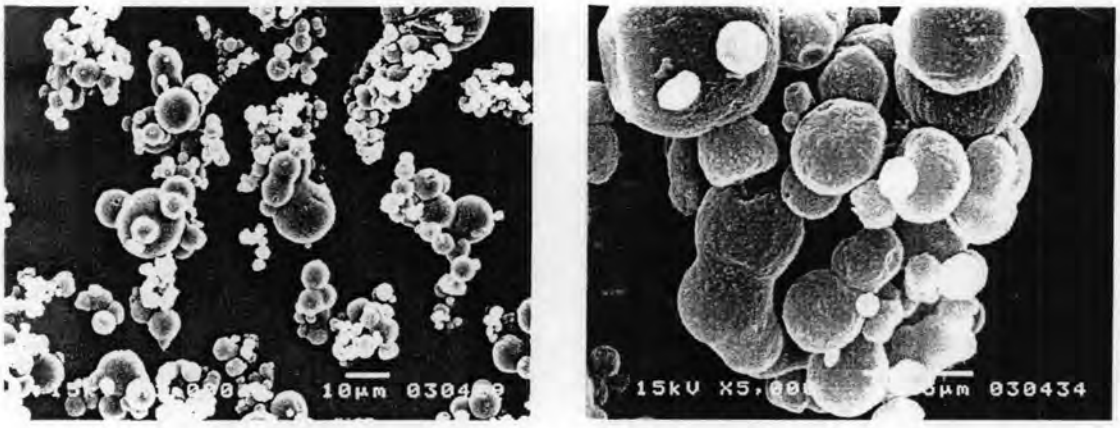

(a) Experiment no. 12: T 96 °C, P 10 %, C 5.775 %w/w

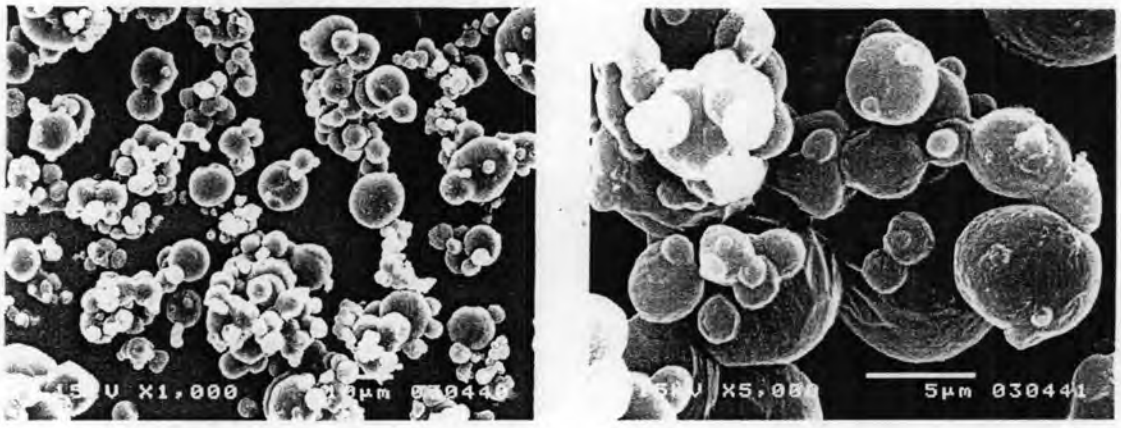

(b) Experiment no. 12: T 164 °C, P 10 %, C 5.775 %w/w

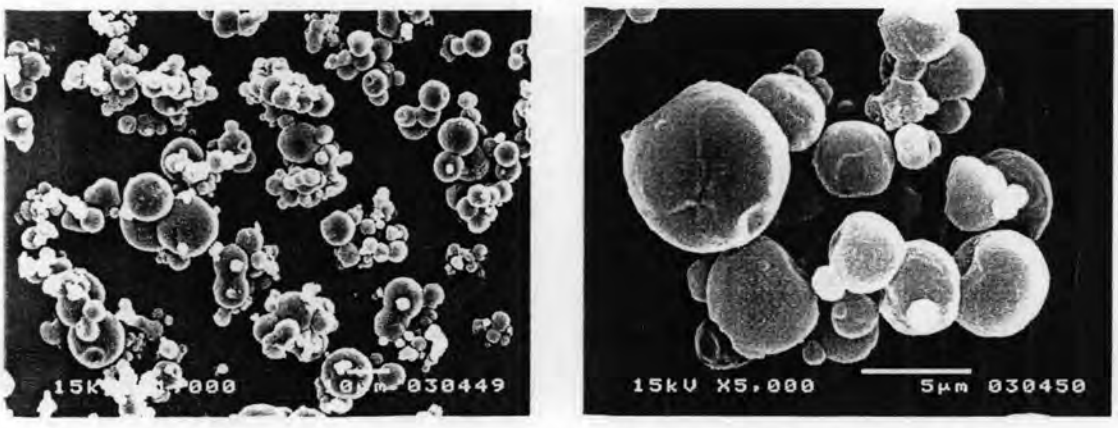

(c) Experiment no. 12: T 130 °C, P 2 %, C 5.775 %w/w

Figure 67 Scanning electron micrographs of the spray-dried powders containing HPC/Chol(8:2):M:LSZ (1:1:0.1) for the axial points in the central composite design. On the left side: magnification 1000x and scale bar = 10 µm. On the right side: magnification 5000x and scale bar = 5 µm.

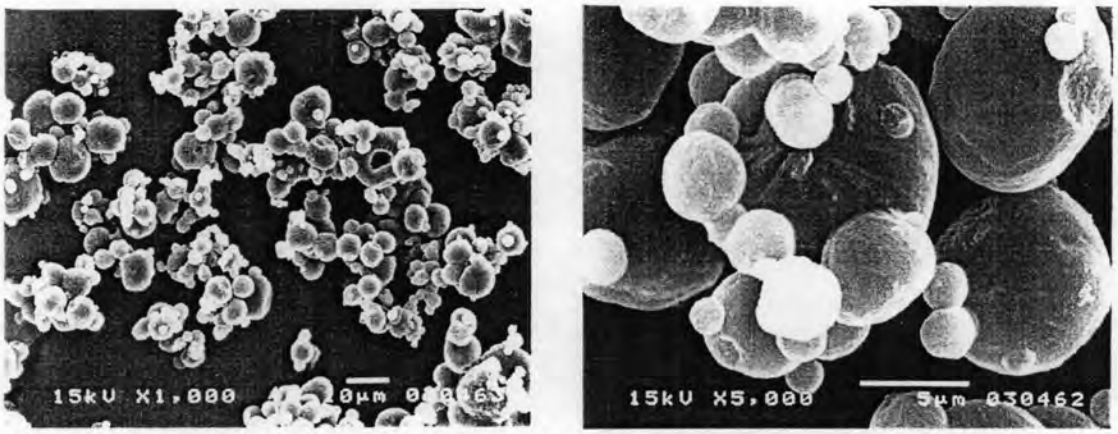

(d) Experiment no. 12: T 130 °C, P 18 %, C 5.775 %w/w

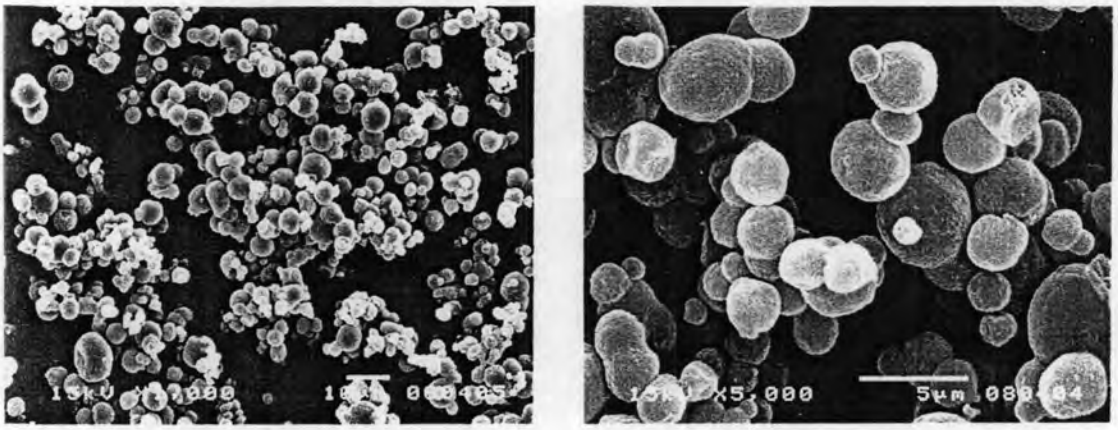

(e) Experiment no. 12: T 130 °C, P 10 %, C 1.05 %w/w

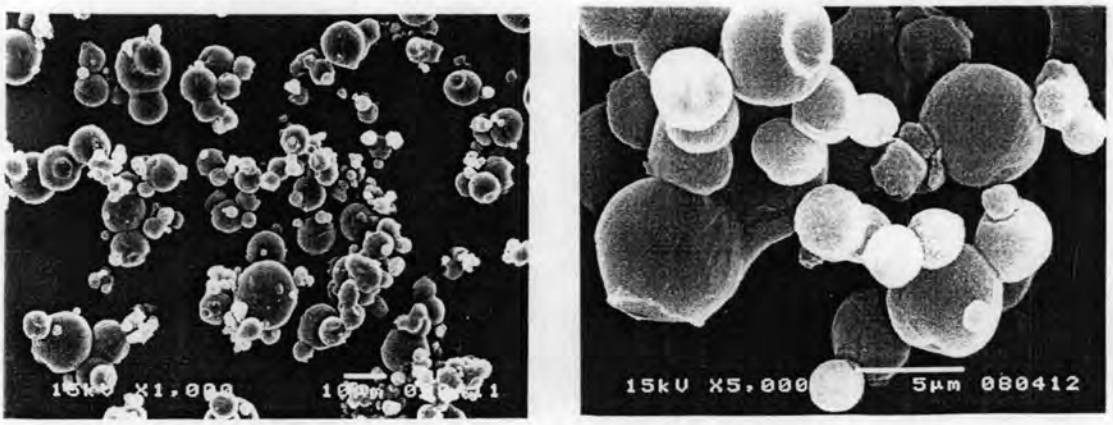

(f) Experiment no. 12: T 130 °C, P 10 %, C 10.5 %w/w

Figure 67 (Continued)

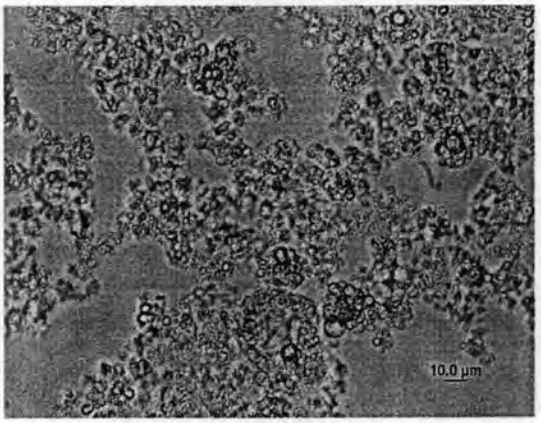

(b) Experiment no. 12

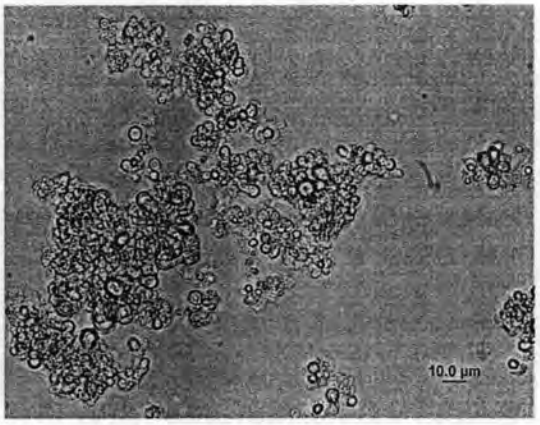

(b) Experiment no. 13

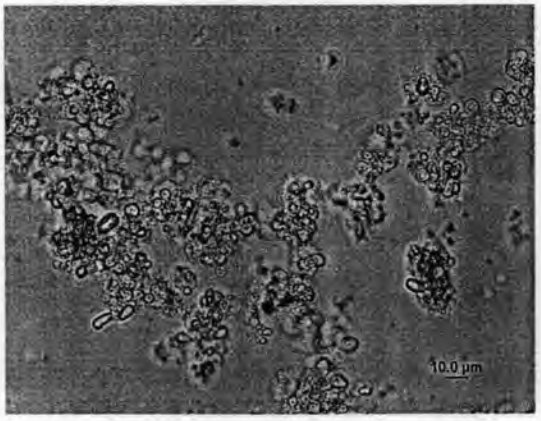

(d) Experiment no. 14

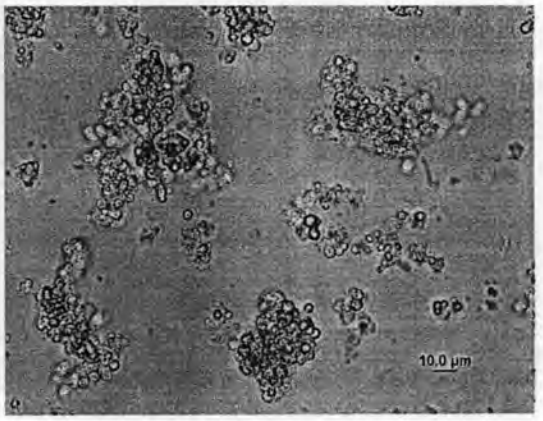

(d) Experiment no. 15

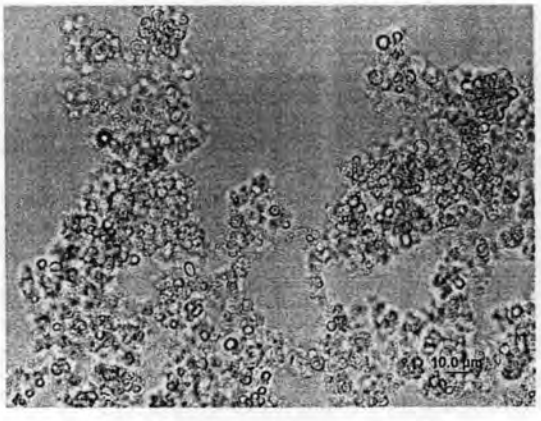

(f) Experiment no. 16

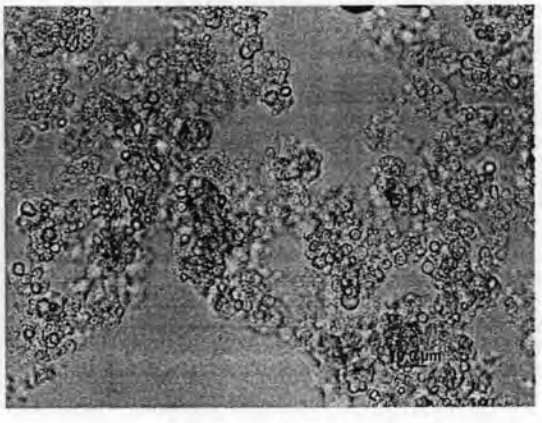

(f) Experiment no. 17

Figure 68 Optical micrographs of the reconstituted liposomes from the spray-dried liposomal powders in HBS at 37 °C for the axial points in the central composite design. Magnification 400x. Scale bar = 10 µm.

Table 52 ANOVA for the quadratic model of yield response (R^2 = 0.957, pred R^2 = 0.673)

Source of Variation	df	Sum of Squares	Mean Square	*F* Value	*P*-Value
Model	9	697.293	77.477	17.353	0.0005**
A-Inlet temperature (°C)	1	299.746	299.746	67.136	0.0001*
B-Pump speed (%)	1	59.203	59.203	13.260	0.0083**
C-Total solid content (%w/w)	1	28.736	28.736	6.436	0.0388***
AB	1	0.392	0.392	0.088	0.7757
AC	1	56.658	56.658	12.690	0.0092**
BC	1	0.000	0.000	0.000	0.9936
A^2	1	68.668	68.668	15.380	0.0057**
B^2	1	89.751	89.751	20.102	0.0029**
C^2	1	27.915	27.915	6.252	0.0410***
Residual	7	31.253	4.465		
Lack of Fit	5	30.742	6.148	24.071	0.0404***
Pure Error	2	0.511	0.255		
Cor Total	16	728.546			

* Significant at $P < 0.0001$

** Significant at $P < 0.01$

*** Significant at $P < 0.05$

The normal probability plot of the residuals to check the violation of normality assumption revealed no serious violation as shown in Figure 69a. The plot of the residuals versus the fitted values for the yield data did not reveal any obvious pattern which indicated adequacy of the model (Figure 69b). Therefore, the reduced quadratic model (equation 17) could be useful in predicting trends for yield as a function of the spray drying conditions.

Table 53 ANOVA for the reduced quadratic model of yield response (R^2 = 0.957, pred R^2 = 0.783)

Source of Variation	df	Sum of Squares	Mean Square	*F* Value	*P*-value
Model	7	696.901	99.557	28.314	0.0001*
A-Inlet temperature (°C)	1	299.746	299.746	85.249	0.0001*
B-Pump speed (%)	1	59.203	59.203	16.837	0.0027**
C-Total solid content (%w/w)	1	28.736	28.736	8.173	0.0188***
AC	1	56.658	56.658	16.114	0.0030**
A^2	1	68.668	68.668	19.529	0.0017**
B^2	1	89.751	89.751	25.526	0.0007**
C^2	1	27.915	27.915	7.939	0.0201***
Residual	9	31.645	3.516		
Lack of Fit	7	31.134	4.448	17.413	0.0554
Pure Error	2	0.511	0.255		
Cor Total	16	728.546			

* Significant at $P < 0.0001$

** Significant at $P < 0.01$

*** Significant at $P < 0.05$

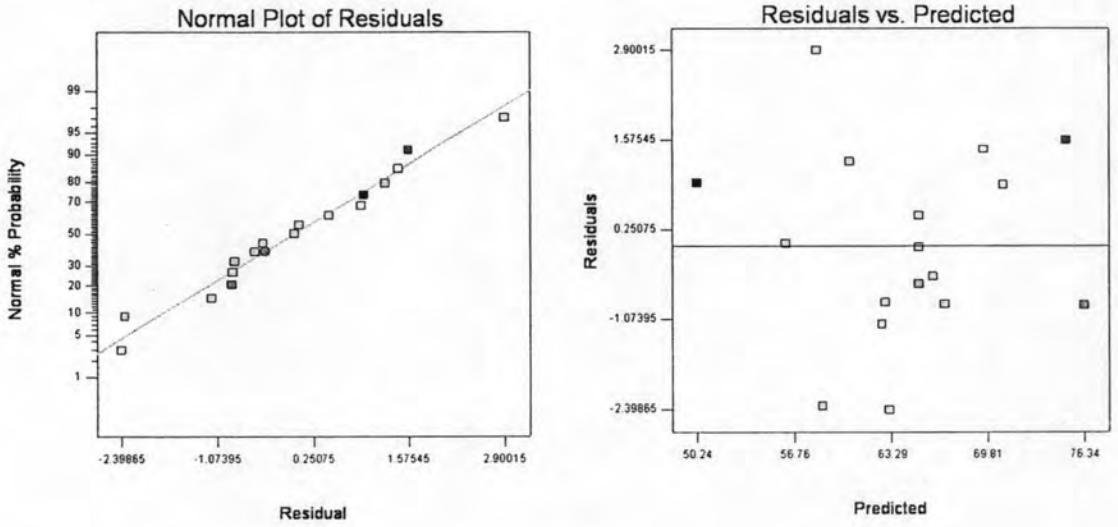

(a) (b)

Figure 69 Residual analysis for the reduced quadratic model of yield response: (a) Normal probability versus residuals and (b) Residuals versus predicted values

The reduced quadratic model for yield response in terms of actual factors was described by equation 17:

$$\text{Yield (\%)} = -89.956 + 2.075(T) - 2.863(P) + 7.955(C) - 0.048(T*C) - 0.006(T)^2 + 0.122(P)^2 - 0.199(C)^2 \quad (17)$$

where T is inlet temperature (°C), P is pump speed (%) and C is total solid content (%w/w). The R^2 value of the reduced quadratic model of yield response was 0.957. This indicated that three variable factors altogether would explain about 95.7 % of the variability in the responses whereas about 4.3 % of the variability in the responses remained to be unexplained. The reduced quadratic model showed prediction (pred) R^2 value of 0.783. The reduced model would be expected to explain about 78.3 % of the variability in new data. The low pred R^2 value may be due to the unusual values of the yield data at experiments no. 7, 16, and 17. However, the model with the pred R^2 value above 0.7 was the acceptable model.

Table 54 and Figure 70 show that the process yield could be increased with an increase in the inlet temperature, a decrease in the pump speed and a decrease in the total solid content when the other two factors was fixed at medium (0) level. The interaction between inlet temperature and total solid content is presented in Figure 70. The relationship between the factors and the responses was further elucidated using contour and response surface plots (Figures 71 and 72, respectively). Contour plots of yield response were obtained by fixing the factor C (total solid content) at its low (-1) (Figure 71a) and high (+1) (Figure 71b) levels. The inlet temperature and pump speed were varied over the range used in the factorial design. Factors A and B were varied because they showed pronounced influence on the yield response. The yield response increased because increased inlet temperature and decreased feed rate allowed complete drying of droplets due to increased outlet temperature. This result agrees well with previous reports (Broadhead et al., 1994; Billon et al., 2000). Broadhead et al. (1994) also showed that the highest yields were obtained from the batches with the lowest moisture content. This result was not evident in this present study over an inlet temperature range of 110-150 °C. An increase in inlet temperature

improved yields to a greater extent when total solid content was low (Figures 70d and 71a). Low total solid content required more thermal energy to ensure the complete evaporation of the solvent, the energy for which was supplied by the inlet temperature. At the low inlet temperature, increasing the total solid content resulted in an increase in the yield (Figure 70d). This may be because increasing total solid content resulted in an increase in size of the dried particles, making them more easily captured through the centrifugal force in the cyclone (Prinn, Costantino, and Tracy, 2002).

Table 54 Coefficient estimate of the quadratic model for yield, particle size and entrapment efficiency (EE) responses

Factor term	**Coefficient estimate**		
	Yield	**Particle size**	**EE**
Intercept	65.138	8.509	13.311
A-Inlet temperature (°C)	4.664	0.981	-2.633
B-Pump speed (%)	-2.124	0.066	0.913
C-Total solid content (%w/w)	-1.449	0.989	0.006
AB	0.221	-0.058	0.121
AC	-2.661	-0.198	0.041
BC	0.006	0.238	-0.499
A^2	-2.412	-0.613	-0.602
B^2	3.048	0.096	-1.086
C^2	-1.557	-0.081	0.386

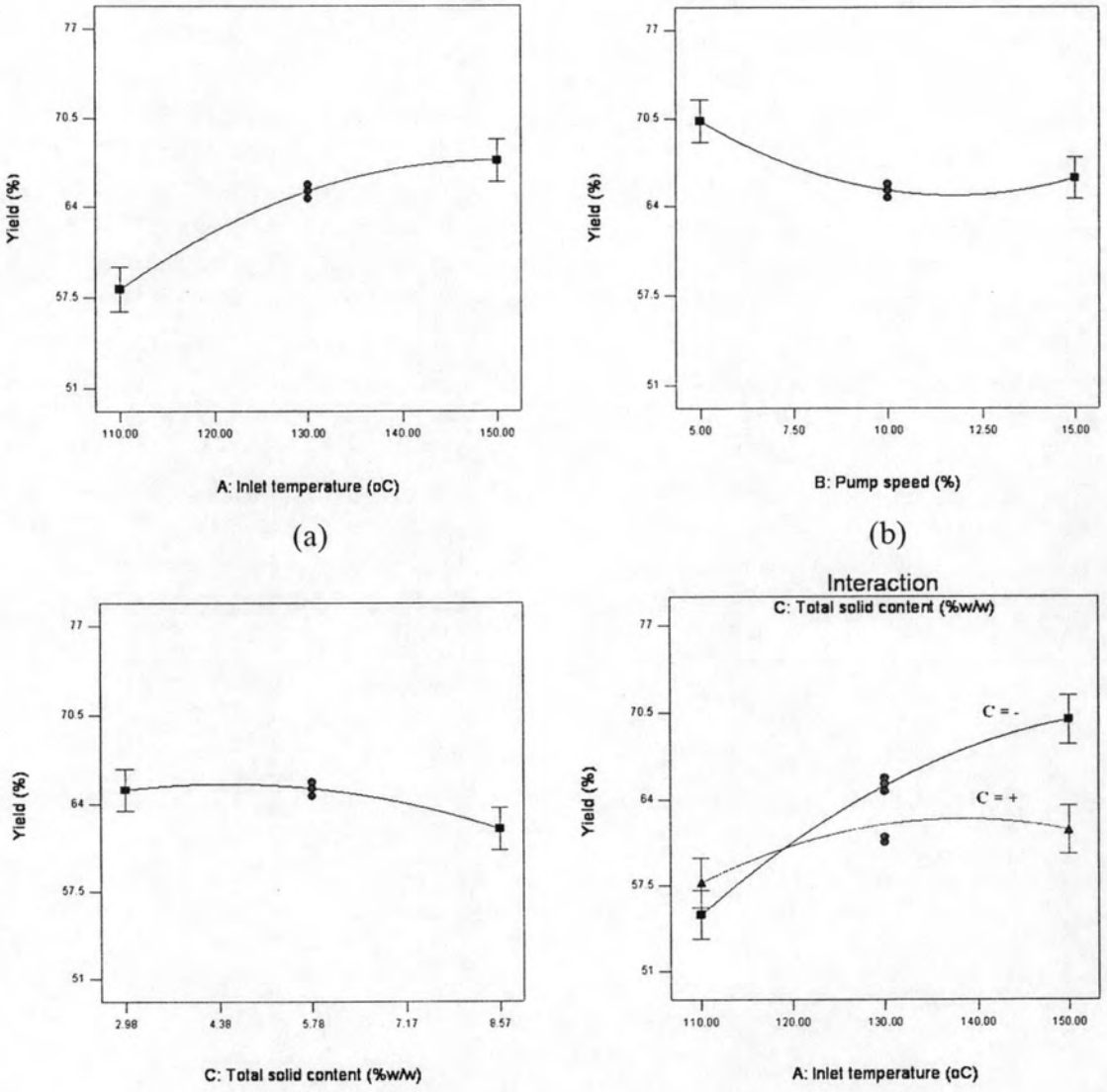

Figure 70 Main effect plots of (a) inlet temperature, (b) pump speed, (c) total solid content at the medium (0) level of the other two factors, and (d) AC interaction for yield response

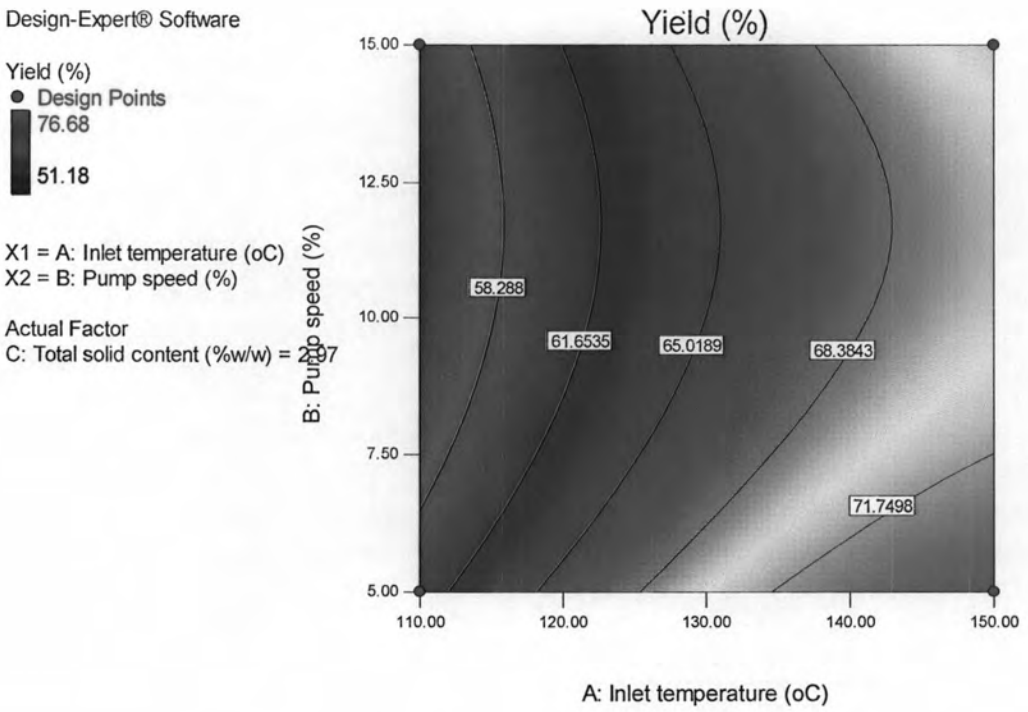

(a) low (-1) level of factor C

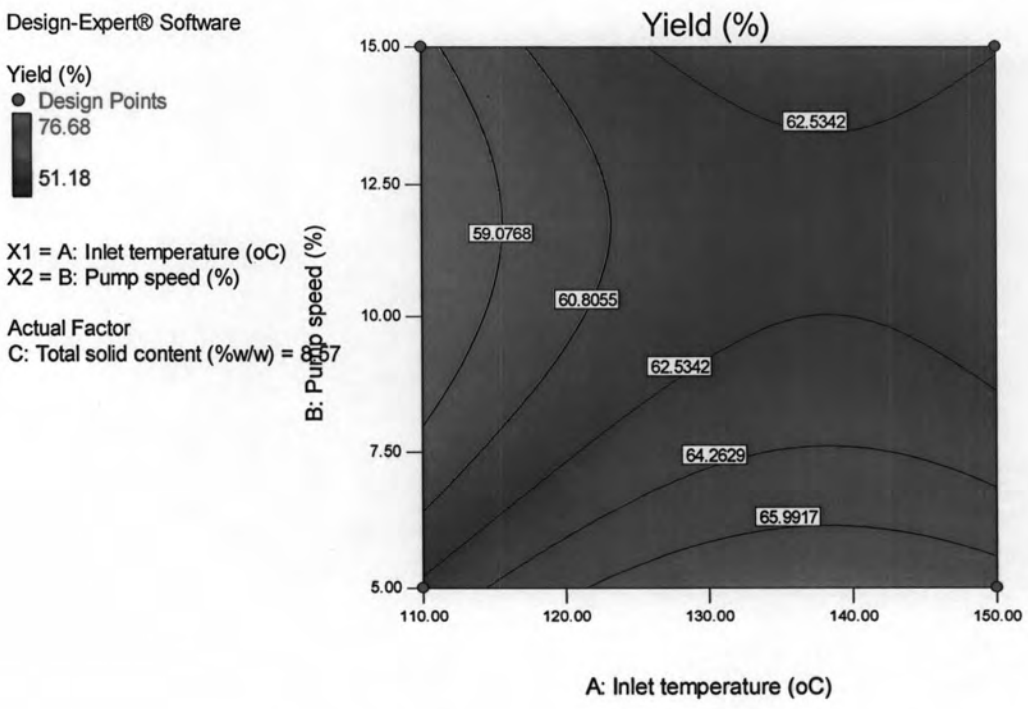

(b) high (+1) level of factor C

Figure 71 Contour plots of yield response at (a) low (-1) and (b) high (+1) levels of factor C (total solid content)

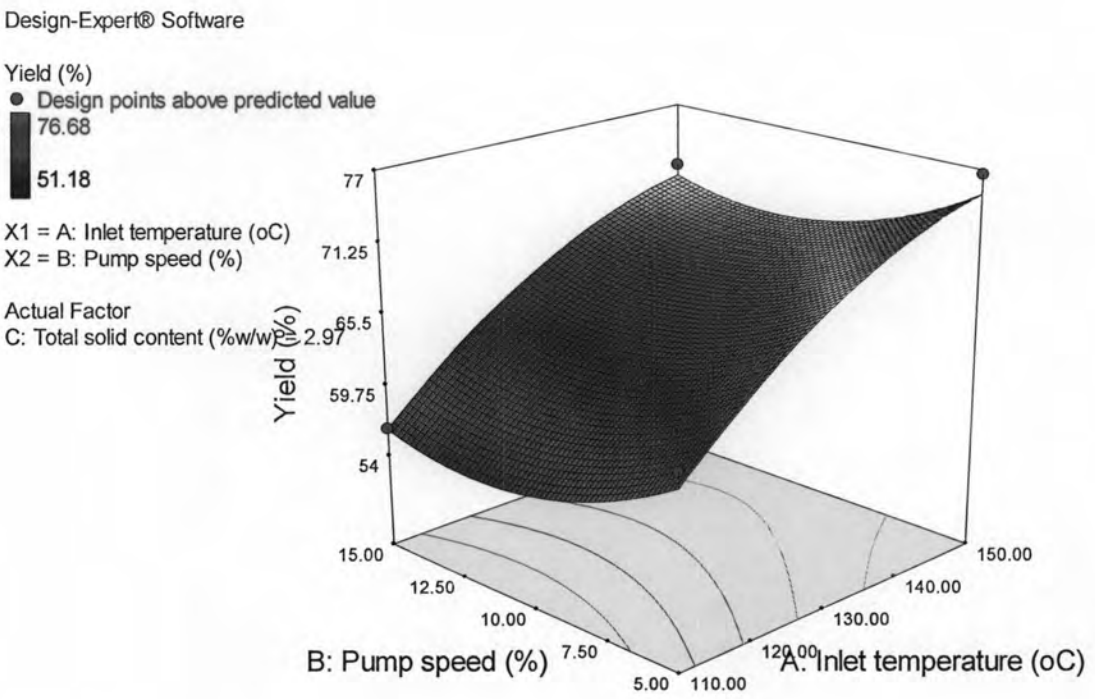

(a) low (-1) level of factor C

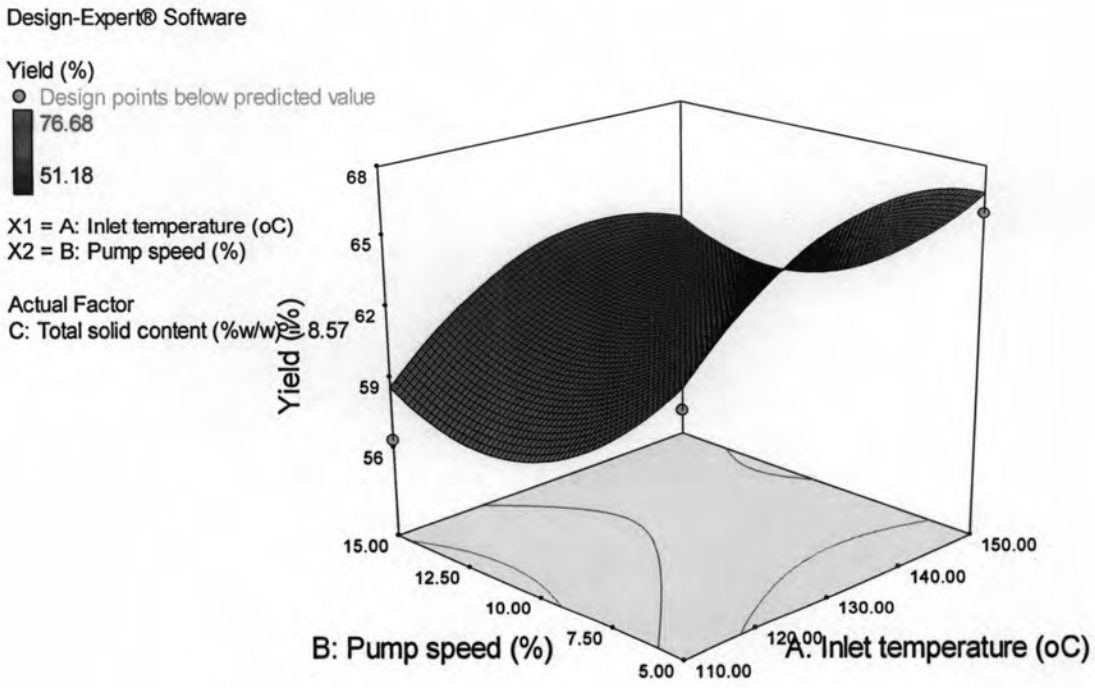

(b) high (+1) level of factor C

Figure 72 Response surface of yield at (a) low (-1) and (b) high (+1) levels of factor C (total solid content)

9.2 Fitting of Particle Size Data to the Quadratic Model

The mass median diameters ($D_{0.5}$) of the spray-dried liposomal powders prepared with conditions over the ranges used in this study were between 4.69 and 10.17 μm (Tables 42 and 52). ANOVA in Table 55 indicates that the pump speed used had no effect on the particle size of the spray-dried liposomal powders (P = 0.5255). Therefore, the pump speed factor was removed from the model. The design became a 2^2 factorial in factor A and C with two replicates. ANOVA in Table 56 shows a high significance ($P < 0.0001$) of the reduced quadratic model for particle size response. The particle size of the spray-dried liposomal powders was highly affected by the inlet temperature ($P < 0.0001$) and total solid content ($P < 0.0001$) of the spray dispersion (Tables 56). The normal probability plot of the residuals (Figure 73a) and the plot of the residuals versus the predicted particle size (Figure 73b) appeared satisfactory. Therefore, the reduced quadratic model was able to be used in predicting particle size as a function of the spray drying conditions. The reduced quadratic model for particle size was described by equation 18:

$$D_{0.5}\ (\mu m) = -25.816 + 0.448(T) + 0.353(C) - 0.002(T)^2 \quad (18)$$

where T is inlet temperature (°C) and C is total solid content (%w/w). The reduced quadratic model showed good characteristic in term of prediction R^2 value of 0.878. Lack of fit was not significant ($P > 0.05$).

Figure 74 indicates that the relationship between the particle size and the inlet temperature was non-linear, while that between the particle size and the total solid content was linear. Contour plot and response surface of the particle size response were obtained by fixing the factor B (pump speed) at the medium (0) level and varying inlet temperature and total solid content over the range used in the factorial design (Figures 75 and 76, respectively). Factor B was kept constant because of its insignificant effect on the particle size response. The particle size was reduced by decreasing the inlet temperature and the total solid content (Figures 74 and 75). Increased inlet air temperature corresponded to higher outlet air temperature which

could result in more aggregation and fusion of the particles. Figure 77 shows that an increase in the outlet temperature tended to increase the particle size of the spray-dried liposomal powders. The effect of temperature on particle size is dependent on the material being dried (Crosby and Marshall, 1958). Broadhead et al. (1994) and Stahl et al. (2002) reported a tendency for the particle size to increase with increasing inlet temperature for spray drying of β–galactosidase and insulin, respectively. Low solute concentration is a means of producing small particles but this in turn reduces efficiency by requiring long spray-drying times (Masters, 1991; Chawla et al., 1994; Maa et al., 1997; Mosen et al., 2004). Low solute concentration decreases the amount of solid in each droplet exiting the nozzle. Therefore, when the water in the droplet evaporates, smaller particles are obtained.

Table 55 ANOVA for the quadratic model of particle size response ($R^2 = 0.973$, pred $R^2 = 0.802$)

Source of Variation	df	Sum of Squares	Mean Square	*F* Value	*P*-value
Model	9	32.832	3.648	28.091	0.0001**
A-Inlet temperature (°C)	1	13.257	13.257	102.082	0.0001*
B-Pump speed (%)	1	0.058	0.058	0.446	0.5255
C-Total solid content (%w/w)	1	13.406	13.406	103.231	0.0001*
AB	1	0.026	0.026	0.204	0.6654
AC	1	0.312	0.312	2.403	0.1650
BC	1	0.451	0.451	3.475	0.1046
A^2	1	4.439	4.439	34.182	0.0006**
B^2	1	0.090	0.090	0.689	0.4338
C^2	1	0.076	0.076	0.582	0.4705
Residual	7	0.909	0.130		
Lack of Fit	5	0.850	0.170	5.735	0.1551
Pure Error	2	0.059	0.030		
Cor Total	16	33.741			

* Significant at $P < 0.0001$

** Significant at $P < 0.01$

Table 56 ANOVA for the reduced quadratic model of particle size response (R^2 = 0.941, pred R^2 = 0.878)

Source of Variation	df	Sum of Squares	Mean Square	*F* Value	*P*-value
Model	3	31.756	10.585	69.320	0.0001*
A-Inlet temperature (°C)	1	13.257	13.257	86.816	0.0001*
C-Total solid content (%w/w)	1	13.406	13.406	87.793	0.0001*
A^2	1	5.093	5.093	33.351	0.0001*
Residual	13	1.985	0.153		
Lack of Fit	11	1.926	0.175	5.908	0.1535
Pure Error	2	0.059	0.030		
Cor Total	16	33.741			

* Significant at $P < 0.0001$

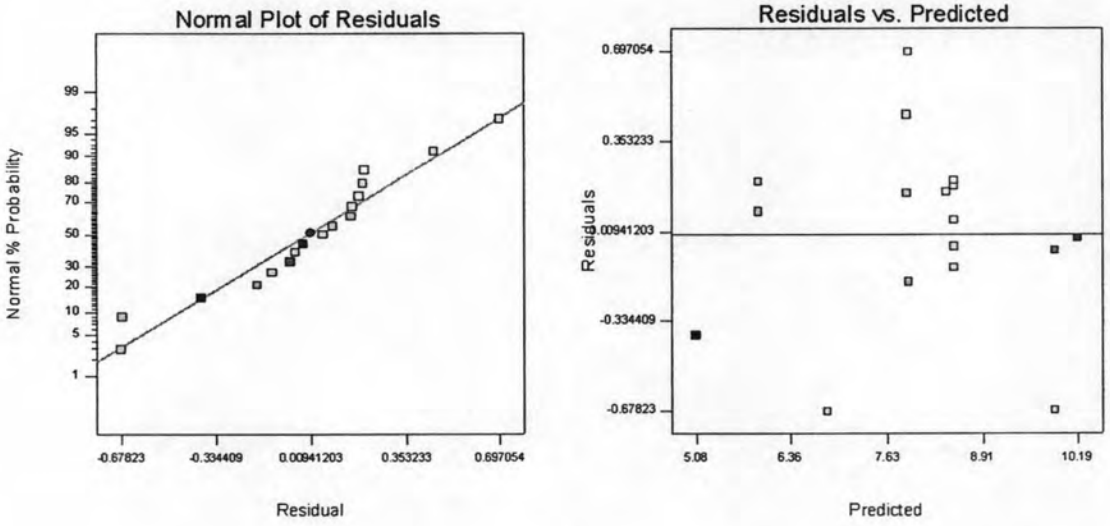

(a) (b)

Figure 73 Residual analysis of the reduced quadratic model for particle size response: (a) Normal probability versus residuals and (b) Residuals versus predicted values

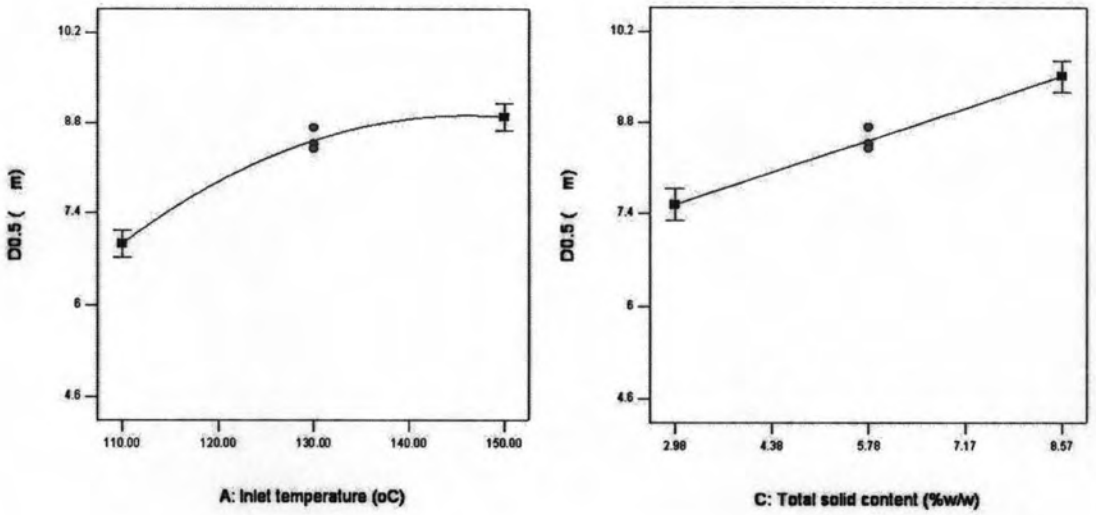

(a) (b)

Figure 74 Main effect plots of (a) inlet temperature and (b) total solid content for particle size response at the medium (0) level of the other two factors

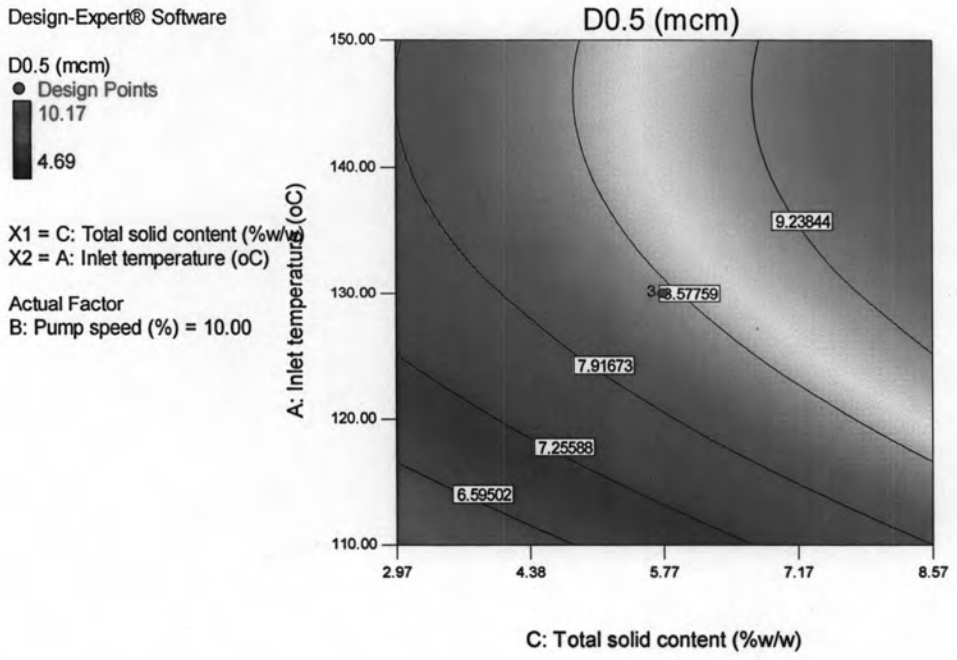

Figure 75 Contour plot of particle size response at the medium (0) level of factor B (pump speed)

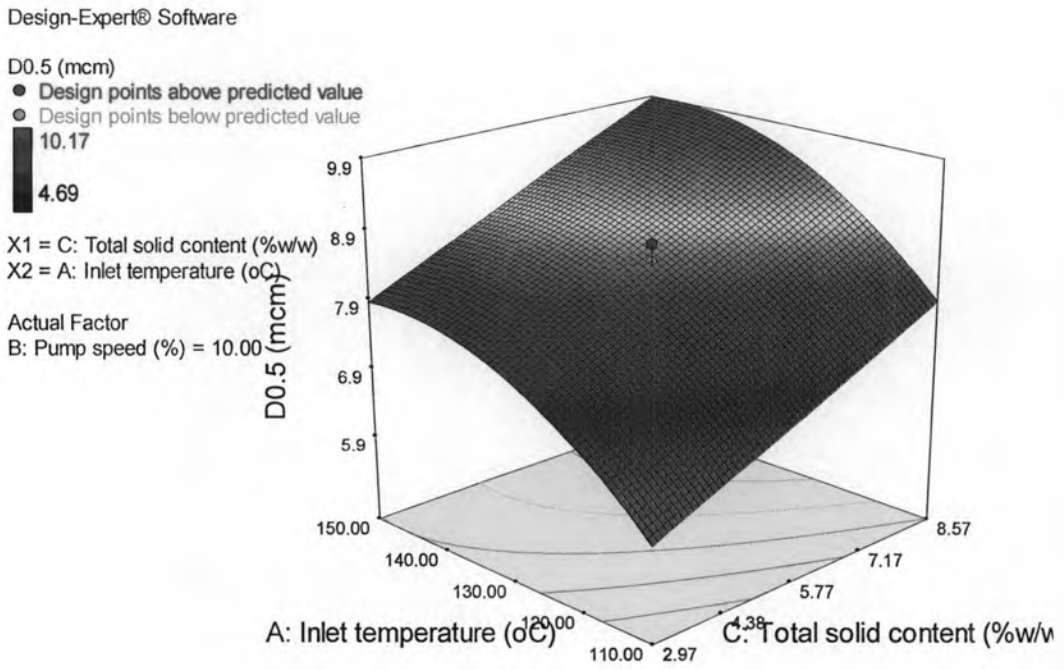

Figure 76 Response surface of particle size at the medium (0) level of factor B (pump speed)

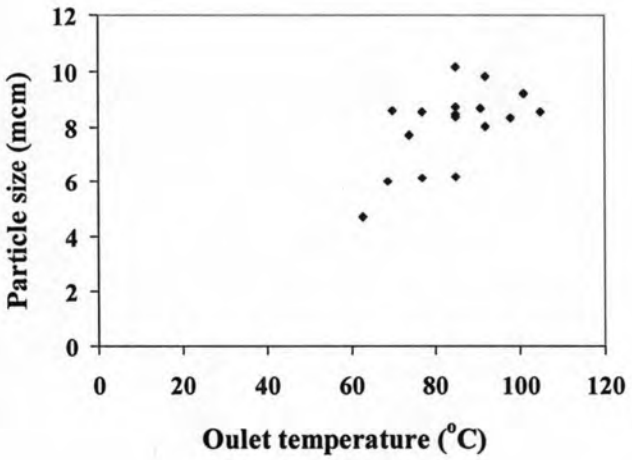

Figure 77 Correlation between the particle size of the spray-dried liposomal powders and the outlet temperature

9.3 Fitting of Entrapment Efficiency Data to the Quadratic Model

The entrapment efficiencies of lysozyme in the reconstituted liposomes from the spray-dried liposomal powders prepared with conditions used in this study were between 7.13 and 16.02 μg LSZ/mg lipid (Tables 42 and 51). Table 57 indicates that the entrapment efficiency was highly affected by the inlet temperature ($P < 0.0001$) and the pump speed ($P < 0.0001$). The total solid content over the ranges used in this study had no significant effect on the entrapment efficiency ($P = 0.9476$). However, this term could not be removed from the fitted equation because the BC interaction term was highly significant ($P < 0.01$) (Table 57). In other words, the factor C had a great effect on the level of the factor B. Since important information may be lost, it is always preferable to remain terms from the full model unless a remarkable improvement in model performances is achieved (Montgomery, 2005). In addition, underestimation of effects may be generated as a consequence of a not hierarchical model.

After removing the insignificant terms, residual analysis (Figure 78) indicates that the assumptions of normality and equality of variance were violated. Therefore, the natural log (ln) was used to transform the entrapment efficiency data. Residual analysis following the log transformation indicates that the assumptions held and the model was adequate (Figure 79). ANOVA in Table 58 shows a high significance ($P < 0.0001$) of the reduced quadratic model for the entrapment efficiency response following the log transformation which was described by equation 19:

$$\ln(EE) = 0.753 + 0.033(T) + 0.072(P) - 0.01(C) + 0.0003(T*P) - 0.003(P*C) - 0.0002(T)^2 - 0.004(P)^2 + 0.004(C)^2 \quad (19)$$

where EE is entrapment efficiency (μg LSZ/mg lipid), T is inlet temperature (°C), P is pump speed (%) and C is total solid content (%w/w). Lack of fit was not significant ($P > 0.05$). The reduced quadratic model following the log transformation showed good characteristic in term of prediction R^2 value of 0.970. Therefore, it could be

used in predicting entrapment efficiency response as a function of the spray drying conditions.

Table 57 ANOVA for the quadratic model of entrapment efficiency response (R^2 = 0.994, pred R^2 = 0.982)

Source of Variation	df	Sum of Squares	Mean Square	*F* Value	*P*-value
Model	9	128.562	14.285	135.628	0.0001*
A-Inlet temperature (°C)	1	95.534	95.534	907.060	0.0001*
B-Pump speed (%)	1	10.928	10.928	103.758	0.0001*
C-Total solid content (%w/w)	1	0.000	0.000	0.005	0.9476
AB	1	0.118	0.118	1.117	0.3257
AC	1	0.014	0.014	0.129	0.7298
BC	1	1.990	1.990	18.894	0.0034**
A^2	1	4.277	4.277	40.609	0.0004**
B^2	1	11.395	11.395	108.187	0.0001*
C^2	1	1.719	1.719	16.320	0.0049**
Residual	7	0.737	0.105		
Lack of Fit	5	0.111	0.022	0.07064	0.9913
Pure Error	2	0.627	0.313		
Cor Total	16	129.299			

* Significant at $P < 0.0001$

** Significant at $P < 0.01$

Figures 80 shows that the entrapment efficiency increased with decreasing inlet temperature and increasing pump speed at the medium (0) level of the other two factors. The magnitude of AB interaction effect was minute and of little practical importance (Table 58 and Figure 80). After a log transformation for model fitting, contour plot and response surface on original scale of the entrapment efficiency were generated by fixing the factor C (total solid content) at the low (-1) and the high (+) levels and varying the inlet temperature and the pump speed over the range used in the factorial design (Figures 81 and 82, respectively). Factors A and B were varied because they displayed major influence on the entrapment efficiency response.

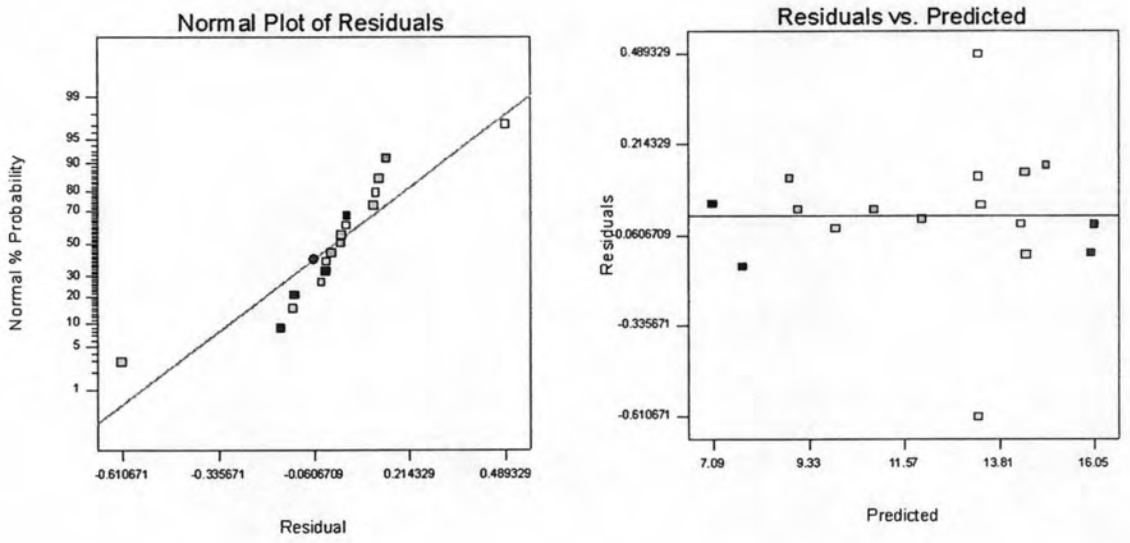

(a) (b)

Figure 78 Residual analysis of the reduced quadratic model for entrapment efficiency response: (a) Normal probability versus residuals and (b) Residuals versus predicted values

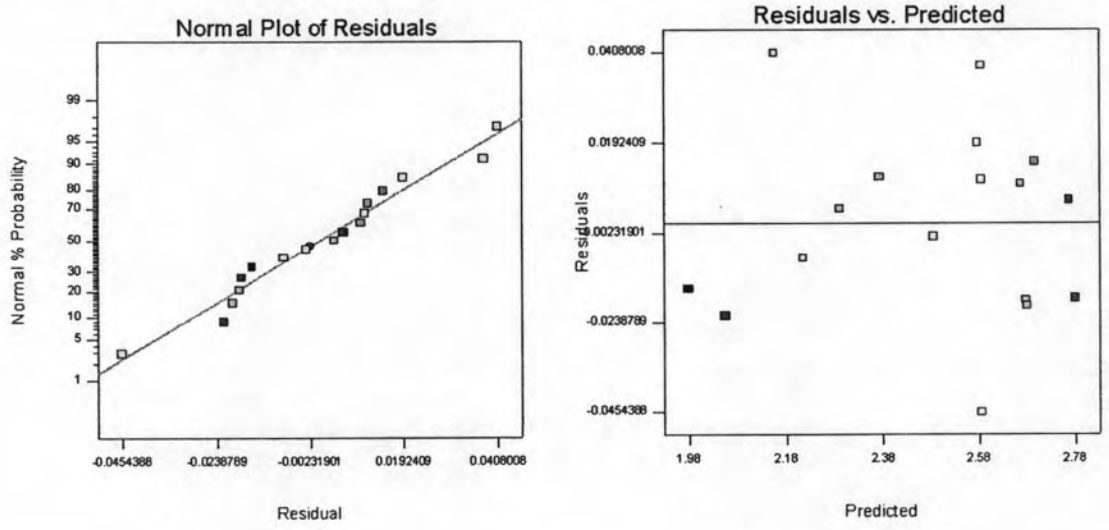

(a) (b)

Figure 79 Residual analysis of the reduced quadratic model for entrapment efficiency response following the log transformation: (a) Normal probability versus residuals and (b) Residuals versus predicted values

Table 58 ANOVA for the reduced quadratic model of entrapment efficiency response following the log transformation ($R^2 = 0.992$, pred $R^2 = 0.970$)

Source of Variation	df	Sum of Squares	Mean Square	*F* Value	*P*-value
Model	8	1.030	0.129	128.693	0.0001*
A-Inlet temperature (°C)	1	0.741	0.741	740.224	0.0001*
B-Pump speed (%)	1	0.094	0.094	93.977	0.0001*
C-Total solid content (%w/w)	1	0.000	0.000	0.225	0.6478
AB	1	0.007	0.007	6.759	0.0316***
BC	1	0.017	0.017	17.175	0.0032**
A^2	1	0.064	0.064	63.931	0.0001*
B^2	1	0.082	0.082	82.023	0.0001*
C^2	1	0.011	0.011	10.609	0.0116***
Residual	8	0.008	0.001		
Lack of Fit	6	0.004	0.001	0.411	0.8319
Pure Error	2	0.004	0.002		
Cor Total	16	1.038			

* Significant at $P < 0.0001$

** Significant at $P < 0.01$

*** Significant at $P < 0.05$

Decreasing inlet temperature improved considerably the entrapment efficiency irrespective of the other factors (Figure 81). High inlet temperature might result in more rapid drying of lysozyme and mannitol solutions when compared to liposome drying. Consequently, segregation of liposomes and lysozyme occurred resulting in non-homogeneous dispersion of lysozyme in liposomal powders. Upon reconstitution, low entrapment resulted from poor penetration of lysozyme into liposomes through the non-homogeneous mass. An increase in total solid content improved entrapment efficiency when pump speed was low (Figure 80d). At high

pump speed, decreasing total solid content resulted in increased entrapment efficiency (Figure 80d). The low solute concentration combined with the increased pump speed resulted in slow drying, allowing sufficient time for homogeneous mixture of lysozyme and lipid in the powders.

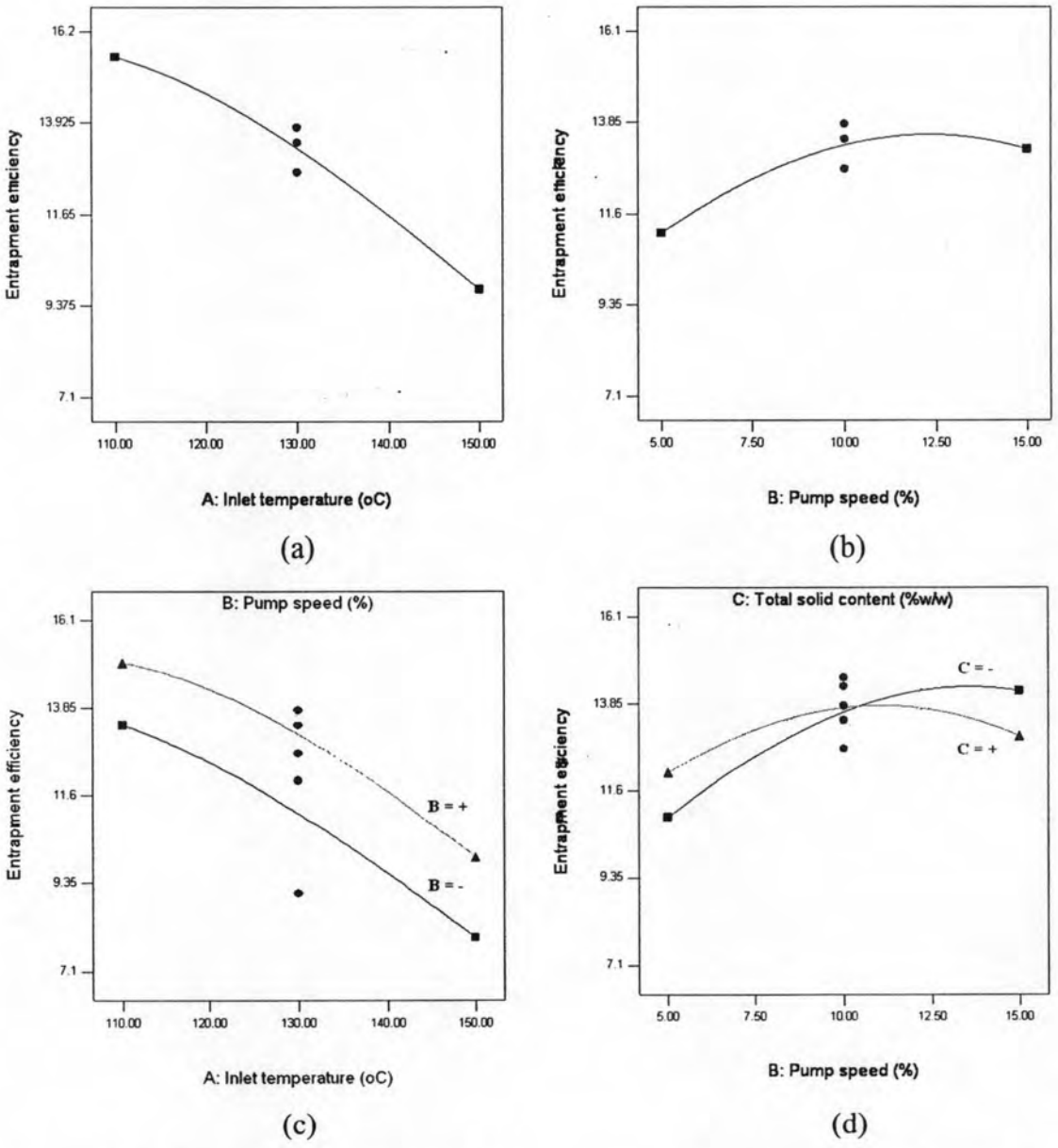

Figure 80 Main effect plots of (a) inlet temperature, (b) pump speed at the medium (0) level of the other factors, (c) AB interaction and (d) BC interaction on original scale for entrapment efficiency response following the log transformation

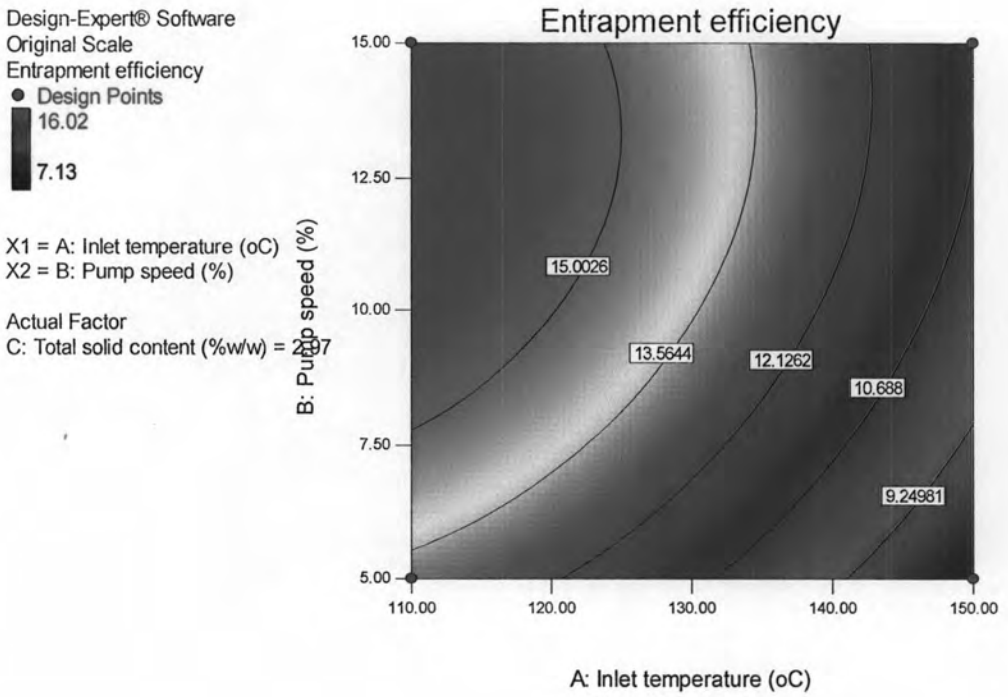

(a) low (-) level of factor C

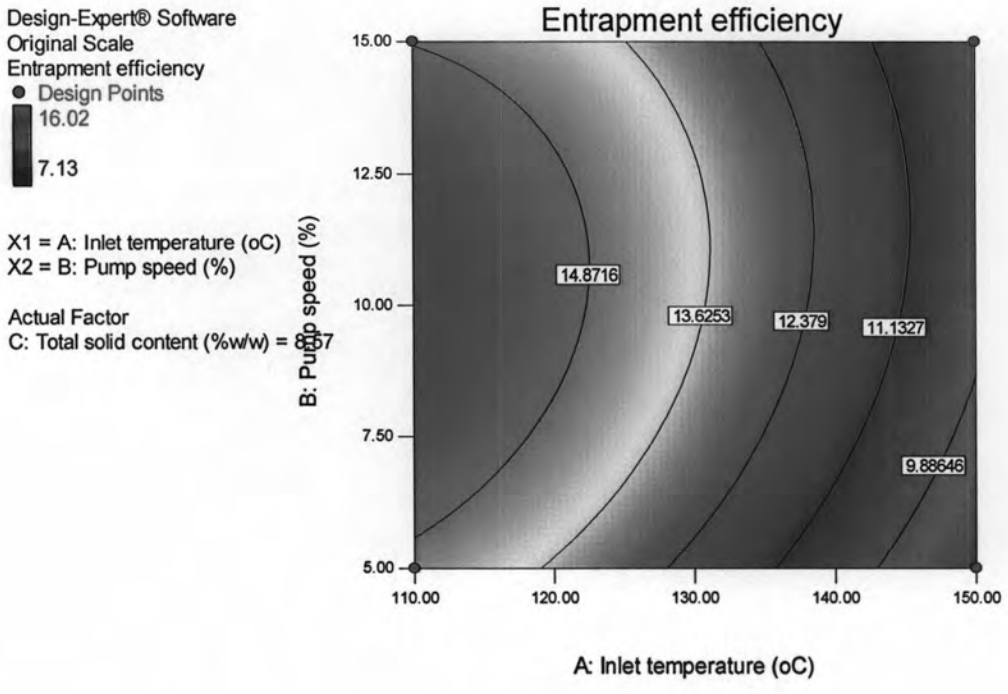

(b) high (+) level of factor C

Figure 81 Contour plots on original scale of entrapment efficiency response following the log transformation at (a) low (-) and (b) high (+) levels of factor C (total solid content)

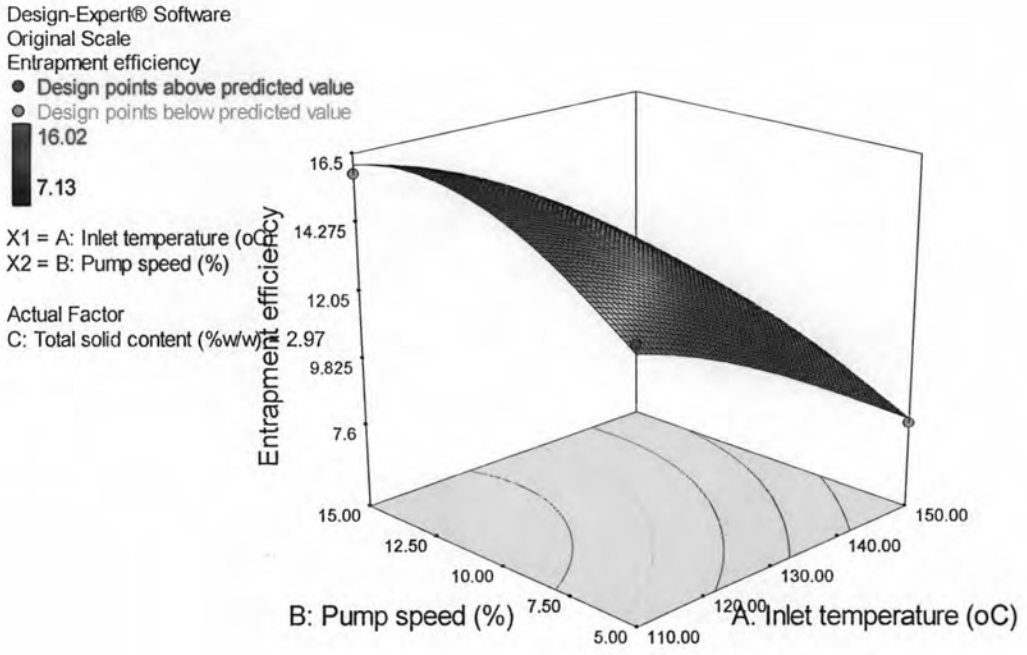

(a) low (-) level of factor C

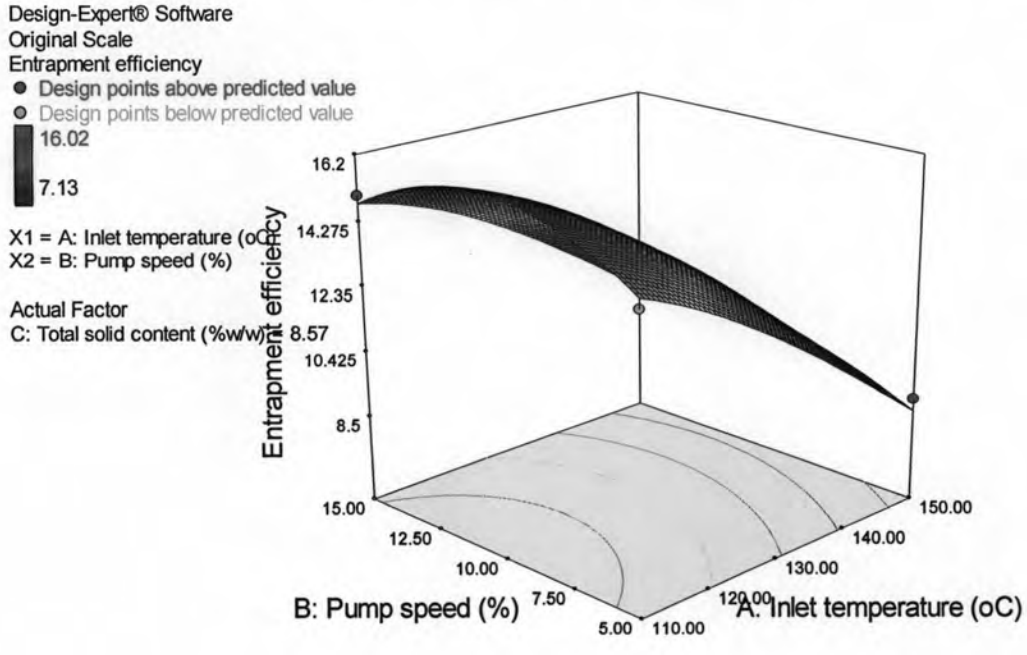

(b) high (+) level of factor C

Figure 82 Response surface on original scale of entrapment efficiency following the log transformation at (a) low (-) and (b) high (+) levels of factor C (total solid content)

Table 59 shows other properties of the spray-dried lysozyme-loaded liposomal powders obtained from experimental design for the spray drying condition optimization. The apparent density values of the lysozyme-loaded liposomal powders prepared with different spray drying conditions were rather similar and ranged from 1.2603 to 1.3209 g/cm^3. The sizes of the reconstituted liposomes ranged from 3.82 to 5.32 μm. The spray drying conditions used in this study had no impact on the biological activity of lysozyme.

Table 59 Other properties of the spray-dried lysozyme-loaded liposomal powders for the central composite design (mean ± SD)

Exp.	Factors			Properties			
	T (°C)	P (%)	C (%w/w)	T_o (°C)	Apparent density (g/cm^3) (n = 5)	Reconstituted liposome size* ($D_{[4,3]}$, μm) (n = 3)	Remaining activity of LSZ (%) (n = 4)
1	110	5	2.975	77	1.3085 ± 0.0087	4.52 ± 0.01	101.24 ± 7.90
2	150	5	2.975	98	1.3209 ± 0.0049	5.20 ± 0.01	100.43 ± 3.11
3	110	15	2.975	69	1.3019 ± 0.0077	4.00 ± 0.02	100.87 ± 2.81
4	150	15	2.975	92	1.2940 ± 0.0096	4.80 ± 0.01	100.93 ± 1.78
5	110	5	8.575	74	1.2985 ± 0.0063	4.18 ± 0.00	99.93 ± 1.79
6	150	5	8.575	101	1.2826 ± 0.0066	5.32 ± 0.01	99.61 ± 2.23
7	110	15	8.575	70	1.3032 ± 0.0110	4.14 ± 0.02	102.00 ± 3.81
8	150	15	8.575	92	1.2926 ± 0.0087	5.03 ± 0.01	101.20 ± 3.64
9	130	10	5.775	85	1.2751 ± 0.0072	5.14 ± 0.01	102.73 ± 1.85
10	130	10	5.775	85	1.2778 ± 0.0083	4.81 ± 0.00	101.14 ± 2.82
11	130	10	5.775	85	1.2786 ± 0.0084	4.59 ± 0.01	100.78 ± 4.08
12	96	10	5.775	63	1.2740 ± 0.0081	3.82 ± 0.01	101.75 ± 1.32
13	164	10	5.775	105	1.2693 ± 0.0094	5.01 ± 0.01	100.40 ± 0.80
14	130	2	5.775	91	1.2603 ± 0.0067	4.24 ± 0.00	99.34 ± 1.40
15	130	18	5.775	77	1.2953 ± 0.0025	4.91 ± 0.01	100.82 ± 4.92
16	130	10	1.05	85	1.2723 ± 0.0049	4.49 ± 0.01	98.66 ± 3.77
17	130	10	10.5	85	1.2862 ± 0.0073	4.52 ± 0.00	102.34 ± 4.15

* measured by Mastersizer 2000

10. Optimization of Spray Drying Conditions

From the results of the experimental design in Section 9, the optimum spray drying process conditions were studied using the criteria as present in Table 60. Table 61 summarizes the optimum spray drying conditions with predicted responses determined from the response surface to achieve maximum of yield and entrapment efficiency and minimum of particle size. The optimum condition no. 1 was chosen to evaluate the predictability of the regression quadratic models because of the highest desirability function (Table 61 and Figure 83). Predicted values of response variables for the optimum condition no. 1 are shown in Table 62. The observed values for yield, particle size and entrapment efficiency responses fell inside the prediction intervals of the corresponding responses at a 95 % confidence level (Table 63). A good agreement between actual and predicted values of all responses was observed with the low estimated biases below 8 % (Table 63). The observed values of yield, particle size and entrapment efficiency obtained from three batches displayed good precision of the process (low SD, Table 63). The mass median diameters ($D_{0.5}$) of three batches ranged from 5.71 to 6.15 μm. These results indicated that the experimental design could be used for optimization of the spray drying factors to develop the lysozyme-loaded liposomal powders for possible pulmonary delivery with a relatively low number of experiments. This is one of the advantages of such method which has large application in pharmaceutical development.

Table 60 Criteria for optimization of spray drying factors

Variables	Goal	Lower limit	Upper limit	Importance
Inlet temperature (°C)	in range	110	150	3
Pump speed (%)	in range	5	15	3
Total solid content (%w/w)	in range	2.975	8.575	3
Yield (%)	maximize	51.18	76.68	4
$D_{0.5}$ (μm)	minimize	4.69	7	5
Entrapment efficiency	maximize	7.13	16.02	4

Table 61 Optimum spray drying factors and predicted response variables

Number	Factors			Predicted responses			Desirability
	T (°C)	P (%)	C (%w/w)	Yield (%)	$D_{0.5}$ (μm)	EE (μg LSZ/ mg lipid)	
1	110.00	5.00	2.98	60.46	5.93	13.16	0.500
2	110.00	5.00	3.03	60.55	5.95	13.16	0.497
3	110.51	5.00	2.98	60.77	5.99	13.13	0.494
4	110.00	5.29	3.04	60.09	5.96	13.38	0.493
5	110.00	5.60	2.98	59.52	5.94	13.61	0.491
6	110.73	5.00	2.98	60.90	6.01	13.11	0.491
7	110.65	5.26	2.98	60.43	6.00	13.31	0.489
8	111.01	5.00	2.98	61.07	6.04	13.09	0.487
9	110.00	5.00	3.37	61.04	6.07	13.15	0.482
10	110.00	6.52	2.98	58.25	5.93	14.24	0.477
11	111.92	5.00	2.98	61.61	6.14	13.01	0.474
12	110.00	7.39	3.13	57.46	5.99	14.76	0.458
13	110.00	15.00	2.98	56.22	5.93	16.14	0.451
14	110.44	14.99	2.98	56.47	5.98	16.12	0.450
15	110.23	8.09	2.98	56.69	5.96	15.15	0.449
16	110.00	8.26	2.98	56.41	5.94	15.25	0.447
17	111.58	15.00	2.98	57.16	6.11	16.06	0.444
18	111.76	15.00	2.98	57.27	6.12	16.05	0.443
19	110.64	14.55	2.98	56.27	6.00	16.22	0.441
20	110.00	8.92	2.98	55.89	5.93	15.57	0.437
21	110.00	9.33	2.98	55.64	5.93	15.74	0.431
22	110.00	9.46	2.98	55.56	5.93	15.79	0.429
23	110.23	13.12	2.98	55.30	5.96	16.42	0.420
24	110.86	11.25	2.98	55.47	6.03	16.25	0.414

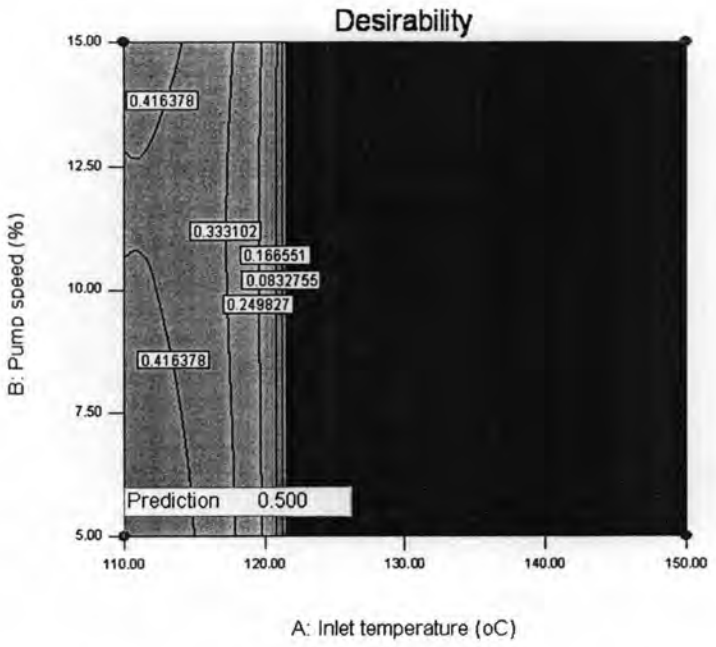

Figure 83 Contour plot of desirability for optimization of the spray drying condition at low level of factor C

Other physicochemical properties of the optimum formulation no. 1 are summarized in Table 64. The apparent density was 1.2802 g/cm^3. The bulk and tapped density were 0.31 and 0.43 g/cm^3, respectively. The theoretical aerodynamic diameter (D_{aer}) of individual particles was calculated for each batch and found to be around 4 μm. Hanes et al. (2003) reported that particles with an aerodynamic diameter between 0.02 and 0.05 μm and 2-5 μm were capable of alveolar deposition. Dry powders having particle size > 5 μm and a tap density < 0.4 g/cm^3 were suggested to be aerodynamically light particles (Vanbever, Mintzes, and Wan, 1999). Aerodynamically light powders are more capable of escaping inertial and gravitational deposition in the oropharyngeal region, and site-specific targeting to the deep lung (Edwards et al., 2005). However, the theoretical aerodynamic diameter might not reflect the true aerodynamic diameter. Therefore, the mass median aerodynamic diameter (MMAD) should be determined using cascade impactor analysis for in vitro characterization of the aerodynamic properties of the spray-dried liposomal powders in the further study.

Table 62 Predicted responses for the optimum formulation no. 1 (T = 110 °C, P = 5 % and C = 2.975 %w/w)

Response	Predicted value	95% Prediction Interval
Yield (%)	60.46	55.40 – 65.53
$D_{0.5}$ (μm)	5.93	5.01 – 6.86
EE (μg LSZ/mg lipid)	13.16	12.02 – 14.42

Table 63 Actual value and bias of response variables for optimum condition no. 1 (T = 110 °C, P = 5 % and C = 2.975 %w/w)

Response	Yield (%)		$D_{0.5}$ (μm)		EE (μg LSZ/mg lipid)	
Predicted	60.46		5.93		13.16	
Batch	Actual	Bias (%)	Actual	Bias (%)	Actual	Bias (%)
1	64.94	7.40	6.13	3.30	14.01	6.43
2	58.63	-3.03	6.15	3.64	13.86	5.29
3	61.15	1.13	5.71	-3.78	13.63	3.54
Mean	61.57	1.83	6.00	1.05	13.83	5.09
SD	3.18	5.25	0.25	4.19	0.19	1.45

The Carr's compressibility index, which is generally considered as an appropriate method for evaluation of the flow properties of solids, was determined from tapped and bulk density values. Carr's Index values of less than 25 usually show good flow characteristics, while values beyond 40 indicate poor powder flowability (Sebti and Amighi, 2006). From Table 64, the optimum formulation no. 1 showed intermediate flow characteristics which might be due to their small particle size. However, a relatively small amount of sample (3 g) was used in this present study. Since the reliability of the method used could be influenced by equipment specification and working protocol, a larger sample size (e.g. 100 g) might give a more accurate result.

The influence of vesicle size on phagocytosis in the alveoli has been widely studied (Rudt and Muller, 1992; Agu et al., 2001; Aliasgar and Ambikanandan, 2004; Zhou et al., 2005). Very small particles persisted longer in the lungs because they prefer to translocate to the connective tissues and are cleared by epithelial cells. In contrast, particles with larger particle sizes (> 1 μm) are mainly phagocytosed by alveolar macrophages (Geiser, 2002). In this present study, the volume mean diameter of the reconstituted liposomes from the optimum formulation was about 4.7 μm (Table 64). Thus, phagocytosis of these particles by alveolar macrophages seemed plausible when aerosolized to the lungs, making it promising to use these particles for vaccine delivery.

Table 64 Other properties of the spray-dried lysozyme-loaded liposomal powders prepared with optimum condition no. 1 (T = 110 °C, P = 5 % and C = 2.975 %w/w)

Properties	Batch 1	Batch 2	Batch 3	Mean	SD
Outlet temperature (°C)	74	74	75	74.33	0.58
Moisture content (%w/w)	3.23	3.2	3.16	3.20	0.04
Apparent density (g/cm^3) (n = 5)	1.2693	1.2816	1.2897	1.2802	0.0103
Bulk density (g/cm^3)	0.3	0.31	0.31	0.31	0.01
Tapped density (g/cm^3)	0.45	0.44	0.40	0.43	0.03
Theoretical aerodynamic diameter (D_{aer}) (μm)	4.11	4.06	3.62	3.93	0.27
Carr's compressibility index (%)	32.5	30	24	28.83	4.37
Remaining activity of LSZ (%) (n = 4)	102.24	101.3	103.06	102.20	0.88
Reconstituted liposome size* ($D_{[4,3]}$, μm) (n = 3)	4.64	4.74	4.68	4.69	0.05

* measured by Mastersizer 2000

The morphological characteristics of the lysozyme-loaded liposomal powders produced with the optimum spray drying condition no. 1 and the corresponding reconstituted liposomes were investigated using SEM as shown in Figures 84 and 85. The reconstituted liposomes appeared very aggregate, though spherical, and had diameters around 3-4 μm (Figure 85) which is consistent with the images observed by optical microscopy (Figure 62a). Polarizing photomicrograph (Figure 86) confirmed the formation of lamellar vesicles after the spray-dried liposomal powders were reconstituted with HBS at 37 °C.

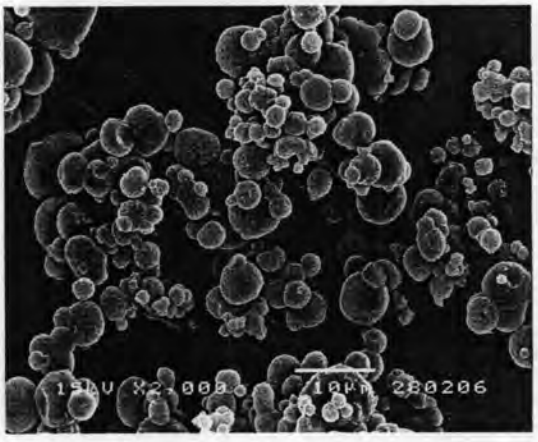

Figure 84 SEM image of the spray-dried lysozyme-loaded liposomal powders produced with the optimum condition no. 1. Magnification 2000x. Scale bar = 10 μm.

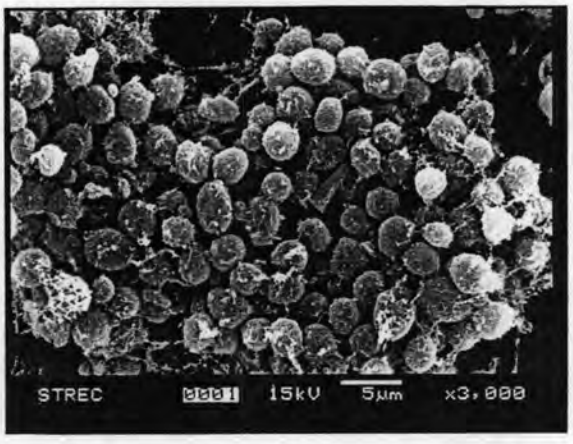

Figure 85 SEM image of the reconstituted liposomes from the optimum condition no. 1 in HBS at 37 °C. Magnification 3000x. Scale bar = 5 μm.

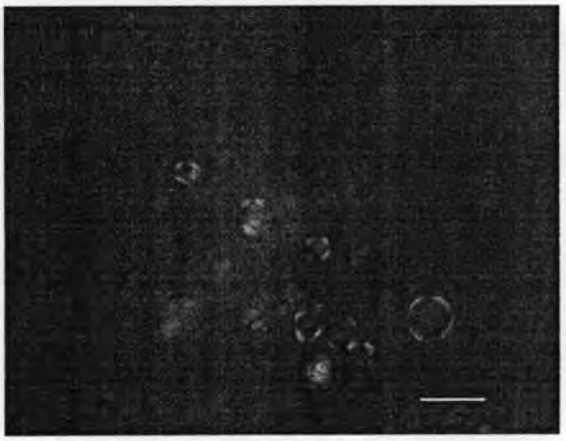

Figure 86 Polarizing micrograph of the reconstituted liposomes from the optimum formulation no. 1 in HBS at 37 °C. Magnification 1000x. Scale bar = 10 μm.

Lysozyme content of the spray-dried liposomal powders obtained from the optimum condition no. 1 was measured using QPBCA protein assay kit with six samples from the same batch. The result showed a mean of lysozyme loading efficiency close to 100 % (Table 65). This indicated that no loss of lysozyme occurred during spray drying. The % CV value of the lysozyme content was 3.07 %.

Table 65 Lysozyme content and loading efficiency of the spray-dried lysozyme-loaded liposomal powders with the optimum condition no. 1

Run no.	**1**	**2**	**3**	**4**	**5**	**6**	**Mean**	**SD**
LSZ content (%w/w)	5.00	4.90	4.75	4.74	4.88	4.59	4.81	0.15
Loading efficiency (%)	105.07	102.84	99.65	99.52	102.58	96.35	101.00	3.10

DSC thermograms of the spray-dried formulations prepared with the inlet temperature of 96 °C and 110 °C showed exothermic peak at around 133-148 °C (Figure 87). These exothermic peaks may correspond to the recrystallization of amorphous fraction of mannitol in the spray-dried liposomal powders prepared with low inlet temperature. However, these exothermic peaks were not evident when either mannitol or liposomes was spray-dried using the same condition in Figure 87(a).

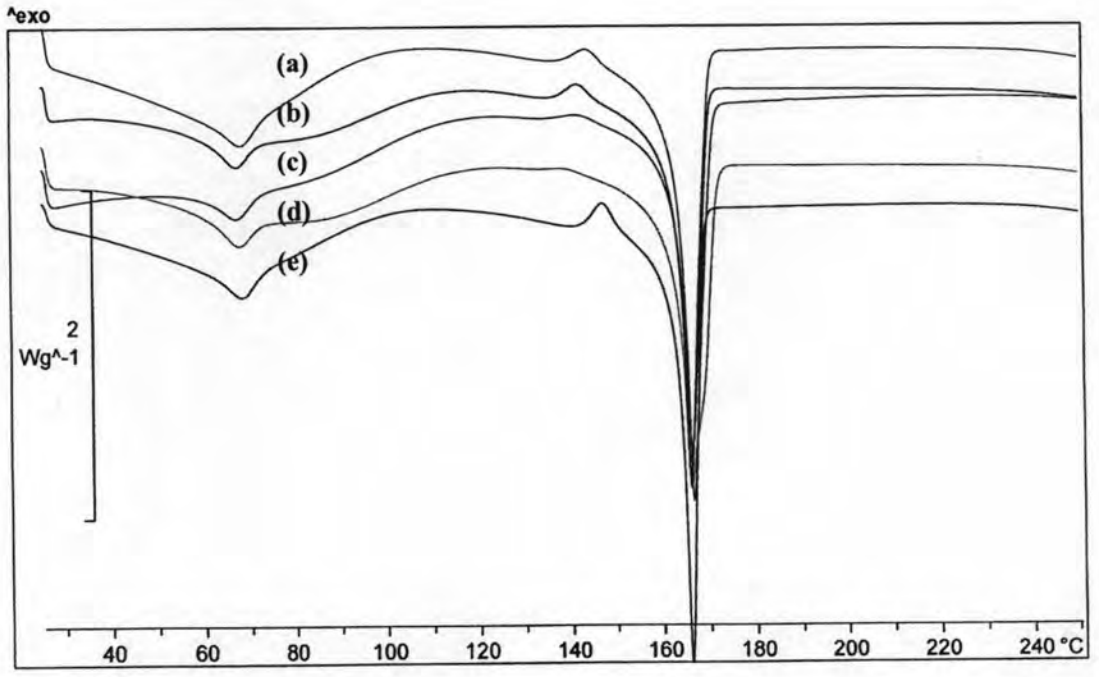

Figure 87 DSC spectra of the spray-dried liposomal powders prepared with the inlet temperature below 110 °C (Experiment 1 (a), 3 (b), 5 (c), 7 (d) and 12 (e))

Finally, the spray-dried liposomal powders should be further developed to obtain smaller particle size which is suitable for delivery of drugs to deep lung. Because the optimum condition no. 1 selected was the condition at low (-1) levels of all spray drying factors, a further reduction of inlet temperature or total solid content might be able to give smaller particle sizes. However, process yield and entrapment efficiency might be adversely affected. Alternatively, an increase in the energy available for atomization such as atomizing air flow rate should decrease particle size

of the spray-dried liposomal powders (Broadhead et al., 1992). In addition, the spray-dried liposomal formulations should be also developed to yield smaller size of the reconstituted liposomes for better drug targeting to alveolar macrophages. Increasing Chol content above 30 mole% may result in a reduction in liposome size. However, amount of additive should be increased accordingly in spray-dried formulation to yield appropriate powders. In addition, the limitations of spray drying process included problems with efficient particle collection and the potential instability of materials sensitive to high temperatures such as proteins/peptides. Anti-adherents (e.g. amino acids) and stabilizers (e.g. disaccharides) might be included for improvement of yield and protein stability, respectively, during spray drying process.